ISTANBUL TECHNICAL UNIVERSITY ★GRADUATE SCHOOL OF SCIENCE ENGINEERING AND TECHNOLOGY

ESTIMATION OF PARTIAL SATURATION TO BE INDUCED IN LIQUEFIABLE SANDS FOR MITIGATION USING ARTIFICIAL NEURAL NETWORK APPROACH

M.Sc. THESIS

Çağdaş ÇAYAKAN

Department of Civil Engineering

Earthquake Engineering Programme

JUNE 2012

ISTANBUL TECHNICAL UNIVERSITY ★GRADUATE SCHOOL OF SCIENCE ENGINEERING AND TECHNOLOGY

ESTIMATION OF PARTIAL SATURATION TO BE INDUCED IN LIQUEFIABLE SANDS FOR MITIGATION USING ARTIFICIAL NEURAL NETWORK APPROACH

M.Sc. THESIS

Çağdaş ÇAYAKAN
(501091223)

Department of Civil Engineering

Earthquake Engineering Programme

Thesis Advisor: Assist. Prof. Dr. E. Ece BAYAT

JUNE 2012

İSTANBUL TEKNİK ÜNİVERSİTESİ ★ FEN BİLİMLERİ ENSTİTÜSÜ

YAPAY SİNİR AĞLARI YÖNTEMİYLE SIVILAŞMA İYİLEŞTİRMESİ İÇİN KUMLARDA UYGULANACAK KISMI DOYGUNLUK TAHMİNİ

YÜKSEK LİSANS TEZİ

Çağdaş ÇAYAKAN
(501091223)

İnşaat Mühendisliği Anabilim Dalı

Deprem Mühendisliği Programı

Tez Danışmanı: Y. Doç. Dr. E. Ece BAYAT

HAZİRAN 2012

Çağdaş ÇAYAKAN, a **M.Sc.** student of ITU **Institute of Science** student ID 501091223, successfully defended the **thesis** entitled "**ESTIMATION OF PARTIAL SATURATION TO BE INDUCED IN LIQUEFIABLE SANDS FOR MITIGATION USING ARTIFICIAL NEURAL NETWORK APPROACH**", which she prepared after fulfilling the requirements specified in the associated legislations, before the jury whose signatures are below.

Thesis Advisor : **Assist. Prof. Dr. E. Ece BAYAT** ....
İstanbul Technical University

Jury Members : **Prof. Dr. Derin N. URAL** ....
İstanbul Technical University

Assist. Prof. Dr. Nurhan ECEMİŞ ....
İzmir Institute of Technology

Date of Submission : 04 May 2012
Date of Defense : 08 June 2012

Afacan'a,

FOREWORD

I would like to express my special thanks to my advisor, Assist. Prof. Dr. E. Ece Bayat, for her guidance and encouragement throughout this work.

I also want to thank my dearest friends for their support and patience.

Finally, I would express my deepest gratitude to my mother, Ayla Çayakan and my father, Mehmet Çayakan for their endless support and belief during this study. I would not be able to achieve any of my goals without their encouragement.

June 2012 Çağdaş ÇAYAKAN

(Civil Engineer)

TABLE OF CONTENTS

Page

ABBREVIATIONS

IPS	**:** Induced Partial Saturation
RuPSS	**:** Model for predicting Excess Pore Water Pressure in Partially Saturated Sand
$\mathbf{r_u}$	**:** Excess pore water pressure ratio
S	**:** Degree of Saturation
$\mathbf{D_r}$	**:** Relative Density
$\boldsymbol{\gamma}$	**:** Shear Strain Amplitude
$\boldsymbol{\sigma_v'}$	**:** Initial Effective Stress
M	**:** Earthquake Magnitude
ANNs	**:** Artificial Neural Networks
SPT	**:** Standard Penetration Test
CPT	**:** Cone Penetration Test

LIST OF TABLES

LIST OF FIGURES

Page

ESTIMATION OF PARTIAL SATURATION TO BE INDUCED IN LIQUEFIABLE SANDS FOR MITIGATION USING ARTIFICIAL NEURAL NETWORK APPROACH

SUMMARY

Liquefaction of sands is one of the most devastating effects of earthquakes to our environment, resulting in bearing capacity failures, lateral spreading, differential settlements. Liquefaction is the loss of shear strength in fully saturated loose sands due to excess pore water pressure build-up during a repeated loading or dynamic excitation, such as an earthquake. In order to reduce the liquefaction related failures to our built environment, there are current mitigation techniques implemented in practice. However, there is an urgent need for more practical and cost effective mitigation techniques. Induced-Partial Saturation (IPS) which has been recently proposed by Yegian et al. in 2007 aims to mitigate liquefaction by generating air/gas in fully saturated liquefiable sand sites. A series of shaking table experiments were performed to investigate excess pore water generations in partially saturated sands prepared at different degrees of saturation and an empirical model RuPSS (excess pore water pressure ratio (r_u) in partially saturated sands) was developed by Eseller-Bayat in 2009, to estimate r_u in partially saturated sands either mitigated by IPS or naturally occurring in that condition. RuPSS predicts r_u within an uncertainty based on mathematical equations depending on 5 main parameters (degree of saturation, S, relative density, D_r, shear strain, γ, earthquake magnitude, M and initial effective stress, σ'_v).

The prediction of excess pore water pressures by a mathematical model was challenging and had complications in correlating effects of multiple parameters. In this thesis a new study was performed to develop ANN models for better prediction of excess pore water pressures generated in partially saturated sands during an earthquake. Another goal of using the ANNs was to perform sensitivity analysis and to determine the effect of the most dominant parameters on the generation of excess pore water pressures in partially saturated sands. The results demonstrate that degree of saturation (S) is the parameter which has the most dominant effect on r_u. Also, based on ANN models, prediction plots were developed for loose and medium dense sands for use in practice.

In the second phase of the research, the degrees of saturation that need to be induced in a liquefiable sand site in Japan, were estimated for a design value of r_u. Edushake was used to get the shear strains developed in each soil layer due to a given earthquake at that site. Using the maximum shear strains induced (γ_{max}), relative densities (D_r) estimated based on the standard penetration test results, earthquake magnitude (M), the required degrees of saturation to be induced in each layer of the soil profile were predicted for a limiting value of design r_u (excess pore water pressure ratio) by using both ANNs and the mathematical models. For the specific

site used in the study, reduction of degree of saturation by 20% was sufficient to reduce r_u down to less than 0,1 for the majority of sand layers. Only for a weak sand layer just above the outcrop, 50% reduction in degree of saturation was suggested due to very high strains (γ>0,3%) induced. The predictions by both models were close to each other confirming the functionality of ANN models for predicting r_u. Moreover, ANN models can be improved with more data when available in the future with the application of the IPS technique in the field.

YAPAY SİNİR AĞLARI YÖNTEMİYLE SIVILAŞMA İYİLEŞTİRMESİ İÇİN KUMLARDA UYGULANACAK KISMI DOYGUNLUK TAHMİNİ

ÖZET

Yapay sinir ağları, insan beyninin sinir yapısından ve çalışma mekanizmasından etkilenerek geliştirilmiştir. Günümüzde bir çok alanda uygulaması olduğu gibi, inşaat mühendisliği alanında da oldukça kullanılmaktadır. Bu çalışmada, yapay sinir ağları yaklaşımıyla Yegian et al. Tarafından 2007 yılında, deprem sırasında zeminde oluşabilecek sıvılaşma durumunu engellemek amacıyla önerilen Kısmi-Doyguna İndirgeme tekniği için sahada uygulanması gereken kısmı doygunluk tahmini yapılmıştır.

Gevşek, suya doygun bir kum zemin, deprem yüklerine maruz kalırsa, sıkışmaya çalışır ve hacmi azalır. Hacimdeki bu azalma, boşluk suyu basıncını arttırır ve artan boşluk suyu başlangıç efektif gerilme değerine ulaşırsa, efektif gerilme sıfır olur ve kum sıvı gibi davranır. Kumun sıvı gibi davranması ise literatürde sıvılaşma olarak tanımlanmaktadır. Sıvılaşma, deprem etkisiyle, taşıma gücü kayıpları, yanal yayılma ve diferansiyel oturmalarla sonuçlanabilen en yıkıcı olaylardan biridir.

Sıvılaşmanın yıkıcı etkisini yok etmek adına, günümüzde çeşitli zemin iyileştirme yöntemleri geliştirilmiştir. Zemin iyileştirmelerinde ki temel amaç, mekanik etkilerle zemin boşluk suyu oranının azaltılmasıyla ya da zemindeki boşlukların çeşitli karışımlarla doldurulmasıyla sıvılaşmaya karşı direnci arttırmaktır. Zemin iyileştirmesinde kullanılan popüler teknikler sıkılaştırma, güçlendirme, enjeksiyon/ karıştırma ve drenaj olarak sıralanabilir. Bu tekniklere ek olarak, sıvılaşma etkisini engellemek adına diğerlerinden daha pratik ve ekonomik olması avantajıyla Kısmi-Doyguna İndirgeme (IPS) yeni bir yöntem olarak geliştirilmiştir. Kimyasal bileşimi soydum perborat olan Efferdent kuru kumla karıştırılarak su ile reaksiyona girer ve H_2O_2 oluşturarak oksijen açığa çıkmasına sebep olur. Böylece kısmi doygun kumlarda, farklı doygunluk dereceleri elde edilir. Farklı doygunluk derecelerine ve farklı rölatif sıkılığa sahip olan kumlara farklı kesme birim deformasyonları da uygulanarak boşluk suyu basıncındaki azalmanın gözlenmesiyle, kısmı doygun kumlarda sıvılaşma olmadığı tespit edilmiştir.

Kısmi Doyguna İndirgeme tekniğinin başarısını ölçme ve kısmi doygun kumlarda deprem sırasında oluşacak boşluk suyu basıncı tahmini için 2009 yılında Eseller-Bayat tarafından RuPSS (kısmi doygun kumlarda boşluk suyu basıncı oranı) ampirik modeli geliştirilmiştir. RuPSS modeli boşluk suyu basınç oranını üç aşamada hesaplamayı öngörür. İlk aşamada model, deprem şiddetine bağlı olan eşdeğer tekrarlı çevrim sayısını göz önünde bulundurmadan oluşabilecek maksimum boşluk suyu basınç oranını (r_{umax}) (zeminin çevrim sayısı devam edildiği sürece erişebileceği ve orda sabit kalacağı maksimum değer) bulmayı öngörür. İkinci aşamada eşdeğer deprem çevrim sayısının (N_γ), r_{umax}'e ulaşmak için gereken çevrim sayısına (N_{max}) oranına (N_γ/N_{max}) bağlı olarak boşluk suyu basınç oranının maksimum boşluk suyu

basınç oranına bölümünü (r_u/r_{umax}) tahmin etmeyi önerir. Bir başka deyişle, deprem eşdeğer çevrim sayısının boşluk suyu basıncını maksimum değerinden ne oranda aşağıya düşürdüğünü tahmin eder. Son aşama olarak da birinci aşamada bulunan r_{umax}, ikinci aşamada bulunan azalma oranı ile (r_u/r_{umax}) çarpılarak kısmi doygun zeminde belli bir deprem sırasında oluşabilecek boşluk suyu basıncını tahmin eder. Deney verilerine bağlı olarak, r_{umax}'ın, doygunluk derecesine (S), rölatif sıklığa (D_r) ve zeminde oluşan tekrarlı kesme birim deformasyonuna (γ) ve N_{max}'ın ise S, D_r , γ ve ilk efektif gerilmeye (σ'_v) bağlı olduğu görülmüştür. Eseller-Bayat tarafından r_{umax} için bağlı olduğu parametrelere dayalı matematiksel bir denklem geliştirilmiş, ancak N_{max}'in bağlı olduğu parametrelerle ilişkisinin karmaşıklığı nedeniyle de doğrudan r_{umax}'e bağlı bir matematiksel denklem geliştirilmiştir. Bu çalışmada yapay sinir ağları tekniği kullanılarak N_{max}'ın doğrudan bağlı olduğu parametrelerle ilişkisinin belirlenmesi ve aynı zamanda her parametrenin N_{max} davranışına etkisinin duyarlılık analizi ile belirlenmesi hedeflenmiştir. İkinci bir yapay sinir ağları modeli de r_{umax} tahmini için gerçekleştirilmiş ve duyarlılık analizi ile her parametrenin r_{umax} üzerindeki etkisi belirlenmiştir.

Maksimum boşluk suyu basıncı (r_{umax}) için geliştirilen yapay sinir ağı modeli için, sarsma masasında özel bir sıvılaşma kutusunda gerçekleştirilen 96 test verisi kullanılmıştır. Bu veriler, doygunluk derecesi (S), rölatif sıkılık (D_r), kesme birim deformasyonu (γ) ve maksimum boşluk suyu basıncı oranı (r_{umax}) parametrelerinden oluşmaktadır. Davranışa en uygun yapay sinir ağı modeli "Geri yayılma sinir ağı (BPNN)" olarak belirlenmiştir. BPNN modelin, matematiksel modele kıyasla 90% güven aralığında $\pm$0,1 hata ile daha iyi tahmin yaptığı görülmüştür. Oluşturulan modelin eğitilmesinde, kullanılan her girdi parametresinin, çıkış parametresine etkisi de incelenmiş ve doygunluk derecesinin, maksimum boşluk suyu basıncı oranı üzerinde en büyük etkiye sahip olduğu gözlemlenmiştir. İkinci büyük etkinin kesme birim deformasyonu, diğerinin ise rölatif sıkılık olduğu tespit edilmiştir. Yapay sinir ağı modelinin en uygun modeli kullanılarak eğitilmesi sonucu, pratikte boşluk suyu basıncı oranı tahmininde kullanılması amaçlı, gevşek ve orta sıkı kumlarda belirli kesme birim deformasyonları için, doygunluk derecesine bağlı olarak maksimum boşluk suyu basıncı (r_{umax}) tahmin grafikleri oluşturulmuştur.

İkinci bir yapay sinir ağı modelinde 57 test verisi, maksimum boşluk suyu basıncı oranına ulaşabilmek için gerekli olan çevrim sayısı (N_{max}) tahmini için eğitilmesinde kullanılmıştır. Bu veriler, doygunluk derecesi (S), rölatif sıkılık (D_r), kesme birim deformasyonu (γ) ve N_{max} parametreleridir. Davranışa en uygun yapay sinir ağı modeli "Genel regresyonlu sinir ağı (GRNN)" olarak belirlenmiştir. GRNN modelin, matematiksel modele kıyasla 90% güven aralığında $\pm$11 hata ile daha iyi tahmin yaptığı görülmüştür. Tıpkı maksimum boşluk suyu basıncı oranında olduğu gibi doygunluk derecesinin, maksimum boşluk suyu basıncı oranı üzerinde en büyük etkiye sahip olduğu gözlemlenmiştir. İkinci büyük etkinin rölatif sıkılık, diğerinin ise kesme birim deformasyonu olduğu tespit edilmiştir. Yapay sinir ağı modelinin en uygun modeli kullanılarak eğitilmesi sonucu, pratikte boşluk suyu basıncı oranı tahmininde kullanılması amaçlı, gevşek ve orta sıkı kumlarda belirli kesme birim deformasyonları için doygunluk derecesinin maksimum boşluk suyu basıncı oranına ulaşabilmek için gerekli olan çevrim sayısı (N_{max}) tahmin grafikleri oluşturulmuştur.

Uygulanacak kısmi doygunluk tahmini için son olarak, örnek vaka çalışması yapılmıştır. Sıvılaşma potansiyeli olan ve temiz kuma sahip bir saha seçilerek öncelikli olarak, tekrarlı kayma gerilmesi kriteriyle sıvılaşma analizi yapılmıştır. Sıvılaştığı tespit edilen zemin katmanları için iyileştirme tekniği olarak Kısmi

Doyguna İndirgeme tekniği kullanıldığında optimum uygulanması gereken kısmi doygunluk derecelerinin tahmini yapılmıştır. Sahaya ait rölatif sıkılıklar, düzeltilmiş SPT vuruş sayılarıyla her bir tabaka için hesaplanmıştır. Sahaya ait ölçülen SPT darbe sayıları her bir tabaka için kayma hızına dönüştürülmüştür. Edushake programı ile, elde edilen kayma hızları ve zemine ait birim ağırlıklar da kullanılarak, 1-D yer hareketi analizi yapılmıştır. Bu analiz sonucu her bir tabaka için maksimum kesme birim deformasyonları elde edilmiştir. Elde edilen maksimum kesme birim deformasyonları, hem yapay sinir ağları modelinde hem de matematiksel modelde kullanılmak üzere tekrarlı kesme birim deformasyonuna dönüştürülmüştür. İlk olarak tamamen doygun zeminin 80% doygunluk derecesine indirgenmesi ile oluşan r_{umax} ve r_u degerleri hem YSA modelleri hem de matematiksel model ile tahmin edilip karşılaştırılmıştır. YSA modelleri ile tahmin edilen boşluk suyu basınç oranlarının matematiksel modele çok yakın olduğu görülmüştür. Buna ek olarak, doygunluk derecesinin sadece 20% azaltılması ve oldukça büyük bir yer hareketi etkimesine rağmen boşluk suyu basıncı oranlarında genelde 0,1 den az değerlere kadar düşüş tahmin edilmiştir. Sonuç olarak zeminin büyük bir kısmında 80% lik bir kısmi doygunluğa indirgemenin boşluk suyu basıncını azaltmada yeterli olduğu görülmüştür. Doygunluk derecesi 80%'e indirgenmiş olup, kesme birim deformasyonu çok yüksek (γ>0,3%) olduğu durumlarda ise boşluk suyu basınç oranının 1'e yakın yani kritik değerlere yaklaştığı görülmüştür. Vaka analizinin ikinci aşamasında herhangi bir dizayn r_u değeri için (r_u=0,5) zemin derinliği boyunca ne derecelerde kısmi doyguna indirgenme uygulanması gerektiği tahmin edilmiştir. Zemin derinliğinin büyük bir kısmında doygunluk derecesinin sadece 80%'e indirgenmesiyle elde edilen boşluk suyu basıncı oranının 0,1'den az değerlerde olması 80% kısmi doygunluk derecesinin yeterli olacağını göstermiştir. İstenirse daha yüksek kısmi doygunluk dereceleri de uygulanabilir ancak zeminin her yerinde eşit bir dağılımın sağlanması ve 80%'nin üzerinde maksimum boşluk suyu basınç oranının 1'e yakın değerlere yaklaşma ihtimalinden dolayı güvenli tarafta kalmak için 80% derecede indirgeme önerilmiştir. Zeminin kaya katmanına çok yakın kısmında zayıf bir kum tabakasının bulunması Edushake programında çok yüksek birim deformasyonlarının elde edilmesine neden olmuştur. Bu yüksek birim deformasyonları için yapılan tahminler o katmanlarda r_u'nun 0,5 den az olması için kısmi doygunluk derecesinin 50%'ye indirgenmesi önerilmiştir.

Vaka analizinde, yapay sinir ağları modellerinin kısmi doyguna indirgeme tekniği ile iyileştirilecek zeminlerde boşluk suyu basınç oranını (r_u) başarıyla tahmin ettiği ve matematiksel model ile yakın sonuçlar verdiği gözlenmiştir. Bu çalışmada geliştirilen yapay sinir ağı modelleri gelecekte saha verilerinin de eklenmesiyle geliştirilip, daha iyi tahminler vermesi gerçekleştirebilir.

1. INTRODUCTION

Liquefaction of sands is one of the most devastating effects of earthquakes to our environment, resulting in bearing capacity failures, lateral spreading, differential settlements. Liquefaction is the loss of shear strength in fully saturated loose sands due to excess pore water pressure build-up during a repeated loading or dynamic excitation, such as an earthquake. Research is ongoing on understanding the liquefaction phenomenon whereas ground improvement techniques are also being explored to reduce the liquefaction related damages. Ground improvement techniques being implemented in practice can be listed as densification, reinforcement, grouting/mixing and drainage .

In addition to these techniques Yegian and Eseller (2007) developed a new technique, Induced-Partial Saturation (IPS), that would be a cost-effective and a practical solution to prevent the occurrence of the liquefaction. The technique involves generation of gas bubbles in loose saturated sand thus inducing partial saturation (IPS) leading to not only strength gain against liquefaction, but also potentially eliminating the occurrence of liquefaction under any size earthquake.

Eseller-Bayat (2009) performed a series of cyclic simple shear strain tests on sand specimens partially saturated by IPS and investigated the effect of the fundamental parameters (S, D_r, γ, M, σ_v') on r_{umax} .Then, an empirical model (RuPSS) based on mathematical equations was developed to predict excess pore water pressures generated in specimens mitigated by IPS or naturally in partially saturated condition (Figure 1.1).

According to the results by Eseller-Bayat (2009), the behavior of partially saturated sands during the cyclic strain motions was quite complex. Therefore, the prediction of excess pore water pressures by a mathematical model was challenging and had complications in correlating effects of multiple parameters. Based on the research performed by Eseller-Bayat and the RuPSS mathematical model as reference, a new study was performed to predict excess pore water pressures generated in partially saturated sands during an earthquake more accurately, by using the Artificial Neural Networks (ANNs) programming Neuroshell 2. Another goal of using the ANNs was to perform sensitivity analysis and to determine the effect of the most dominant parameters on the generation of

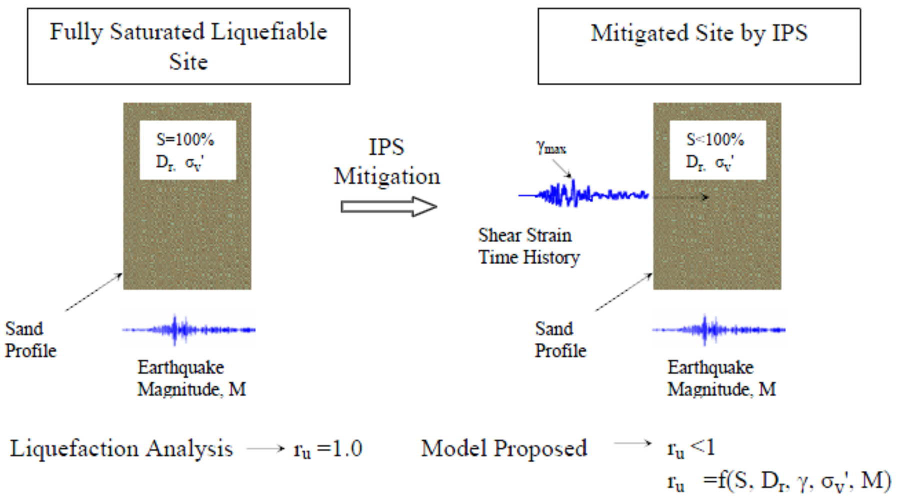

Figure 1.1 : Schematic showing the application of IPS and RuPSS model (Eseller-Bayat, 2009).

excess pore water pressures in partially saturated sands. Also, ANN model can be improved with more data when available in the future with the application of the IPS technique in the field.

In the second phase of the research, the degrees of saturation that need to be induced in a liquefiable sand site were estimated for a design value of r_u. Edushake (EduPro Civil System, 1998) was used to get the shear strains developed in each soil layer due to a given earthquake at that site. Using the maximum shear strains induced (γ_{max}), relative density (D_r) based on the standard penetration test results, earthquake magnitude (M) the required degrees of saturation to be induced in each layer of the soil profile were predicted for a limiting value of design r_u (excess pore water pressure ratio) by using both models: ANNs and RuPSS (the mathematical model).

2. LIQUEFACTION AND CURRENT MITIGATION TECHNIQUES

2.1 Soil Liquefaction

The term liquefaction, originally coined by Mogami and Kubo (1953), has historically been used in conjunction with a variety of phenomena that involve soil deformations caused by monotonic, transient, or repeated disturbance of saturated cohesionless soils under undrained conditions (Kramer, 1996). In addition to this explanation, in 1975 Seed *et al.* stated that "Liquefaction denotes a condition where a soil will undergo continued deformation at a constant low residual stress or with no residual resistance, due to the build-up and maintenance of high pore water pressures which reduce the effective confining pressure to a very low value; pore pressure build-up may be due either to static or cyclic stress applications".

Besides, it has been used to describe a number of related but different phenomena observed in loose, saturated soils. When the state of sand packing is loose enough and the magnitude of cyclic shear stress is great enough, the pore water pressure builds up to a full extent in which it becomes equal to the initially existing confining stress. At this state no effective stress or inter granular stress is acting on the sand and individual particles released from any confinement exist as if they were floating in water. Such a state is called liquefaction (Rauch, 1997).

2.1.1 Conditions for liquefaction

There are three factors that need to combine for liquefaction ground failure to occur. The first is that the soil must consist primarily loose sand. The second element needed is fully saturated sand. Either heavy rain or a high water table can provide this. The third element is a severe shaking of the ground due to an earthquake. When all three of these factors combine ground liquefaction failure can occur.

The sediment layer and water content do not need to be close to the surface. Liquefaction failure can occur well below the ground in layers. When the underground layer fails the above layers can also fail (http://geomaps.wr.usgs.gov/sfgeo/liquefaction).

2.1.2 Flow liquefaction and cyclic mobility

Flow liquefaction is a phenomenon in which the static equilibrium is destroyed by static or dynamic loads in a soil deposit with low residual strength. Residual strength is the strength of a liquefied soil. Static loading, for example, can be applied by new buildings on a slope that exert additional forces on the soil beneath the foundations. Earthquakes, blasting, and pile driving are all example of dynamic loads that could trigger flow liquefaction. Once triggered, the strength of a soil susceptible to flow liquefaction is no longer sufficient to withstand the static stresses that were acting on the soil before the disturbance.

The flow liquefaction process can be described in two stages. First, the excess pore pressure that develops at low strains moves the effective stress path to the flow liquefaction surface (FLS), at which point the soil becomes unstable. When the soil reaches this point of instability under undrained conditions, its shear strength drops to the residual strength (Vaid and Chern, 1983).

In Figure 2.1(a), plots of stress paths for five undrained shear tests are shown. Three test specimens (C, D, and E) were subjected to loads greater than their residual strengths, and experienced flow liquefaction. Since flow liquefaction cannot take place if the static shear stress is lower than the steady state strength, the flow liquefaction surface is truncated by a horizontal line through the steady state point, as it is seen in Figure 2.1(b). Flow liquefaction will be initiated if the stress path crosses the flow liquefaction surface during undrained shear regardless of whether the loading is cyclic or monotonic loading (Kramer, 1996).

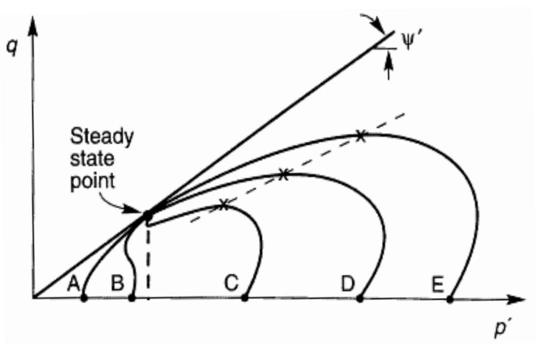

(a)

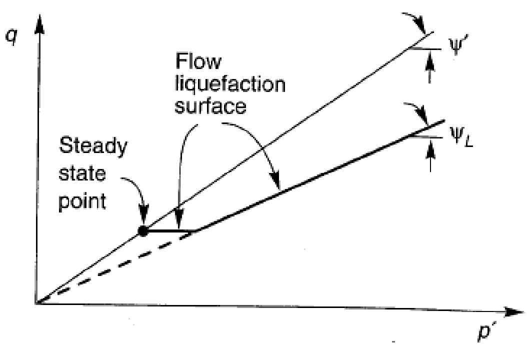

(b)

Figure 2.1 : Graphical explanation of flow liquefaction surface (Kramer, 1996).

Failures caused by flow liquefaction are often characterized by large and rapid movements which can produce the type of disastrous effects experienced by the Kawagishi-cho apartment buildings, which suffered a remarkable bearing capacity failure during the *Niigata Earthquake 1964.* The Turnagain Heights landslide, *Alaska Earthquake* to be triggered by liquefaction of sand lenses in the 130-acre slide area provides another example of flow liquefaction. Sheffield Dam suffered a flow failure triggered by the Santa Barbara Earthquake in 1925. A 300 ft section (of the 720 feet long dam) moved as much as 100 ft downstream. The dam consisted mainly of silty sands excavated from the reservoir and compacted by routing construction equipment over the fill (Seed, 1968).

Cyclic mobility is a liquefaction phenomenon, triggered by cyclic loading, occurring in soil deposits with static shear stresses lower than the soil strength. Deformations due to cyclic mobility develop incrementally because of static and dynamic stresses that exist during an earthquake. Lateral spreading, a common result of cyclic mobility, can occur on gently sloping and on flat ground close to rivers and lakes. The 1976 Guatemala earthquake caused lateral spreading along the Motagua River (Ishihara, 1985).

A special case of cyclic mobility is level-ground liquefaction. Because static horizontal shear stresses that could drive lateral deformations do not exist, level-ground liquefaction can produce large movement known as ground oscillation during earthquake shaking. Level-ground liquefaction failures are caused by the upward flow of water that occurs when seismically induced excess pore pressures dissipate (Kramer, 1996).

2.2 Ground Failure Resulting from Soil Liquefaction

Once the likelihood of soil liquefaction has been identified, an engineering evaluation must focus on the mode and magnitude of ground failures that might result. The National Research Council of the USA (1985) lists eight types of failure commonly associated with soil liquefaction in earthquakes:

• *Sand boils,* which usually result in subsidence and relatively minor damage.

• *Flow failures of slopes* involving very large down-slope movements of a soil mass.

• *Lateral spreads* resulting from the lateral displacements of gently sloping ground.

• *Ground oscillation* where liquefaction of a soil deposit beneath a level site leads to back and forth movements of intact blocks of surface soil.
• *Loss of bearing capacity* causing foundation failures.
• *Buoyant rise of buried structures* such as tanks.
• *Ground settlement*, often associated with some other failure mechanism.
• *Failure of retaining walls* due to increased lateral loads from liquefied backfill soil or loss of support from liquefied foundation soils.

2.3 Evaluation of Soil Liquefaction Potential

In order to evaluate soil liquefaction potential, a number of approaches developed. Most common of these approaches are detailed below: cyclic stress approach, cyclic strain approach, energy dissipation approach, effective stress-based response analysis approach and probabilistic approach.

2.3.1 Cyclic stress approach

Conversion of irregular earthquake cyclic strains into uniform strain cycles is similar to that used in the cyclic stress approach. It is conceptually quite simple: the earthquake-induced loading, expressed of cyclic shear stresses, is compared with the liquefaction resistance of soil, also expressed in terms of cyclic shear stresses. At locations where the loading exceeds the resistance, liquefaction is expected to occur.
The liquefaction potential analysis is generally based on 2 methods: 1. Using field case histories for previous earthquakes and 2. An evaluation of the cyclic stress or strain conditions to be developed in the field by design earthquake where evidence of liquefaction was or was not observed (Seed et al., 1983). The liquefaction analysis after earthquakes with using field history for soils is based on empirical correlations, in situ soil tests such as Standard Penetration Tests (SPT) or Cone Penetration Tests (CPT) and Shear wave Velocity Tests (V_s).
During the determination of liquefaction potential, using standard penetration test (SPT) is the most common preference. Simplified method of evaluating liquefaction potential were developed and termed as Simplified Procedure by Seed & Idriss (1971). The simplified procedure is the most preferred analysis to evaluate liquefaction potential of a site. Simplified procedure can be only applied for soils susceptible to liquefaction and under the ground water table. Cyclic stress ratio (CSR) caused by earthquake and cyclic resistance ratio (CRR) which represents the

liquefaction resistance of the in situ soil are usually determined to obtain factor of safety by multiplying CSR to CRR. Along the result that is smaller than 1, the constitution is, liquefaction occurs in soil.

2.3.2 Cyclic strain approach

In an effort to develop a more robust approach to the liquefaction problem, Dobry and Ladd (1980) and Dobry et al. (1982) described an approach that used cyclic strains rather than cyclic stresses to characterize earthquake-induced loading and liquefaction resistance. The approach is based on experimental evidence that shows densification of dry sands to be controlled by cyclic strains rather than cyclic stresses and the existence of the threshold volumetric shear strain below which densification does not occur.

2.3.3 Energy dissipation approach

According to dissipated energy is related to both cyclic stresses and cyclic strains, it is related to earthquake ground motions. Nemat-Nasser and Shokooh (1979) developed a simple, unified theory that related densification under drained conditions and pore pressure generation under undrained conditions to dissipated energy.

2.3.4 Effective stress-based response analysis approach

By setting the incremental volumetric strain to zero to represent undrained conditions, changes in effective stresses can be computed. Such models can be incorporated into nonlinear ground response and dynamic response analyses.

2.3.5 Probabilistic approach

Probabilistic approaches were developed to deal with the loading and resistance aspects of liquefaction problems. 2 ways are being used to describe the uncertainties in liquefaction resistance. One group of methods based on probabilistic characterization of the parameters shown by laboratory tests to influence pore pressure generation to compute the probability of liquefaction due to particular set of loading conditions. The other group of methods are based on in situ test based characterization of liquefaction resistance (Kramer, 1996).

2.4 Soil Liquefaction Mitigation Techniques

Many ground improvement techniques are available to mitigate soil liquefaction. On the basis of the mechanism by which they improve the engineering properties of the soil, the most common of these can be divided into four major categories: densification techniques, reinforcement techniques, grouting/mixing techniques, and drainage techniques.

2.4.1 Densification techniques

Densification is one of the most effective and commonly used means of improving soil characteristics for mitigation of seismic hazards. At the same time, it should be recognized that the increased stiffness of densified soil deposit will cause it to respond differently to earthquake motion; displacement amplitudes are likely to decrease, but accelerations may be somewhat greater than they would have been had the soil not been improved. The most common approaches to densification include vibro techniques, dynamic compaction, blasting, and compaction grouting. Of these techniques, the first three make use of the tendency of granular soils to densify when subjected to vibrations. As such, their effectiveness is greatest for cohesionless soils such as clean sands and gravels.

2.4.1.1 Vibro techniques

Vibro techniques use probes that are vibrated through a soil deposit in a grid pattern to densify the soil over the entire thickness of the deposit. Vibro techniques can be divided into those based. On horizontal vibration (*vibroflotation*) and those based on vertical vibration (*vibro rod systems*).

2.4.1.2 Dynamic compaction

Dynamic compaction is performed by repeatedly dropping a heavy weight in a grid pattern on the ground surface. It is a method that is used to increase the density of soil deposits. Dynamic compaction is generally effective to depths of 30 to 40 ft (9 to 12 m) although extremely high impact energies may produce densification at greater depths. Because the process is rather intrusive - it can produce considerable noise, dust, flying debris, and vibration - it is rarely used near occupied or vibration-sensitive structures. (Kramer, 1996)

2.4.1.3 Blasting

It is a method of densification that uses explosive charges to destroy the existing soil structure and rearrange particles in a more compact state. The use of blasting was used to densify soils to depths of 40 m (130 ft) as documented by Solymar (1983).

2.4.1.4 Compaction grouting

A grout rod is drilled to the maximum depth of improvement, then a low slump grout is injected under pressure, and a grout bulb forces the particles together to densify the sand. The grout rod is incrementally moved up and the process is repeated until the entire target layer has been treated. Compaction grouting is difficult at depths less than 6 m (20 ft), due to a lack of confining pressure.

2.4.1.5 Areal extent of densification

An important consideration in the densification of oils for construction of individual structures and foundations is the areal extent of soil improvement required for satisfactory performance during earthquakes. The areal extent should be evaluated on a case-by-case basis since site-specific soil conditions, performance requirements, and failure consequences must be addressed (Kramer, 1996).

2.4.2 Reinforcement techniques

In some cases it is possible to improve the strength and stiffness of an existing soil deposit by installing discrete inclusions that reinforce the soil. These inclusions may consist of structural materials, such as steel, concrete, or timber and geomaterials suck as densified gravel (Kramer, 1996).

2.4.2.1 Stone columns

The gravel densifies the soil adjacent to the stone column and provides a path to relieve the potential buildup of excess pore water pressures. This technique is especially effective in clean sands, but can be used in soils with high fines content if drainage is provided (Mitchell et al., 1998)**.**

2.4.2.2 Compaction piles

This soil improvement technique uses clean sand as a backfill material or, the site may be lowered an amount equal to the densification of the in-situ soil. Sand Compaction Piles can be completed with or without water jets (i.e. wet or dry method). The use of water jets aid penetration and reduce inter-granular forces, thereby encouraging compaction (Dobson and Slocombe, 1982). Wet or dry, this type of treatment is best suited for clean granular soils

2.4.2.3 Drilled inclusions

Structural reinforcing elements can also be installed in the ground by drilling or augering. Drilled shafts, sometimes with very large diameters, have been used to stabilize many slopes. Such shafts may be installed closely enough to tangent or secant pile walls. Soil nails, tiebacks, micropiles, and root piles have also been used (Kramer, 1996).

2.4.3 Grouting and mixing techniques

The engineering characteristics o many soil deposits can be improved by injecting or mixing cementations materials into the soil. These materials both strengthen the contacts between soil grains and fill the void space between the grains. Grouting techniques involve the injection of such materials into the voids of the soil remains intact. Mixing techniques introduce cementitious materials by physically mixing them with the soil, completely disturbing the particle structure of the soil (Kramer, 1996).

2.4.3.1 Grouting

A grout rod is drilled to the maximum depth of improvement, then a low slump grout is injected under pressure, and a grout bulb forces the particles together to densify the sand. The grout rod is incrementally moved up and the process is repeated until the entire target layer has been treated.

2.4.3.2 Mixing

Soil mixing consists of an auger, or row overlapping augers, being rotated to the target depth, followed by cement being pumped near the tip of the augers while the augers are being rotated and lifted. This causes the cement and the soil to mix, producing a soil-crete column (Idriss and Boulanger 2008).

2.4.4 Drainage techniques

Unacceptable movements of slopes, embankments, retaining structures, and foundations can frequently be eliminated by lowering the groundwater table prior to earthquake shaking. The buildup of excess pore water pressure during earthquake shaking can be suppressed using drainage techniques, although drainage alone is rarely relied upon for the mitigation of liquefaction hazards. The installation of stone columns, for example, introduces columns of freely draining gravel into a liquefiable soil deposit (Kramer, 1996).

2.5 Experimental Study of Induced Partial Saturation (IPS) Technique

Induced-Partial Saturation (Yegian et al., 2007) is an alternative potential method to most liquefaction mitigation techniques which is developed to be a solution to liquefaction hazards. IPS has more advantages over other techniques in being practical and less expensive. IPS aims to prevent liquefaction by generating gas/air in the pores of fully saturated sands by improving earthquake resistance of loose sands.

In laboratory studies 3 different methods were applied to entrap air/gas in sands: 1) electrolysis, 2) drainage-recharge 3) chemical Efferdent powder. In electrolysis, hydrogen and oxygen gases were generated in the saturated sand specimen. The degree of saturation can be changed by controlling the current intensity. In drainage-recharge, the pore water was drained from the bottom of the fully saturated sand specimen and the drained water was introduced to the specimen again. Remarkable amount of water remained above the specimen indicating entrapment of air during recharge, however at a constant degree of saturation. Finally, as a 3rd technique a special chemical compound (Sodium Perborate) which is a main ingredient of the dental product Efferdent was mixed with dry sand and rained into water. When sodium perborate get into reaction with water it generates hydrogen peroxide (H_2O_2) which is a perfect oxygen gas source by adjusting the ratio of the amount of powder to the mass of sand partially saturated sand specimens were obtained at different degrees of saturation.

Cyclic simple shear strain tests were performed by Eseller-Bayat (2009) in partially saturated sand specimens prepared to investigate the reduction in excess pore water pressures. Then, based on the results of these tests an empirical model (RuPSS) was developed by Eseller-Bayat (2009) to predict excess pore water pressures in sands partially saturated through IPS. Figure 2.2 demonstrates the concept of RuPSS model (Eseller-Bayat, 2009).

2.5.1 Results of cyclic simple shear strain tests

A series of cyclic simple shear strain tests with different strain of amplitudes were performed on partially saturated sand specimens prepared at different degrees of saturation, relative densities and excess pore water pressures generated in specimens were measured. The test results were evaluated in order to identify fundamental effects of each parameter (S, Dr, γ) on the excess pore water pressure ratio in partially saturated sands.

Test results demonstrated that partially saturated sands never liquefied i.e r_u never reached 1. The excess pore water pressure (r_u) reaches a maximum value (r_{umax}) and remains steady regardless of the number of cycles applied. Number of cycles required to reach r_{umax} (N_{max}) is always more than number of cycles required to reach liquefaction (N_L) in fully saturated sands.

Based on these observations, an empirical model was developed to predict excess pore water pressures (r_u) in partially saturated sands.

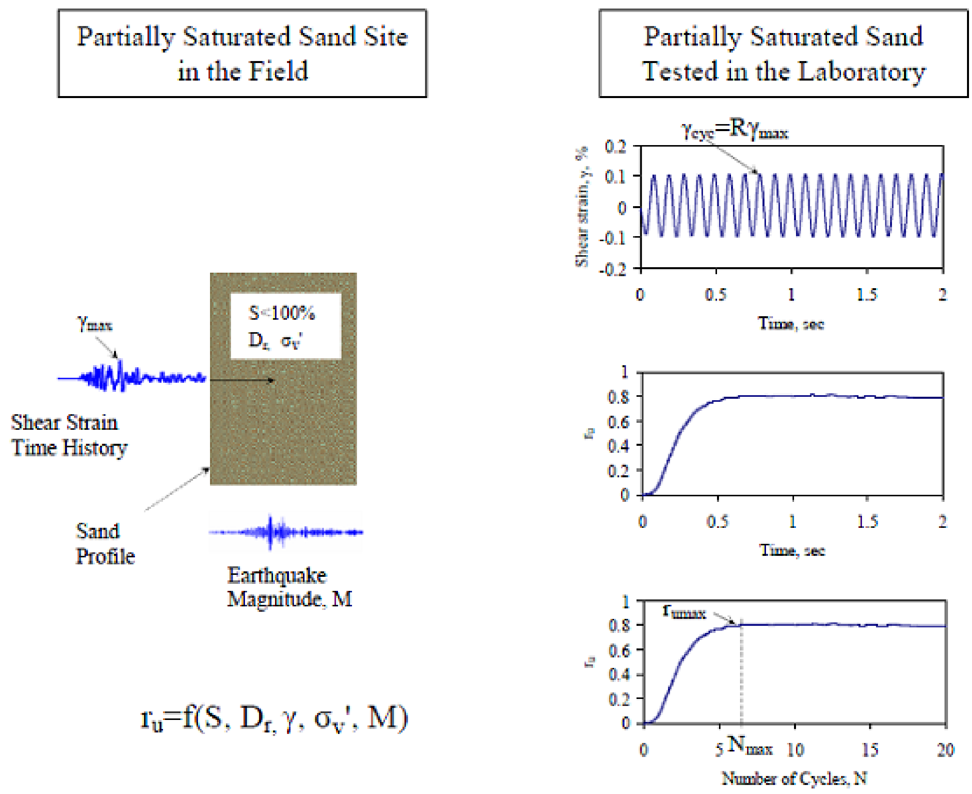

Figure 2.2 : Schematic demonstrating field and laboratory conditions for the RuPSS model.

2.5.2 Empirical model RuPSS for predicting excess pore water pressure ratios in partially saturated sands during earthquakes

An empirical model was developed to predict excess pore water pressure ratios (r_u) in partially saturated sands. When a site is mitigated by IPS, excess pore water pressure ratios (r_u) can be estimated with the proposed model for design level partial degree of saturation (S) or the required partial saturation can be determined for a limiting value of an r_u.

The results demonstrate that IPS provides benefit on liquefaction prevention not only by reducing the maximum excess pore water pressure ratio (r_{umax}) but also by increasing the number of cycles required to reach r_{umax} (N_{max}).

As shown in Figure 1.1, the soil and earthquake parameters that are needed to make prediction of the excess pore water ratio that a site will experience are shown in the argument of the function r_u=f(S, D_r, γ, σ'_v, M).

The model was developed in two stages. In the first stage, a function was developed to estimate the maximum excess pore water pressure ratio (r_{umax}) at a given strain amplitude regardless of the earthquake magnitude, or number of cycles of strain application. In the second stage, the effect of earthquake magnitude or number of cycles of strain application was introduced to estimate the r_u corresponding to the earthquake magnitude (M). RuPSS model can predict r_u in 3 steps as introduced below (Eseller-Bayat,2009);

1) $r_{u\max} = f_1(S, D_r, \gamma)$

2) $\dfrac{r_u}{r_{u\max}} = f_2\left(\dfrac{N_\gamma}{N_{\max}}\right)$

3) $r_u = f_1 \times f_2$

1) Estimation of r_{umax}

A mathematical equation was fitted to the maximum excess pore water pressures measured in partially saturated sands with parameters S and D_r and tested under a specific strain amplitude (γ) (Eseller-Bayat, 2009). The equation has a base function *f* and scaling factor functions F_D and F_γ.

$$r_{u\max} = f_1(S, D_r, \gamma) \quad \textbf{(2.1)}$$

$$r_{u\max} = f(S, D_r = 20\%, \gamma = 0.1\%) \times F_D(S, D_r) \times F_\gamma(S, \gamma) \quad \textbf{(2.2)}$$

f is the base function of S at $D_r = 20\%$ and γ=0.1%
F_D is scaling factor function for D_r's other than D_r = 20%
F_γ is scaling factor function for γ's other than γ=0.1%

$$f = S^{0.5} \times e^{-\left[\frac{1-S}{0.54}\right]^4} \quad \textbf{(2.3)}$$

$$F_D = 1 - 8.75 \times (D_r - 0.2) \times (1 - S) \times e^{\left[-\frac{(1-S)^2}{2 \times (1 - 0.84 \times (0.2/D_r)^{0.25})^2}\right]} \quad \textbf{(2.4)}$$

$$F_\gamma = 1 - 1.75 \times (-\log \frac{\gamma}{0.001}) \times (1 - S) \times e^{\left[-3.1(1-S)^2\right]} \quad \textbf{(2.5)}$$

The mathematical model for r_{umax} predicts the maximum excess pore water pressure loose to medium dense sands within an acceptable error range. r_{umax} can be predicted with an error of ± 0,08 with 68% confidence interval. Figure 2.3 shows the goodness of fit of the data for γ=0,1%.

In order to use the r_{umax} mathematical equation in practice, relative densities can be estimated using the field test data (SPT, CPT etc.) and cyclic simple shear strain (γ) can be estimated as an equivalent cyclic shear strain using the maximum value (γ_{max}) of shear strain record obtained in the soil due to a characteristic earthquake, as shown in equation 2.6.

$$\gamma = \gamma_{\max} \times R \quad \textbf{(2.6)}$$

$$R = \frac{M - 1}{10}$$

R: Strain Ratio

M: Earthquake Magnitude

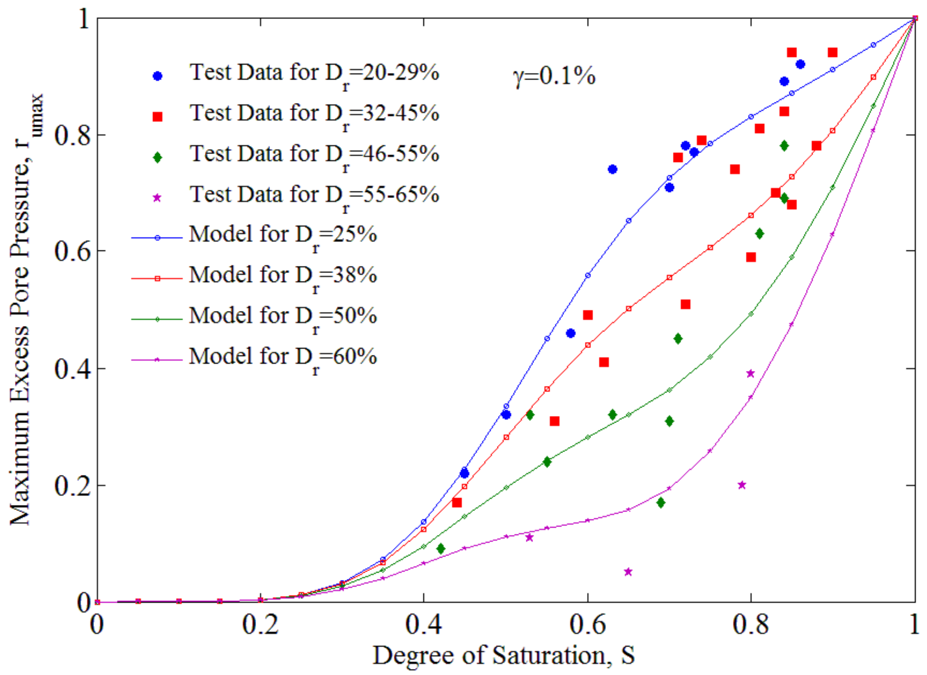

Figure 2.3 : Comparison of experimental data with the predicted r_{umax} model for γ=0,1% (Eseller-Bayat, 2009).

2) Estimation of r_u/r_{umax}

Excess pore water pressures generated in partially saturated sands can be reduced depending on the earthquake magnitude (which represents the strain amplitude and the number of cycles applied in laboratory tests). The rate of reduction was formulated based on the experimental results and correlated to the ratio of N_γ/N_{max} where N_γ is numbers of equivalent cyclic shear strains and N_{max} is number of cycles required to reach r_{umax} (Eseller-Bayat, 2009).

$$\frac{r_u}{r_{u\max}} = f_2\left(\frac{N_\gamma}{N_{\max}}\right) = \left(\frac{\sin\left[\left(\frac{N_\gamma}{N_{\max}} - 0.5\right)\times\pi\right] + 1}{2}\right)^{0.54} \quad \text{for } N_\gamma / N_{\max} \le 1 \tag{2.7}$$

$$\frac{r_u}{r_{u\max}} = 1 \quad \text{for } N_\gamma / N_{\max} > 1 \tag{2.8}$$

Number of equivalent shear strain cycles for different magnitudes M (N_γ) was estimated using the correlation for number of equivalent cyclic shear strains for M=7.5 (for stress levels R=0.65) by Seed et al. (1975) and the correlations for conversion to other stress levels (R=R) by Astunias and Dobry (1982).

$$N_\gamma = 0.057e^{0.72M} \times 0.114 \times e^{(\frac{1}{R})^{1.8}} \qquad \textbf{(2.9)}$$

If the correlation of R to the earthquake magnitude M (R=(M-1)/10) is introduced into the equation 2.9 it becomes;

$$N_\gamma = 0.0065 \times e^{\left[(\frac{10}{M-1})^{1.8} + 0.72M\right]} \qquad \textbf{(2.10)}$$

Number of cycles required to reach r_{umax} (N_{max}) was found to be dependent on parameters S, D_r, γ and σ'_v . N_{max} was formulated as a function of r_{umax} and σ'_v. Since r_{umax} includes the effects of S, D_r, γ for simplicity purposes N_{max} was directly correlated to r_{umax}. The effect of σ'_v was introduced in a similar way as for number of cycles required to reach liquefaction (N_L) in fully saturated sands (Dobry et al. 1982, Hazirbaba et al. 2005, Chang et al. 2007).

$$N_{max} = 107 \times e^{-(3r_{u\max} + 2011\gamma)} \left(\frac{1}{kPa}\right) \times \sigma_v' \qquad \sigma_v' \text{ is in kPa.} \qquad \textbf{(2.11)}$$

3) Estimation of r_u

Excess pore water pressure ration (r_u) can be estimated using f_1 and f_2 functions

$$r_u = f(S, D_r, \gamma, M, \sigma_v') = f_1 \times f_2 \qquad \textbf{(2.12)}$$

The details of the experiments and the results are included in Eseller-Bayat's PhD dissertation (Eseller-Bayat, 2009).

3. ARTIFICIAL NEURAL NETWORKS (ANNS)

3.1 Introduction

Artificial Neural Networks were developed by imitating the human brain's mechanism and nervous system's process. Artificial Neural Networks brought out the linear or nonlinear correlation between inputs and outputs. Its prior benefit is making predictions for future studies by training the network with existing data. According to this ANNs have been used in many engineering areas to solve the problems. Recently, artificial neural network (ANN) models have been widely applied to various relevant civil engineering areas.

3.2 Basic Structure of Artificial Neural Networks

Artificial Neural Networks main components are neurons and weights. Neurons are used by ANNs to obtain outputs by utilizing functions with inputs. A neuron sums the input values and then applies a nonlinear function to the sum to arrive at the output value (Frederick, 1996). In Figure 3.1, linear regression of ANNs process is presented. Besides, number of neurons determines the networks capability to learn. Shahin et al. (2001) defined neurons as processing elements (PEs) and mentioned that layers (input layer, hidden layer and output layer) contain PEs.

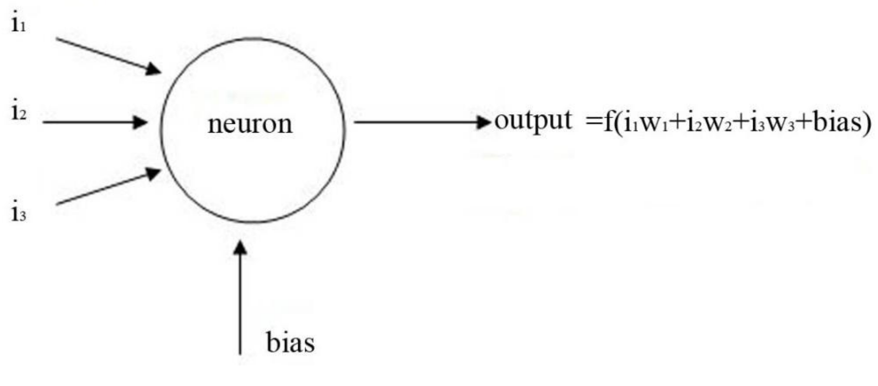

Figure 3.1 : Linear regression model of ANNs process (Cheung and Cannons,2002)

As mentioned above, the other main element is weight. The importance of the inputs imported to the network and their impact on neurons are defined as weights. In order to gain output data in ANNs, the changes in the weights are going to be implemented to the new weights. A neural network has a weight to each input and adjusts its own weights. Hagan et al. (1999) state that how the weights are determined in the algorithm has direct effect on neurons learning ability.

In order to have expected output results, there should be an algorithm applied to the network. The algorithm aims to achieve minimum error between the actual and the network output. Weights can have positive or negative values, that does not depend on the data.

3.3 Main Elements of Artificial Neural Networks

Neurons are ones of the most efficient elements in Artificial Neural Networks. Neurons imitate the biological process. When these biological processes are applied to the artificial process, it can be summarized in 3 parts: Input, Summation and Output.

3.3.1 Input

An input is a variable that a network uses to make a classification or prediction (Frederick,1996). Inputs have properties to maintain the data from outside and deliver the data content from one neuron to other. Inputs that are desired to train the network, constituted by the data from outside. As existing in the first place inputs are defined as problems. Input unit is the significant step to extrapolate the results.

3.3.2 Summation

Summation is the expression of summing the results of multiplying the weight values with each input. The schematic presentation of ANNs operation is displayed in Figure 3.2.

$$\mathrm{Ij} = \theta\mathrm{j} + \sum_{\mathrm{i}=1}^{\mathrm{n}} \mathrm{wji}\ \mathrm{xi} \qquad \textbf{(3.1)}$$

The ANN summation process could be formulized for node j by using equation 3.1. where I_j= the activation level of node j; w_{ji}= the connection weight between nodes j and i; x_i= the input from node I, I=0, 1, …, n; Θ_j= the bias or threshold for node j. (Shahin et al. 2008).

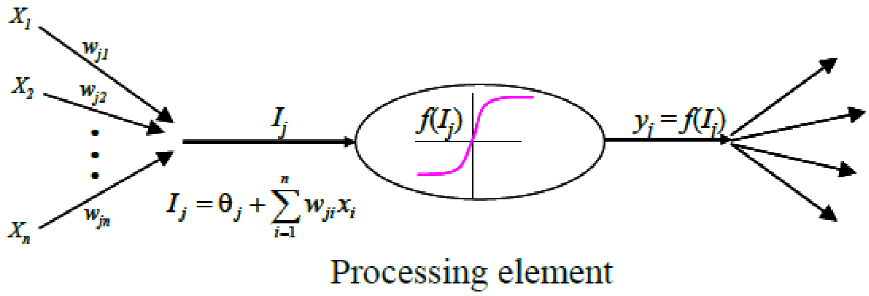

Figure 3.2 : Operation of ANNs (Shahin et al. 2008).

Summation section is not required to be used in every network, in some cases (i.e. complex problems) networks exert summation by themselves by reason of the inputs data significance.

3.3.2.1 Activation and scaling functions

In neural networks, activation functions have serious efficiency to attain anticipated output data results. A way to obtain output data is applying activation functions to the sum of weighted values. There are several types of activation functions, stated below;

Logistic (Sigmoid logistic) - It maps values into the (0, 1) range. When the outputs are categories, this function should be used. Equation 3.2 is the formula of logistic function which is depicted in Figure 3.3.

$$f(x) = \frac{1}{(1+\exp(-x))} \tag{3.2}$$

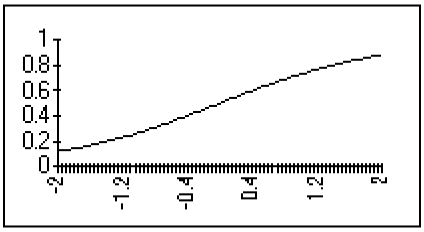

Figure 3.3 : Logistic function.

Linear - Use of this function should generally be limited to the output slab. It is useful for problems where the output is a continuous variable. Learning rates, momentums (that are generally used to stabilize weight changes), and initial weight sizes, should be stuck to smaller values while using this function. Otherwise, the network may produce larger and larger errors and weights, and hence may not ever lower the error. The linear activation function is often ineffective for the same reason if there are a large number of connections coming to the output layer because the total weight sum generated will be high. Equation 3.3 is the formula of linear function which is depicted in Figure 3.4.

$$f(x) = x \tag{3.3}$$

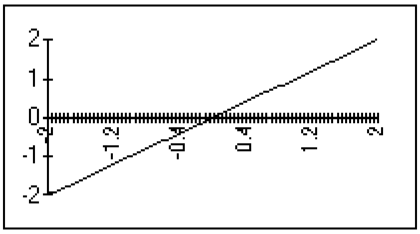

Figure 3.4 : Linear function.

Tanh (hyperbolic tangent) - It is sometimes better for continuous valued outputs, however, especially if the linear function is used on the output layer. If this is used in the first hidden layer, inputs should be scaled into [-1, 1] instead of [0,1]. Equation 3.4 is the formula of tanh function which is depicted in Figure 3.5.

$$f(x) = \tanh(x) \tag{3.4}$$

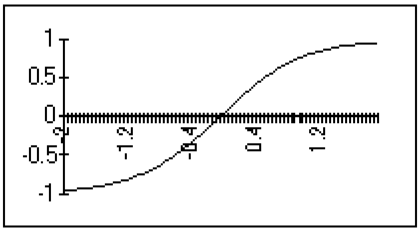

Figure 3.5 : Tanh function.

Sine -Inputs should be scaled into [-1, 1] instead of [0,1] if it's preferred to be used in the first hidden layer. If used on the output layer, scale outputs to [-1,1] also. Equation 3.5 is the formula of sinus function which is depicted in Figure 3.6.

$$f(x) = \sin(x) \tag{3.5}$$

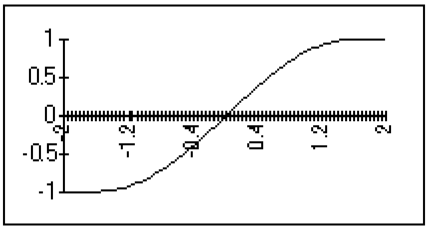

Figure 3.6 : Sine function.

Symmetric Logistic - This is like the logistic, except that it maps to (-1,1) instead of to (0,1). When the outputs are categories, try using the symmetric logistic function instead of logistic in the hidden and output layers. In some cases, the network will train to a lower error in the training and test sets. Equation 3.6 is the formula of symmetric logistic function which is depicted in Figure 3.7.

$$f(x) = \frac{2}{1+\exp(-x)} - 1 \qquad \textbf{(3.6)}$$

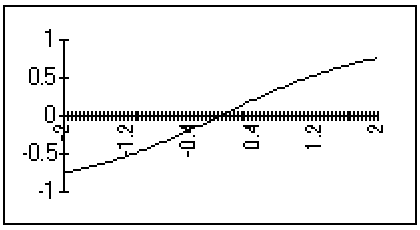

Figure 3.7 : Symmetric logistic function.

Gaussian - This function is unique, because unlike the others, it is not an increasing function. It is the classic bell shaped curve, which maps high values into low ones, and maps mid-range values into high ones. This function produces outputs in [0,1]. Equation 3.7 is the formula of gaussian function which is depicted in Figure 3.8.

$$f(x) = \exp(-x^2) \qquad \textbf{(3.7)}$$

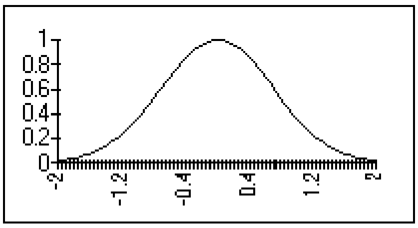

Figure 3.8 : Gaussian function (Frederick, 1996).

When variables are loaded into a neural network, they must be scaled from their numeric range into the numeric range that the neural network deals with efficiently. There are two main numeric ranges the networks commonly operate in, depending upon the type of activation functions you use: zero to one denoted as [0, 1], and minus one to one denoted as [-1, 1]. If the numbers are scaled into the same ranges, but larger numbers are allowed later (i.e., they are not clipped at the bottom or top) then we will denote the ranges <<0, 1>> and <<-1, 1>>. Thus [0, 1] and [-1, 1] denote that Neuroshell 2 will clip off numbers below and above the ranges that it encounters later in new data. In other words, if data from 0 to 100 is scaled to [0, 1], then a later data value of 120 will get scaled to 1. However, if the same data were scaled to <<0, 1>>, then 120 would be scaled to 1,2 (Frederick, 1996).

3.3.3 Output

An output is the value or values the network is trying to predict or the classification values if the network is classifying patterns. A pattern is a single record (or row) of variables that influence a network's predictions or classifications (Frederick, 1996). Outputs can be defined as data that activation function applied. If output is implemented back to one or more neurons, it is possible to call as an input.

3.4 Artificial Neural Network Architecture

The arrangement of neurons into layers and the connection patterns within and between the layers is called the net architecture (Fausett, 1993). Feed forward and Feedback Networks are the types of Neural Network architectures. Simple and generalized architecture should be chosen to solve problems.

Data transport in Feed forward network is one way only. While data is imported from outside, its route is from input to output only. Feed forward networks are separated into 2 categories;

1. Single Layer Architecture: All units are connected to one to another. This type of layer is usually used for pattern classification.

2. Multilayer Architecture: There are multiple different layers connected to each other. Complicated problems preferred to solve with this type of architecture.

Feedback Networks data transfer comes true in both directions. Outputs sometimes become inputs during the training process.

Artificial Neural Networks can have any number of layers and slabs. Nevertheless, the most common type of preferred architecture is 3 layer network. These 3 layers are; Input Layer, Hidden Layer and Output layer. Although there is only one input and one output layer in network, there could be multiple hidden layers (Frederick,1996). Each layer consists of one or more slabs. In all slabs, there are neurons which retain the process.

Input layer's slabs are described as passive, hidden and output layer's slabs described as active (Smith,1997). Input slabs do not modify the imported data but hidden slabs implement activation function and modify the data.

3.5 Training the Network

There are usually 2 ways preferred in machine learning task while training the network: 1. Supervised training and 2. Unsupervised training. Supervised training is a training type that both inputs and outputs are used. It comes with a solution as network already knows what the output should be. Unsupervised training only uses inputs and provides outputs by statistical calculation because of not introduced with output examples.

Artificial Neural Networks biggest issue is the over learning problem. When over learning occurs, an expected minimized error does not reveal. The reasons of an over learning problem are; long training time and training the network with the same examples (Panchal, 2011). In order to prevent over learning issue, good training set should be chosen. Good training set data should constitute the general, each data should represent each class and each data should be introduced once (Cheung and Cannons, 2002).

Learning is the determination of weights. The learning process performs by modifying the weights and applying them to data. It is necessary and important to assign the best values for weights, considering the end result coming from the learning process is based on the weights determined. Although there is no method to designate the weights, the processing elements (neurons) assign the best values for weights after dozens of iterations.

3.5.1 Artificial neural networks algorithms

3.5.1.1 Back propagation neural networks (BPNN)

BPNN is the most common approach in the literature. During training, this network uses both inputs and outputs. As stated in the name of back propagation, its learning process flows backwards as it is seen in Figure 3.9. Although this network is simple and gives more accurate results, BPNN is slow during the training. BPNN has 3 layer architecture: input, hidden and output layer. Every layer may have multiple slabs and every slab is connected with links that have individual learning rates, momentums and initial weights.

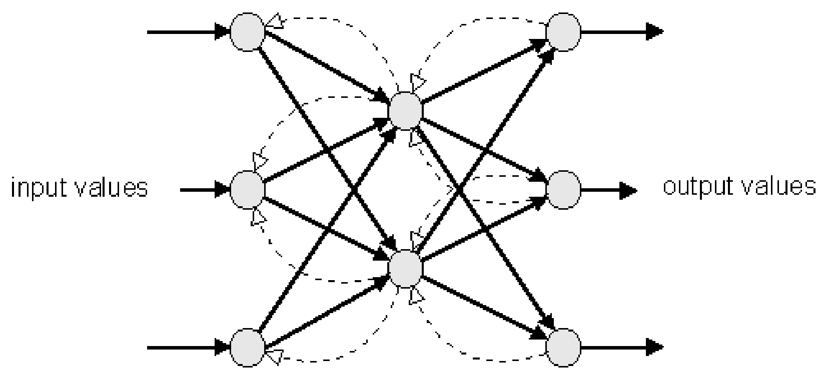

Figure 3.9 : BPNN sample structure.

The learning rate (η) is a value to produce a smaller error during learning process. Learning rate can be expressed as a significant parameter due to its effect on training. The amount of weight modification is equal to the learning rate multiplied by the error (Frederick, 1996). Typical values for the learning rate parameter (η) are within the range of $0,05 < \eta < 0,75$.

In order to accelerate the learning process, enlarging the weight changes is necessary and this could be done by increasing the learning rate. However, learning rate speeds up the learning process, too large learning rate may lead to oscillation or non-convergence.

The momentum (α) factor determines the proportion of the last weight change that is added into the new weight change. The idea about using a momentum is to stabilize the weight change. A reasonable momentum should be limited as: $0 \leq \alpha \leq 0{,}9$.

Initial weight is a value to define the first weight of the learning process. Although there is no method to define initial weight, other weights that are going to be used in network can be estimated by equations 3.9 and 3.10. While the learning process is flowing from hidden layer to output layer as it is seen in Figure 3.10, if assigning initial weight in a considerable range, inputs, learning rate (η) and output error are enough to estimate other weights in network.

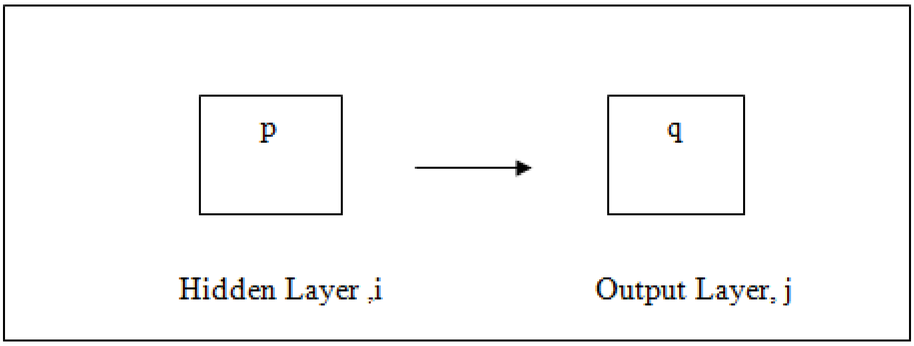

Figure 3. 10 : Representation of the process through hidden layer to output layer.

$$\delta_{qj} = out_{qj} \times (1\text{-}out_{qj}) \times (target_{qj}\text{-}out_{qj}) \quad \textbf{(3.8)}$$

$$\Delta w_{pqj} = \eta \times \delta_{qj} \times out_{pi} \quad \textbf{(3.9)}$$

$$w_{pqj}(n+1)_b = w_{pqj}(n) + \Delta w_{pqj} \quad \textbf{(3.10)}$$

where,

δ_{qj}: the actual value of error for unit q in the output layer j,

out_{qj}: the actual value of out for unit q in the output layer j,

$target_{qj}$: the network value of out for unit q in the output layer j,

η: learning rate,

out_{pi}: the value of out for unit p in the hidden layer i,

w_{pqj} (n): initial weight,

$w_{pqj}\ (n+1)_b$: value of weight at step n+1, before adjustment.

In Figure 3.11, the flow of learning process is from output layer to hidden layer. For both flow directions, weights can be estimated in a similar way. However, the weight change is stabilized by momentum (α) in the direction of hidden to output layer as an only difference. By using equations 3.12 and 3.13, weights in learning process can be estimated.

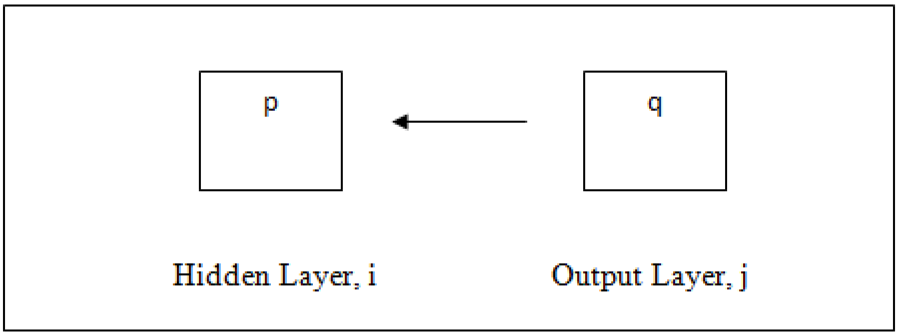

Figure 3. 11 : Representation of the process through output layer to hidden layer.

$$\delta_{pi} = out_{pi} \times (1 - out_{pi}) \times \left(\sum \delta_{qj} w_{pqj}\right) \quad \textbf{(3.11)}$$

$$\Delta w_{pqj}(n+1) = \eta \times \delta_{qj} \times out_{pi} + \alpha \left[\Delta w_{pqj}(n)\right] \quad \textbf{(3.12)}$$

$$w_{pqj}(n+1)_a = w_{pqj}(n) + \Delta w_{pqj}(n+1) \quad \textbf{(3.13)}$$

where,

δ_{pi}: the actual value of error for unit p in the hidden layer i,

out_{pi}: the actual value of out for unit p in the hidden layer i,

η: learning rate,

α: momentum,

out_{pi}: the value of out for unit p in the hidden layer i,

$w_{pqj}\ (n)$: initial weight,

$w_{pqj}\ (n+1)_a$: value of weight at step n+1, after adjustment.

3.5.1.2 General regression neural networks (GRNN)

General Regression Neural Network has one-pass learning algorithm. GRNN was developed as an alternative to BPNN. Unlike BPNN, GRNN is advantageous due to its fast training. As seen from the Figure 3.12, GRNN has 3 layers. Input layer, hidden layer (summation and pattern slabs) and output (decision) layer. In the hidden layer, there is one neuron for every training pattern (Specht, 1991).

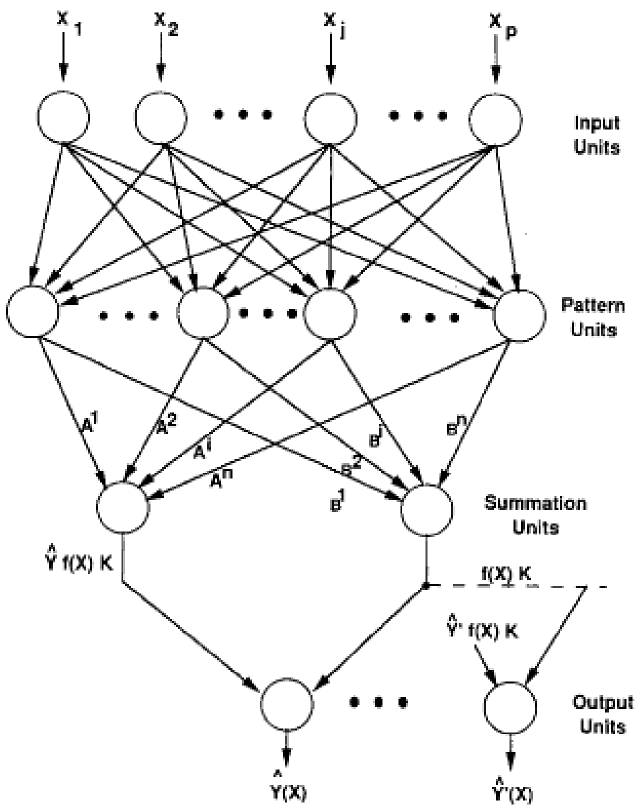

Figure 3.12 : GRNNs block diagram (Specht, 1991).

GRNNs learning mechanism is measuring the distances between two patterns. By using equation 3.14, the distance between two patterns can be measured. Networks output for GRNN, after measuring the distances for each pattern can be estimated by equation 3.15.

$$D_i^2 = (X-X_i)^T (X-X_i) \quad \textbf{(3.14)}$$

$$Y(x)= \frac{\sum_{i=1}^{n} Y_i \exp\left(-D_i^2 \,/\, 2\sigma^2\right)}{\sum_{i=1}^{n} \exp\left(-Di^2 \,/\, 2\sigma^2\right)} \quad \textbf{(3.15)}$$

where,

X: input space

X_i: input vector of the i^{th} training data set

Y_i: output related to X_i

σ: smoothing factor

D_i: the distance between two patterns

Y: network output.

The smoothing factor (σ) is the only parameter that should be adjusted in General Regression Neural Network. The links between slabs or layers, constitute smoothing factor. Although smoothing factor is effective on training and the network success is related to it, there is no intuitive method for revealing the optimum smoothing factor (Hanna et al. 2007, Juang et al. 2003). The smoothing factor is within the range of, $0 < \sigma < 1$.

3.6 Testing the Network

After the weights were determined for the best result, testing is done to examine the network's ability to learn. Testing is used to estimate the error rate after training the network. The outputs are obtained by weighting the examples that are totally new for the network. Common error is to test the neural network using the samples that were used to train the network (Cheung, Cannons, 2002). The output represents the networks training success.

The coefficient of multiple determination is a statistical indicator (R^2) obtained by equation 3.16. It compares the accuracy of the model with using test set data. By equations 3.17 and 3.18, sum of squared error and total corrected sum of squares can be estimated. If the results of R^2 are approaching to 1, the model could be defined as good model.

$$R^2 = 1 - \frac{SSE}{SSYY} \quad \textbf{(3.16)}$$

$$\text{where } SSE = \sum (y - y')^2 \quad \textbf{(3.17)}$$

$$SSYY = \sum (y - \bar{y})^2 \quad \textbf{(3.18)}$$

SSE= sum of the squared error

SSYY= total corrected sum of squares

y = the actual value

y ' = the predicted value of y

and $\bar{y}$ = the mean of the y values.

The Correlation Coefficient (r) - (Pearson's Linear Correlation Coefficient) is a statistical measure of the strength of the relationship between the actual vs. predicted outputs. The r coefficient can range from -1 to +1. The closer r is to 1, the stronger the positive linear relationship, and the closer r is to -1, the stronger the negative linear relationship. When r is near 0, there is no linear relationship.

3.7 Prediction in Network

In addition to training the network, ANNs have ability to make predictions based on training and testing processes which are detailed above. While making predictions by a defined network, the input data to be used for the output prediction which is called production set data are introduced to the network. In test set extraction section it is necessary to assign the number of production set data that are going to be used for prediction. Henceforth, all steps are same with the training and testing processes. After, training and testing the network is finished, production should be selected from option tab. In order to obtain predicted data, data should be applied to file and examine. For future studies, the benefit of ANN is the ability of improvement of the model by providing new input and output data and hence better prediction of the future behavior.

4. ANN MODEL FOR PREDICTION OF EXCESS PORE WATER PRESSURES IN SANDS PARTIALLY SATURATED THROUGH IPS

4.1 Introduction

In this chapter, application of neural networks for predicting the excess pore water pressures generated in partially saturated sands during earthquakes is investigated. In order to obtain maximum excess pore water pressure ratio and the number of cycles that are required to reach maximum excess pore water pressure ratio in partially saturated sands, various ANN models were developed in Neuroshell 2.

As stated in Chapter 2, according to the RuPSS empirical model, r_u can be estimated in 3 steps. In the first step, r_{umax} is estimated and in the second step, r_u/r_{umax} is evaluated as a function of N_γ/N_{max}. Finally, in the third step, r_u can be estimated by the multiplication of r_{umax} with the ratio of r_u/r_{umax}. In this empirical RuPSS model, r_{umax} and N_{max} parameters depend on the soil parameters S, D_r, and σ'_v and earthquake motion parameter γ. These r_{umax} and N_{max} parameters were estimated using mathematical equations developed by Eseller-Bayat (2009), to confirm the mathematical equations as well as to provide an ANN model which can also be fed with more field data when available. An ANN model was developed to estimate r_{umax} and another ANN model was developed to estimate N_{max} based on the experimental data.

4.2 ANNs in Civil Engineering

As Artificial Neural Networks (ANNs) have been used in many engineering areas, ANNs are also applied within the domain of civil engineering. The major types of tasks in civil engineering to which neural networks are currently being applied are: classification/interpretation tasks, diagnosis, modeling and control. Classification and interpretation problems are common applications for ANNs.

Artificial Neural Networks are also being applied to solve inverse mapping problems, where the network is trained on a set of cause-effect data and trained to diagnose observed effects in terms of unknown causes. In an application of an ANN for the identification and control of civil engineering problems, an ANN based model was developed from observed structural response to applied loadings. This model was then used to learn the appropriate control forces for observed dynamic behavior of a specific structure. Another area where neural networks are being applied in civil engineering is for creating models for making predictions and estimations. (Kartam et al., 1997).

As a specific area of civil engineering, in geotechnical engineering, to almost every problem, ANNs have been applied and application of ANNs has been summarized by Shahin et al. (2008) in continuing. Artificial Neural Networks have been used extensively for predicting the axial and lateral load capacities in compression and uplift of pile foundations (Abu-Kiefa 1998; Ahmad et al. 2007; Chan et al. 1995; Das and Basudhar 2006; Goh 1994a; Goh1995a; Goh 1996b; Hanna et al. 2004; Lee and Lee 1996; Nawari et al. 1999; Rahman et al. 2001;Shahin 2008; Teh et al. 1997), drilled shafts (Goh et al. 2005; Shahin and Jaksa 2008) and ground anchors (Rahman et al. 2001; Shahin and Jaksa 2004; Shahin and Jaksa 2005a; Shahin and Jaksa 2005b; Shahin and Jaksa 2006).

Based on the application of ANNs, methodologies have been developed for estimating several soil properties including the pre-consolidation pressure (Celik and Tan 2005), shear strength and stress history (Kurup and Dudani 2002; Lee et al. 2003; Penumadu et al. 1994; Yang and Rosenbaum 2002), swell pressure (Erzin 2007; Najjar et al. 1996a), compaction and permeability (Agrawal et al. 1994; Goh 1995b; Gribb and Gribb 1994; Najjar et al. 1996b; Sinha and Wang 2008), soil classification (Cal 1995) and soil density (Goh 1995b).

As known, the phenomena of liquefaction during earthquakes causes large amount of damages to most civil engineering structures. Although the liquefaction mechanism is well known, the prediction of the value of liquefaction induced displacements is very complex and not entirely understood (Baziar and Ghorbani 2005). In order to predict liquefaction many researchers (Agrawal et al. 1997; Ali and Najjar 1998; Baziar and Ghorbani 2005; Goh 2002; Goh 1994b; Goh 1996a; Goh et al. 1995; Hanna et al. 2007; Javadi et al. 2006; Juang and Chen 1999; Kim and Kim 2006; Najjar and Ali 1998; Ural and Saka 1998; Young-Su ana Byung-Tak 2006) investigated the functionality of ANNs. The problem of predicting the settlement of shallow foundations, especially on cohesion less soils, is very complex, uncertain and not yet entirely understood. This fact has encouraged some researchers (Chen et al. 2006; Shahin et al. 2002a; Shahin et al. 2003a; Shahin et al. 2004a; Shahin et al. 2005a; Shahin et al. 2005b; Shahin et al. 2002b; Shahin et al. 2003b; Shahin et al. 2003c; Shahin et al. 2003d; Sivakugan et al. 1998) to apply the ANN technique to settlement prediction. The problem of estimating the bearing capacity of shallow foundations by ANNs has also been investigated by Padminin et al. (2008) and Provenzano et al. (2004) (Shahin et al., 2008).

4.3 Estimating Maximum Excess Pore Water Pressure Ratio, r_{umax}

To predict the maximum excess pore water pressure ratio (r_{umax}), 96 data obtained from the research conducted by Eseller-Bayat (2009) were used to test various ANN models for the prediction of r_{umax}. The models that were evaluated are summarized in Table 4.1. Model 1 in Back Propagation Neural Network was developed by choosing data selection as arranging all patterns after test set thru training set, assigning scaling function as Linear [-1,1] and constituting activation function in output layer as Linear. Thus, noticeable value of coefficient of determination (R^2=0,96) was obtained by Model 1 in Back Propagation Neural Network.

Table 4.1 : Comparison of ANN models.

	BPNN				GRNN	
Parameters	Model 1	Model 2	Model 3	Model 4	Model 1	Model 2
Data Selection	All patterns after N thru M	All patterns after N thru M	N percent, M percent, randomly chosen	All patterns after N thru M	All patterns after N thru M	All patterns after N thru M
Scaling Function	Linear [0,1]	Linear [-1,1]	Linear [0,1]	Linear [0,1]	Linear [0,1]	Linear [0,1]
Activation Function (output)	Linear	Linear	Linear	Logistic	Genetic	Iterative
R^2	0,9616	0,9333	0,9566	0,9564	0,9575	0,952

While constituting Model 2 in Back Propagation Neural Network, assigning scaling function as Linear [-1,1] was the only difference with Model 1. However, Linear [-1,1] scaling function reduced the coefficient of determination (R^2=0,93) value. Model 3, in Back Propagation Neural Network was evaluated with all parameters except with data selection difference. Unlike Model 1, 25% of data were chosen randomly as test set, 75% of data were chosen randomly as training set in Model 3. Since data selection was changed, the reduction of coefficient of determination (R^2=0,95) was observed in Model 3. While evaluating Model 4 in Back Propagation Neural Network, activation function in output layer was selected as Logistic function which is different than Linear used in Model 1. Nevertheless, Logistic activation function is not acceptable when the data is continuous. Accordingly, Model 4 in Back Propagation Neural Network was ruled out. Model 1 and Model 2 in General Regression Neural Network were constituted with changes in activation function in output layer and the reduction of coefficient of determination (R^2=0,95) was the reason to eliminate these models. According to estimation of highest coefficient of determination (R^2=0,96) and consideration of over learning did not occur, Model 1 in Back Propagation Neural Network returned the best fit of the data.

Table 4.2 : Normalized input and output values for r_{umax} in Neuroshell 2.

Parameters	Degree of Saturation	Relative Density	Shear Strain	Maximum Excess Pore Water Pressure Ratio
Variable Name	S	D_r	γ (%)	r_{umax}
Variable Type	I	I	I	A
Min:	0	0	0	0
Max:	1	1	1	1
Mean	0,51	0,43	0,29	0,44
Std. Deviation	0,28	0,27	0,22	0,30

All normalized data were imported to the network. While defining S, D_r and γ as input parameters and r_{umax} as an output parameter, their normalized minimum and maximum values are computed automatically as seen in Table 4.2. Also, since all data were imported to the network without normalization as seen in Table 4.3, it was observed that network normalize all data. Since neural networks require variables to be scaled into the range 0 to 1 or -1 to 1, the network needs to know the variable's real value range (Frederick,1996).

Usually, two-thirds of the data are suggested for training, one-thirds of data are suggested for testing (HammerStrom, 1993). Therefore, 71 of 96 data were used for training and the remaining 25 data for testing. Data were arranged such that the network can be fed by ranges of data which cover all possible behaviors, and then in test set extraction section, all patterns after N thru M tab was selected. After trying miscellaneous architectures, Multiple Hidden Slabs with Different Activation Functions architecture was preferred as suitable as shown in Figure A.1. Since the type of data for prediction of r_{umax} is continuous Linear [0,1] was assigned as a scaling function in input slab.

Table 4.3 : Input and output values for r_{umax} in Neuroshell 2.

Parameters	Degree of Saturation	Relative Density	Shear Strain	Maximum Excess Pore Water Pressure Ratio
Variable Name	S	D_r	γ (%)	r_{umax}
Variable Type	I	I	I	A
Min:	0,41	0,2	0,01	0,01
Max:	0,9	0,67	0,31	0,94
Mean	0,65	0,41	0,09	0,41
Std. Deviation	0,13	0,13	0,07	0,27

Each link between slabs have their own learning rate, momentum and initial weights. Learning rate was assigned as 0,05 since data is complicated or noisy, momentum was assigned as 0,1 and initial weight was assigned as 0,3 in the links between input and hidden layer. In order to have more accurate results, hidden to output layer links' learning rate was assigned as 0,04 in consideration of producing a smaller error, momentum was kept as same as the links between input and hidden layer because of no difference was observed in estimation of the coefficient of determination (R^2) and initial weight was assigned as 0,3.

Since all data types are continuous, the output should be a continuous variable, and consequently the activation function generated in the output slab is linear. Slabs in the hidden layer could have different activation functions. Hidden slabs activation functions were determined as Gaussian, tanh and Gaussian complete, due to their good relations with the output.

After constituting the model architecture, Back propagation Neural Networks' training and stop training criteria was adjusted as indicated in Figure A.2. For marking pattern selection, both rotation and random choice were tried. According to the best gained result the rotation pattern selection was preferred. For weight updates section, vanilla was used to achieve accurate results in estimation of coefficient of determination (R^2) and to speed up the learning process. Vanilla means that a learning rate is applied to the weight updates but a momentum term is not (Frederick,1996). Thus, using an appropriate learning rate has important role in generating a model.

Calibration computes the squared error for each output in a pattern, totals them and then computes the mean of that number over all patterns in the test set. Calibration finds the optimum network for the data in the test set and saves the network at this optimal point (Frederick,1996). Hence, calibration interval was assigned as 285 within the usual range of 50 and 500 by trial and error. As a consequence of using calibration, network saved on the best set. The stop training criteria was adjusted as, the number of events since the minimum error for the test set reaches 30,000 to train network until greater than 20,000 and 40,000 events. As missing values were not expected, error conditions were therefore considered.

After all the criteria were set, training the data was processed. Figure 4.1 depicts the relation between training set average error and epochs elapsed, and indicates the error's reduction by elapsed epochs while training. Figure 4.2 depicts the relation between test set average error and intervals elapsed while testing the data. The results indicate that peak error was being reduced as intervals elapsed, confirming over learning was eliminated.

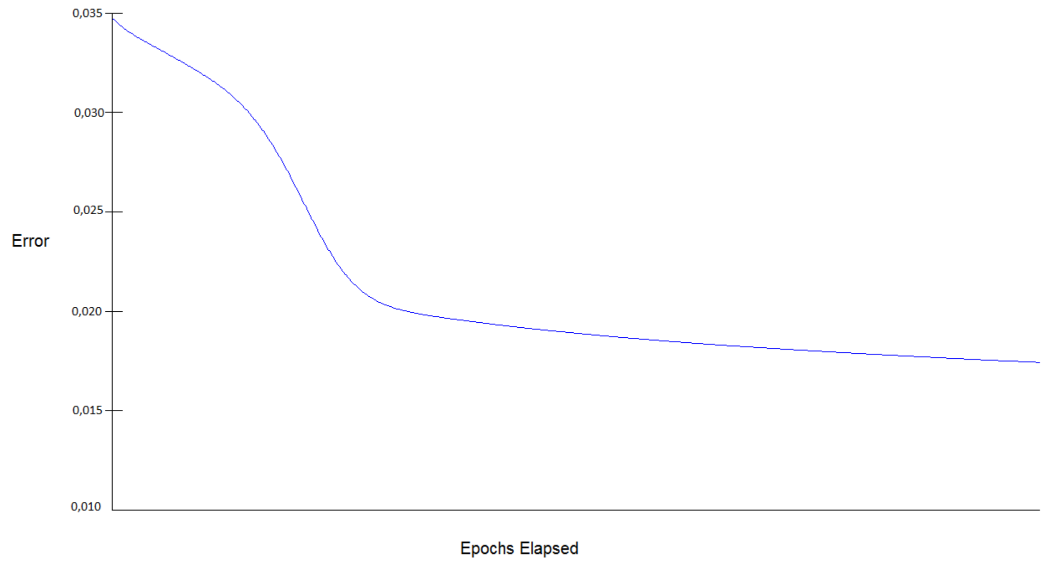

Figure 4.1 : Training set average error graph.

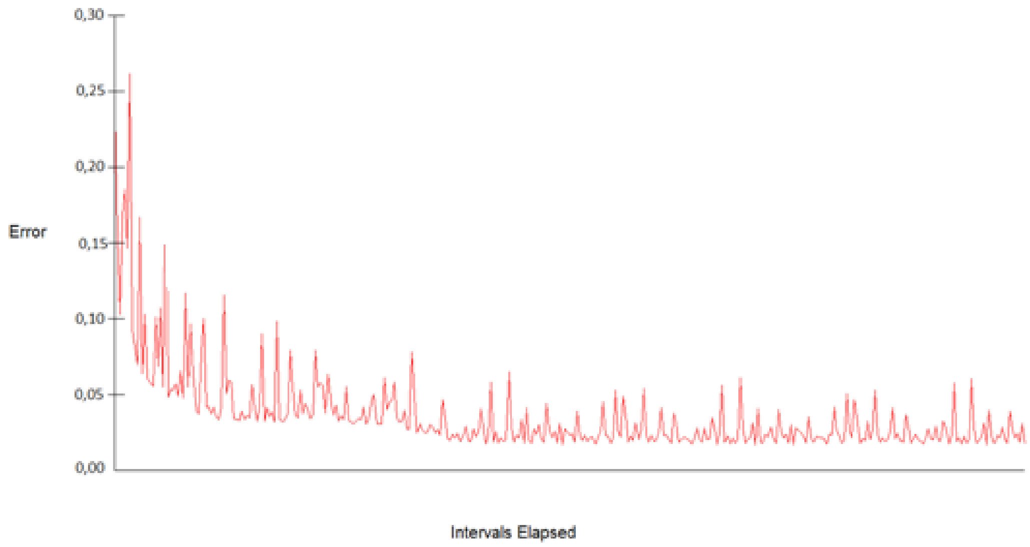

Figure 4.2 : Testing set average error graph.

Relative contribution factor produces a number for each input variable called a contribution factor that is a rough measure of the importance of that variable in predicting the network's output, relative to the other input variables in the same network (Frederick,1996). Relative contribution factors were obtained from the network as followings; 0,49652 (49%) degree of saturation S, 0,22804 (23%) relative density D_r and 0,27543 (28%) shear strain γ. As it is seen from Figure 4.3, degree of saturation (S) is the most effective parameter, shear strain (γ) is the second effective parameter and relative density (D_r) is the least effective parameter in predicting maximum excess pore water pressure ratio (r_{umax}).

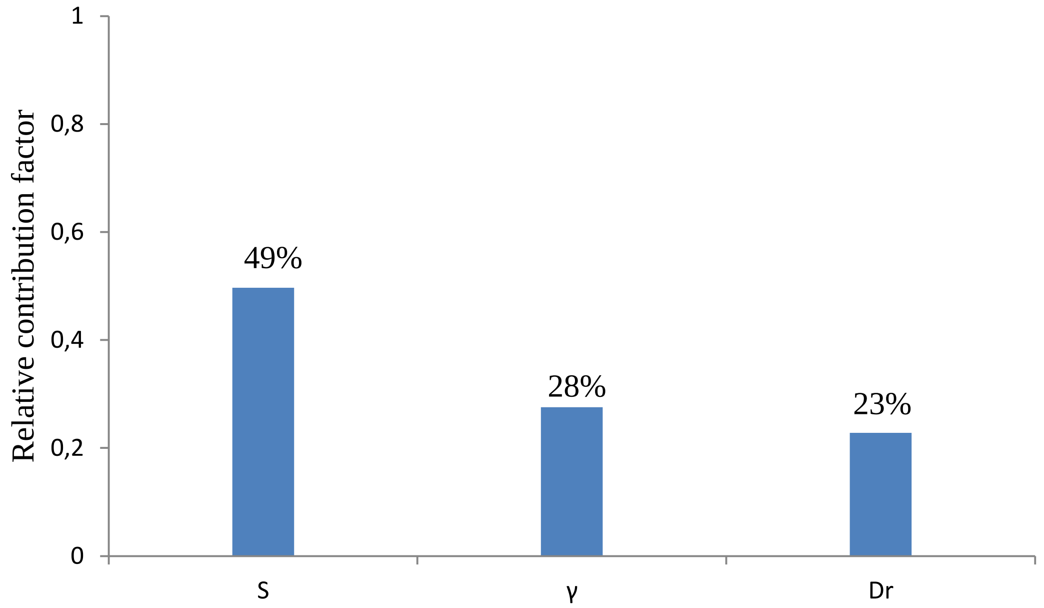

Figure 4.3 : The relative contribution factors of predicting r_{umax} in BPNN.

The contribution factors obtained from the ANN model also agrees with the physical behavior of partially saturated sands when subjected to earthquake motions. The test results and the mathematical model developed by Eseller-Bayat (2009) also demonstrated that the most effective contributing parameter on r_{umax} is degree of saturation S.

The coefficient of determination (R^2) and the statistical measure of the strength of the relationship between the actual vs. predicted outputs (r) results after training and testing the network, were shown in Table 4.4.

Table 4.4 : The statistical results of r_{umax} in Neuroshell 2.

Coefficient of determination R^2	Square of correlation coefficient r^2	Mean squared error	Mean absolute error	Min. absolute error	Max. absolute error	Correlation coefficient r
0,9616	0,9626	0,004	0,052	0	0,175	0,9811

Figure 4.4 demonstrates the relation between error and pattern number for r_{umax} in Neuroshell 2 and Figure 4.5 presents comparison of actual output with network output in Neuroshell 2 with 10% error limit. The proposed r_{umax} predicts the actual r_{umax} within an error range of $-0,1 < \varepsilon < 0,1$ with 90% confidence interval.

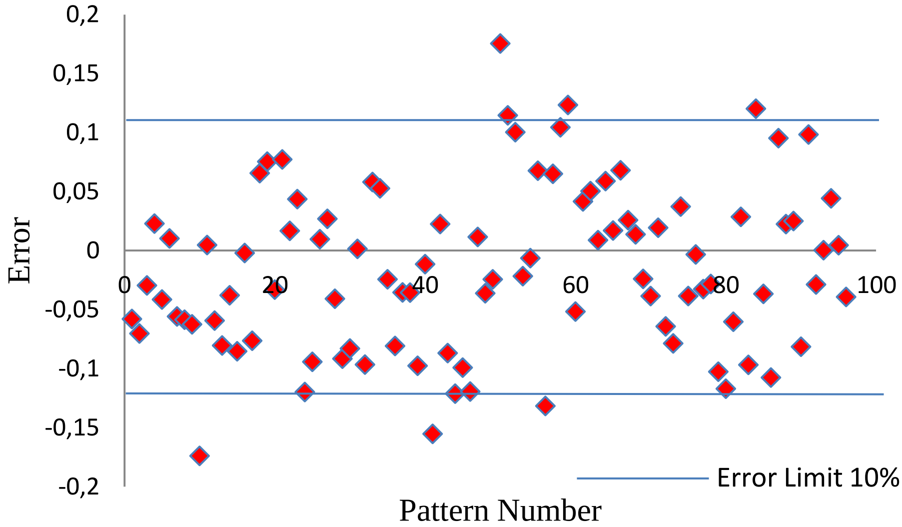

Figure 4.4 : Variables thru patterns and error for r_{umax}.

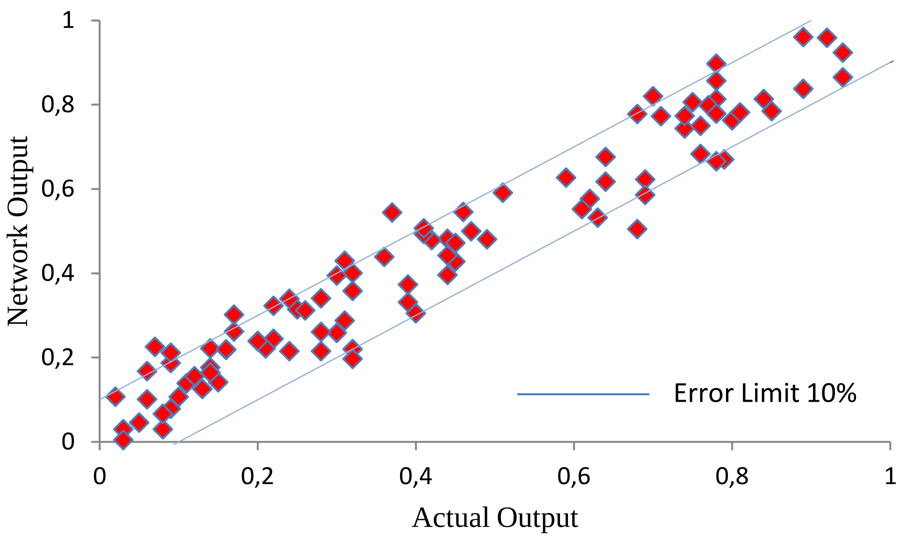

Figure 4.5 : Actual-Network output scatter for r_{umax}.

Maximum excess pore water pressures generated in partially saturated sands under various induced shear strain levels (γ=0,01%, γ=0,05%, γ=0,10% and γ=0,20%) can be predicted using the ANN model developed with BPNN. The model predictions of the r_{umax} are displayed for loose sands (D_r=25%) and medium dense sands (D_r=50%)

within the range of 40% and 90% degree of saturation (S) as shown in Figures 4.6 and 4.7, respectively. The model prediction follows reasonable trends in loose sands, however an irregular trend was observed in medium dense sands at low strain levels for degrees of saturation lower than 60%. This can be attributed to high uncertainty in the test data for low strains and low degrees of saturation in relatively denser sands. The ANN model for medium dense sands can be improved with more data when available. Also, since r_{umax} values are quite low when S< 60% and at low strains, the model for medium dense will be more of interest when degrees of saturation are above S=60%.

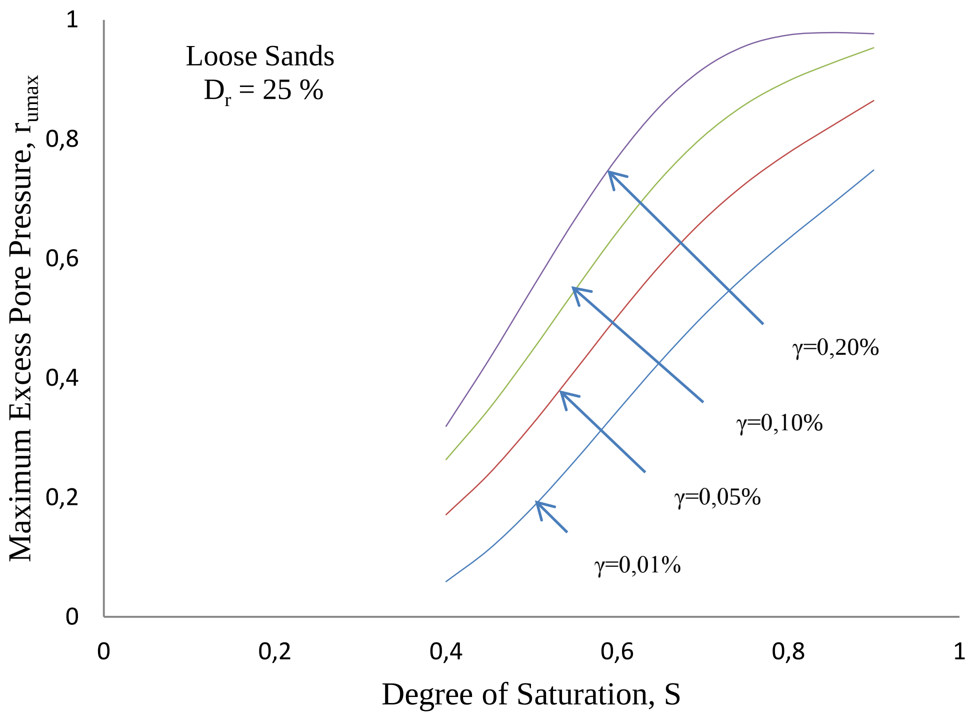

Figure 4.6 : ANN model prediction of maximum excess pore water pressure ratio r_{umax} for loose sands.

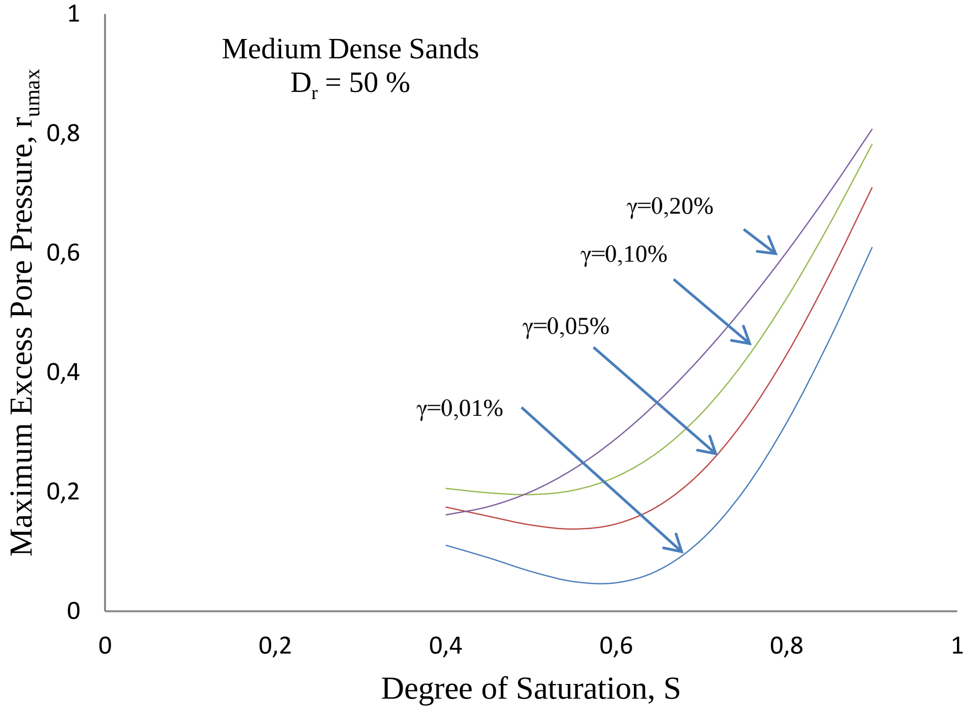

Figure 4.7 : ANN model prediction of maximum excess pore water pressure ratio r_{umax} for medium dense sands.

4.4 Estimating Number of Cycles Required to Reach r_{umax}, N_{max}

To determine the number of cycles that is necessary to reach maximum excess pore water pressure ratio (N_{max}), a new ANN model was developed. As stated in Chapter 2, N_{max} depends on parameters S, D_r, γ and σ'_v. In the mathematical model developed by Eseller-Bayat (2009), N_{max} was related to r_{umax} due to the difficulty in incorporating the effects of 3 parameters (S, D_r, γ) in a mathematical equation. ANN models are very good in dealing such complexities and therefore, N_{max} was predicted based on the parameters S, D_r and γ using artificial neural network. Then the effect of effective stress was incorporated using the empirical equation developed by Eseller-Bayat (2009).

A total of 57 data from the research work by Eseller-Bayat (2009) were used and normalized. The normalized 57 data were imported to the network. S, D_r and γ were defined as input parameters and N_{max} was defined as an output parameter in Table 4.5. In addition, minimum, maximum, mean and standard deviation values were computed both normalization and without normalization in Table 4.5 and in Table 4.6, respectively.

Table 4.5 : Normalized input and output values for N_{max} in Neuroshell 2.

Parameters	Degree of Saturation	Relative Density	Shear Strain	Number of cycles to reach r_{umax}
Variable Name	S	D_r	γ	N_{max}
Variable Type	I	I	I	A
Min:	0	0	0	0
Max:	1	1	1	1
Mean	0,62	0,41	0,27	0,31
Std. Deviation	0,26	0,31	0,22	0,27

As the data were normalized and arranged before import, all the patterns after N thru M is selected to extract the training and testing set. First 43 data were used as training data, remaining 14 data were used as testing data while generating N_{max} model.

Table 4.6 : Input and output values for N_{max} in Neuroshell 2.

Parameters	Degree of Saturation	Relative Density	Shear Strain	Number of cycles to reach r_{umax}
Variable Name	S	D_r	γ	N_{max}
Variable Type	I	I	I	A
Min:	0,42	0,2	0,0106	2,5
Max:	0,9	0,67	0,31	90
Mean	0,71	0,39	0,09	29,5
Std. Deviation	0,12	0,14	0,07	23,1

After several models were constituted, General Regression Neural Network was chosen as a best model when the relation between actual and networks outputs compared. General Regression Neural Network architecture was decided in this instant on the first slab or input layer, the scale function is then defined as Linear [0,1] as chosen in r_{umax}.

All slabs represent the layers in this architecture. As shown in Figure A.3, first slab is input layer and contains 3 neurons i.e. the number of inputs, and scaling function, second slab represents hidden layer and it contains 43 neurons which is the number of training patterns. The final slab contains 1 neuron which is the expected output. The links between slabs include smoothing factor and in this model it was assigned 0,3 as the most appropriate value by trying all the values within the range of 0 and 1.

After architecture was constituted for estimation of N_{max}, training and stop training criteria were set. Since GRNN makes predictions by measuring distance between patterns, for training criteria distance metric had to be selected with consideration of obtaining best results. In contrast to City Block, that is the sum of the absolute values of the differences between the pattern and the weight vector, the vanilla works better and its accuracy is superior. Although all input parameters have impacts on the overall prediction, they don't have same impacts on the output. Since iterative calibration assumes same impact of each input on the output, the use of iterative calibration was not appropriate. Therefore, the genetic is more appropriate for the model for calibration and to determine each parameter's impact. For GRNN, calibration optimizes the smoothing factor based upon the values in the test set. Calibration does this by trying different smoothing factors and choosing the one that generates the least mean squared error between the actual and predicted answers (Frederick, 1996).

A genetic algorithm works by selective breeding of a population of "individuals", each of which is a potential solution to the problem. In this case, a potential solution is a set of smoothing factors, and the genetic algorithm is seeking to breed an individual that minimizes the mean squared error of the test set (Frederick, 1996). While the learning process was running, the genetic breeding pool size was set as 75 by trial and error to obtain best result.

A sensitivity analysis was also performed to determine the relative effects of the input parameters on the $N_{max.}$ In Figure A.4, the sensitivities can be seen that were obtained from genetic calibration. Normalized sensitivities are obtained as, 57,5% for degree of saturation (S), 33% for relative density (D_r) and 9,5% shear strain (γ). Figure 4.8 depicts the relation between error and generations elapsed and indicates that over learning did not occur.

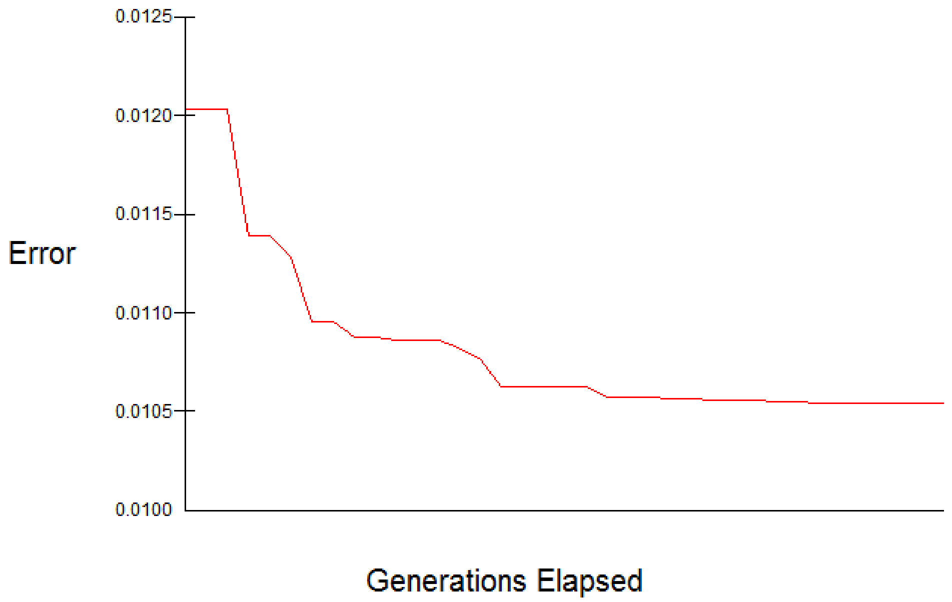

Figure 4.8 : Test set error graph for N_{max} for GRNN.

The sensitivities were found to be reasonable when compared with the physical behavior in the experimental results. The degree of saturation S had tremendous influence on the N_{max} in the excess pore water generation results as seen in Figure 4.9.

After training and testing the network, networks process results can be displayed in Table 4.7.

Table 4.7 : The statistical results of N_{max} in Neuroshell 2.

Coefficient of determination R^2	Square of correlation coefficient r^2	Mean squared error	Mean absolute error	Min. absolute error	Max. absolute error	Correlation coefficient r
0,9145	0,9256	0,006	56	0	0,269	0,9621

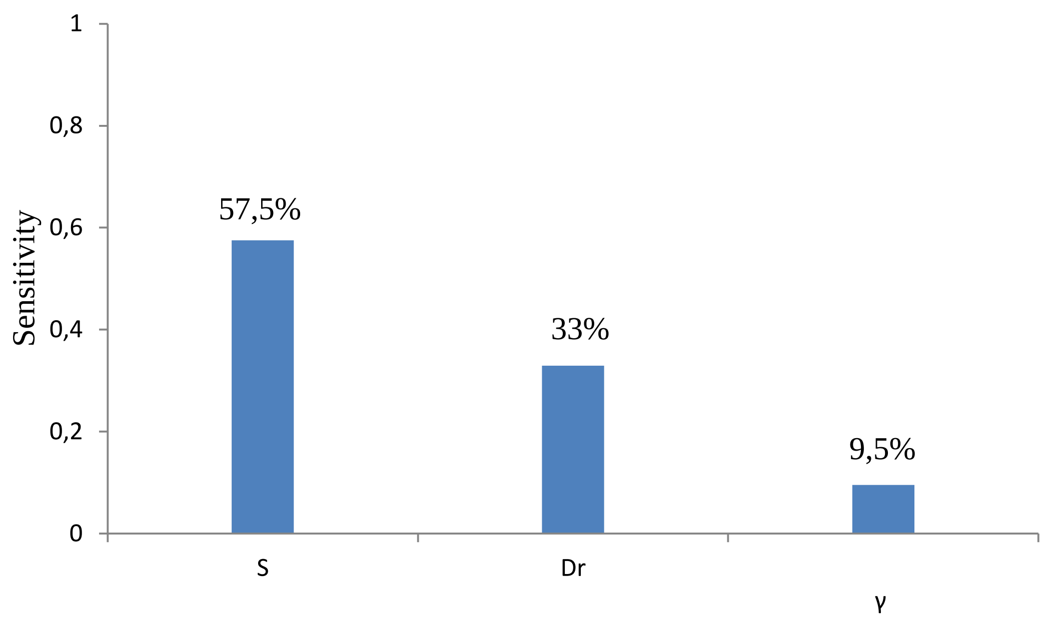

Figure 4.9 : The normalized sensitivities of predicting N_{max} in GRNN.

Figure 4.10 demonstrates the relation between error and pattern number for N_{max} in Neuroshell 2 with and Figure 4.11 presents comparison of actual output with network output for N_{max} in Neuroshell 2 with 10% error limit. The proposed N_{max} predicts the actual N_{max} within an error range of $-11 < \varepsilon < 11$ with 90% confidence interval.

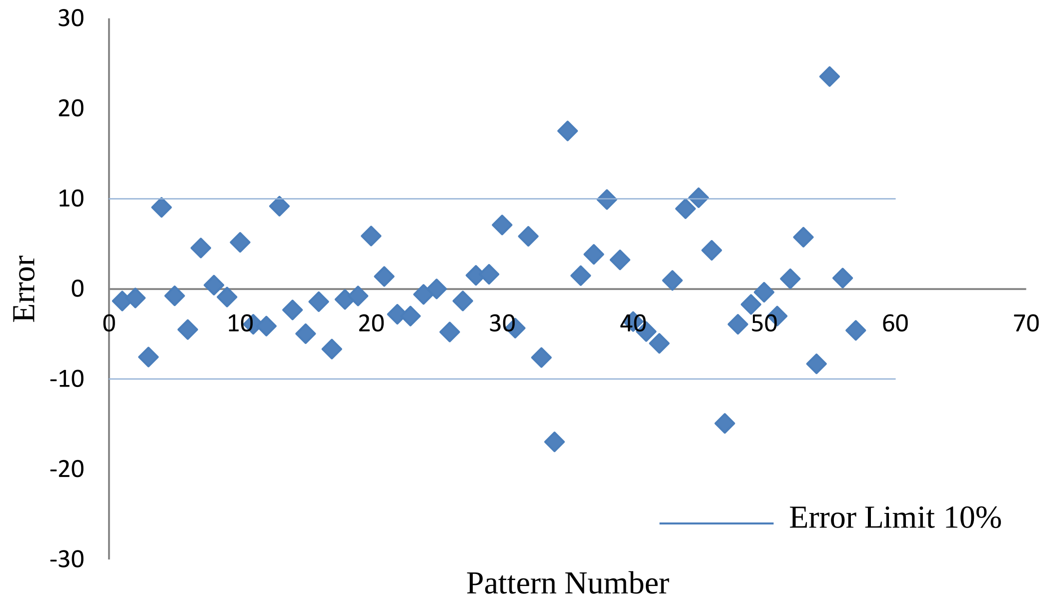

Figure 4.10 : Variables thru patterns and error for N_{max}.

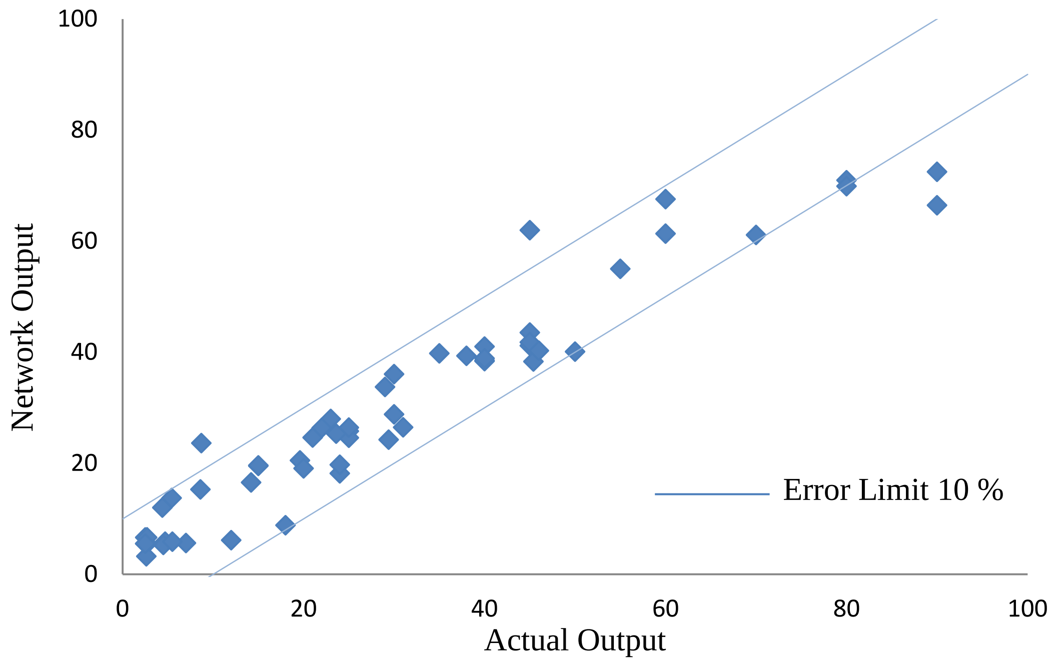

Figure 4.11 : Actual-Network output scatter for N_{max}.

When all training and testing sections were completed, ANN prediction models were generated for loose and dense sands as shown in Figure 4.12 and 4.13, respectively. These prediction plots are for σ'_v=2.5 kPa. For all practical purposes, the effect of effective stress on N_{max} was incorporated by using the effect of effective stress on N_L (number of cycles required to reach r_u=1 in fully saturated sands). The relation between the N_L and effective stress was empirically developed by Eseller-Bayat (2009) using the test results on fully saturated sands as well as the data available in literature (Dobry et al. 1982, Hazirbaba et al. 2005, Chang et al. 2007) as shown in equation 4.1.

$$N_L = \left(5.33 \times e^{-2011\gamma}\left(\frac{1}{kPa}\right)\right) \times \sigma_v' \qquad \textbf{(4.1)}$$

Therefore in order to predict the N_{max} values for other effective stresses in partially saturated sands, the N_{max} prediction outputs were normalized to N_L : N_{max}/N_L. Figure 4.14 and 4.15 demonstrate the normalized N_{max}/N_L plots for loose and medium dense sands respectively. To find N_{max} at other effective stresses, the normalized ANN model prediction can be multiplied by equations 4.2 and 4.3 as below:

$$N_{\max,\sigma_v'} = \left[\left(\frac{N_{\max}}{N_L}\right)_{ANN} \right] N_L \quad \textbf{(4.2)}$$

$$N_{\max,\sigma_v'} = \left[\left(\frac{N_{\max}}{N_L}\right)_{ANN} \right] \left(5.33 \times e^{-2011\gamma} \left(\frac{1}{kPa} \right) \right) \times \sigma_v' \quad \textbf{(4.3)}$$

Here, it was assumed that the effect of σ'_v on N_{max} will be similar to the effect of σ'_v on N_L. This is a conservative assumption since physically as σ'_v increases, the increase in N_{max} will never be less than the increase in N_L. The effective stress will have at least an equal positive effect as in fully saturated sands.

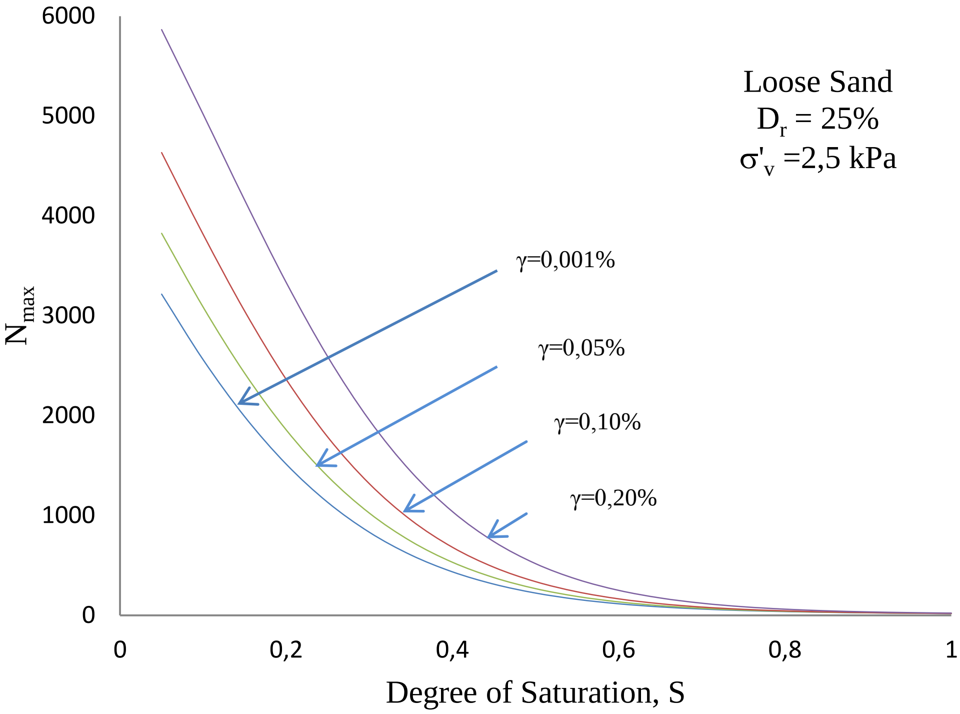

Figure 4.12 : ANN model prediction of N_{max} for loose sands.

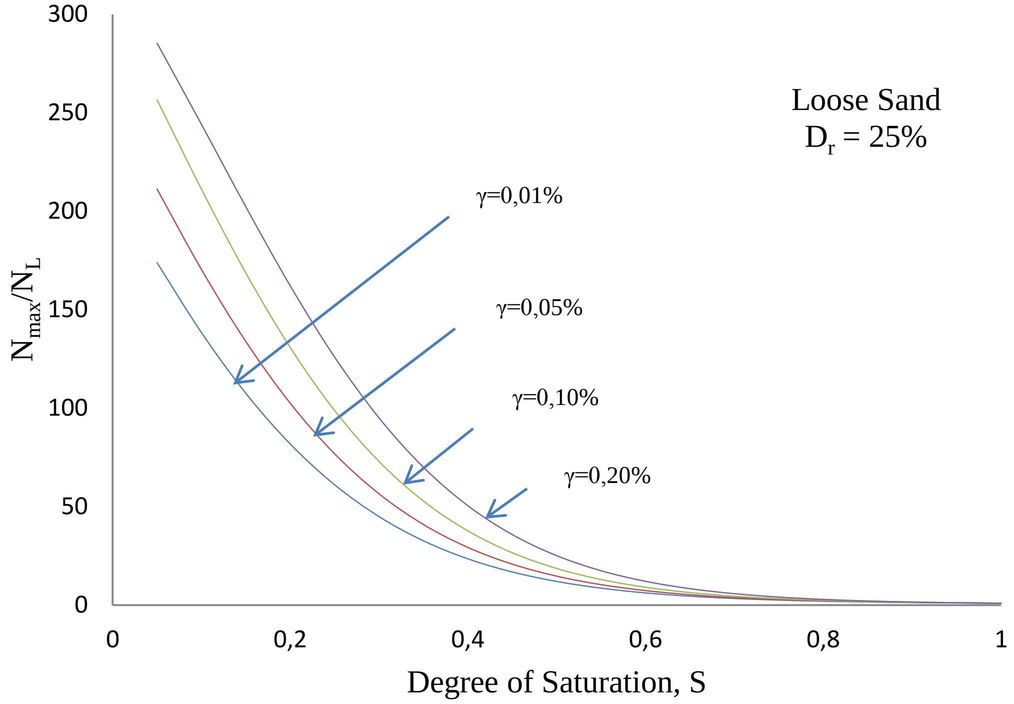

Figure 4.13 : ANN model prediction of normalized N_{max} for loose sands.

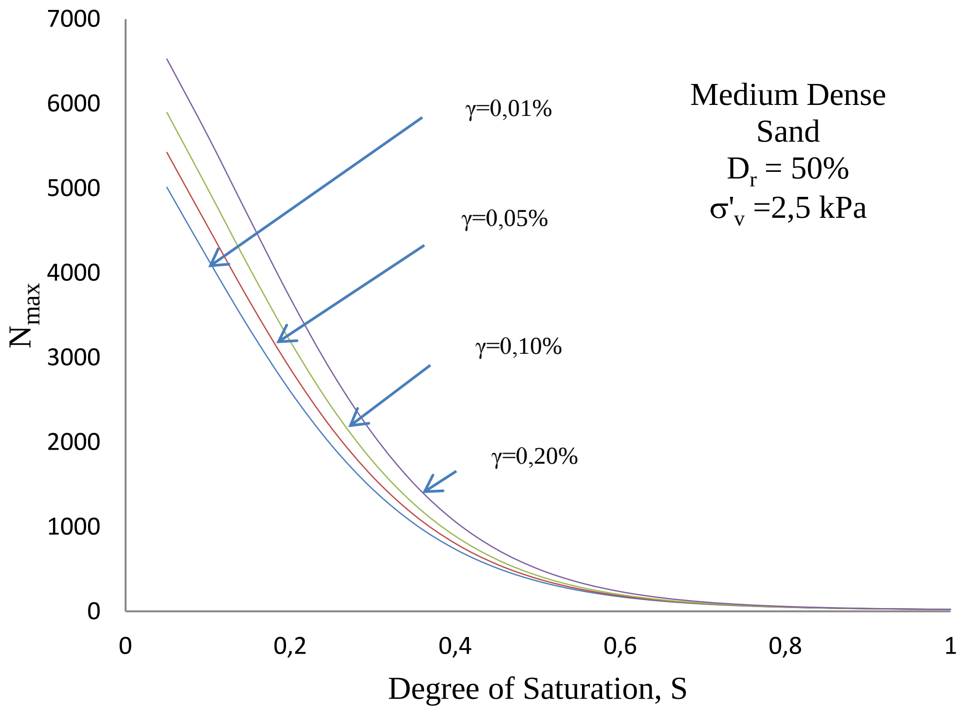

Figure 4.14 : ANN model prediction of N_{max} for medium dense sands.

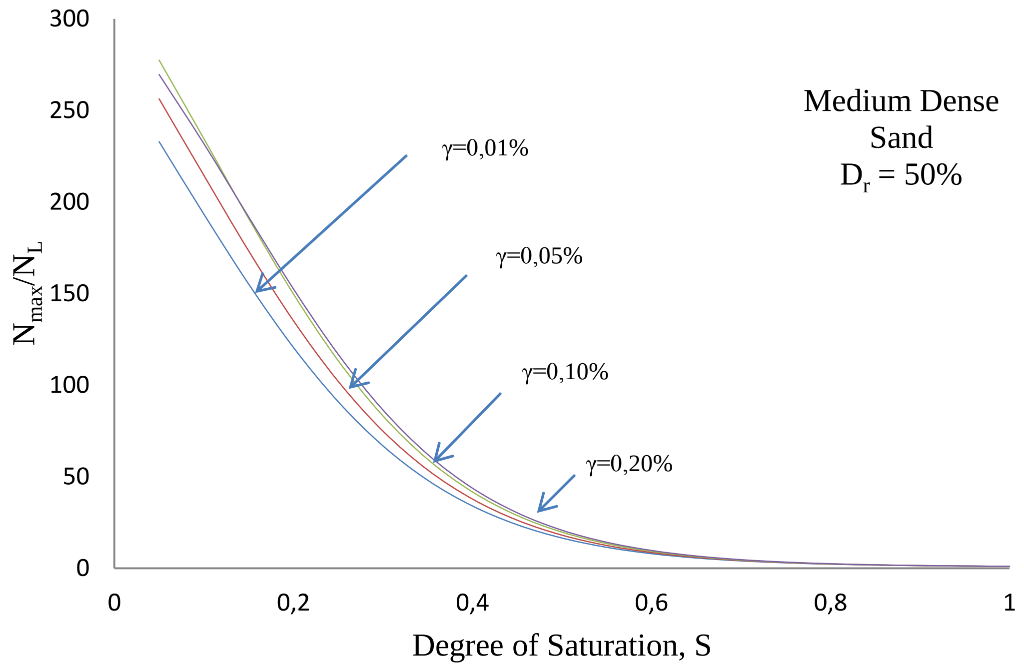

Figure 4.15 : ANN model prediction of normalized N_{max} for medium dense sands.

4.5 Summary

An ANN model for predicting maximum excess pore water pressure ratio (r_{umax}) in partially saturated sands was developed as a function of degree of saturation (S), relative density (D_r) and shear strain (γ). After evaluating different ANN models, a BPNN model which gives highest accuracy with R^2 of 96,2% (coefficient of determination) was determined as the best ANN model. The BPNN model predicts r_{umax} with an higher accuracy than the mathematical model described in Chapter 2 (R^2=92%). Also, the BPNN model can predict r_{umax} with an error range of ±0,1 whereas the mathematical model can predict with an error range of ±0,13 with 90% confidence interval.

Another ANN model was developed to predict N_{max} as a function of S, D_r and γ. After evaluating different ANN models, a GRNN model which gives highest accuracy with R^2 of 91,5% was determined as the best ANN model. N_{max} could not be predicted with a mathematical model as a function of S, D_r and γ due to the complexity of the behavior, instead N_{max} was correlated to r_{umax}. The GRNN model was able to solve this complexity and N_{max} was correlated to S, D_r and γ. Also the effect of each parameter on N_{max} was determined.

To conclude, the ANN prediction model plots developed in here for r_{umax} and N_{max} can be used in RuPSS empirical model when predicting the excess pore water pressure ratios (r_u) in practice, for relatively loose and medium dense sands. For densities in between, a linear interpolation can be adopted in between the r_{umax} and/or N_{max} values found for loose and medium dense sands.

In the next chapter, a case study is presented on a liquefiable sand site which is mitigated by Induced-Partial Saturation (IPS). Partial saturation that need to be induced in the site was predicted by both ANN models introduced in this chapter and the mathematical model and the results were compared.

5. ESTIMATION OF PARTIAL SATURATION TO BE INDUCED IN LIQUEFIABLE SANDS: CASE STUDY

5.1 Introduction

In the previous chapter, 2 ANN models developed for predicting r_{umax} and N_{max} to eventually estimate excess pore water pressure ratio (r_u) in partially saturated sands were presented. In order to define ANN models' functionality and their comparison with the mathematical model, a case study was performed for a liquefiable sand site and partial saturation that need to be induced in the site for mitigation was estimated using both ANN and mathematical models (Eseller-Bayat, 2009) and, these both models results were compared.

5.2 Analysis of a Liquefiable Sand Site in Japan

Liquefaction analysis was performed for a clean and potentially liquefiable sand site as depicted in Figure 5.1 located in Japan, which would be subjected to 1952 Taft earthquake (M=7,6). The SPT blow counts and corrected values are tabulated in Table 5.1. The SPT counts and shear wave velocities obtained from the borehole logs are shown in Figure 5.2 (Kramer, 1996).

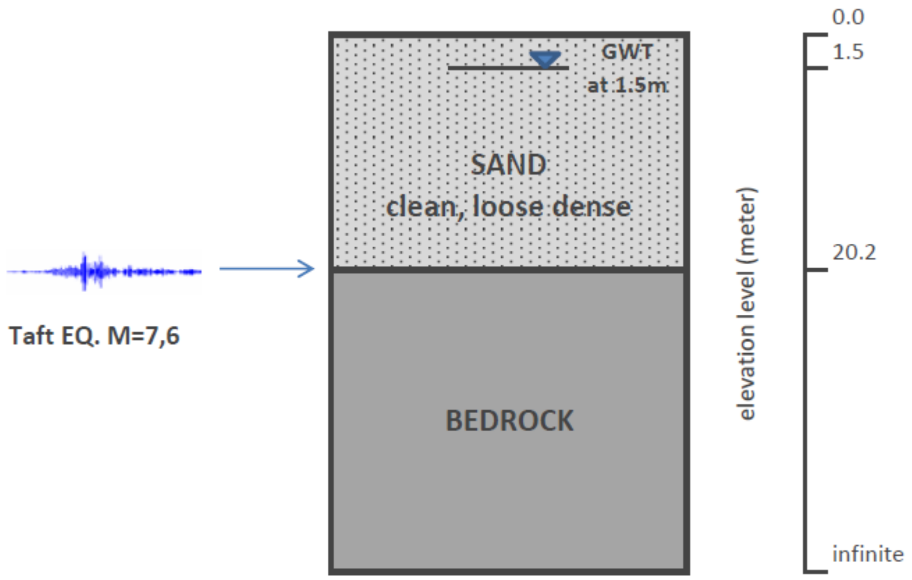

Figure 5.1 : Soil profile.

Table 5.1 : SPT blow counts (Kramer, 1996).

Depth (m)	N_m	$(N_1)_{60}$	Depth (m) Cont'd	N_m Cont'd	$(N_1)_{60}$ Cont'd
1,2	7	17	11,2	23	23
2,2	4	8	12,2	13	12
3,2	3	5	13,2	11	10
4,2	3	5	14,2	11	10
5,2	5	7	15,2	24	21
6,2	9	12	16,2	27	23
7,2	12	15	17,2	5	4
8,2	12	14	18,2	6	5
9,2	14	15	19,2	4	3
10,2	9	9	20,2	38	29

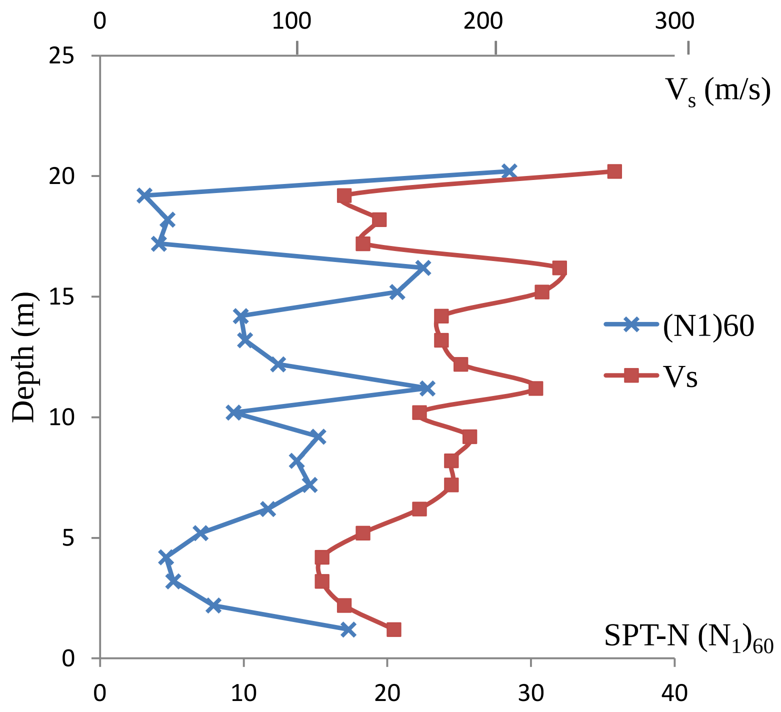

Figure 5.2 : The SPT data and shear wave velocities for the site in Japan.

Liquefaction analysis was performed using Seed's Simplified Procedure to estimate the liquefiable sand layers. The site was divided into 20 sand layers and peak ground acceleration generated as 0,18g for Taft earthquake using Edushake (EduPro Civil System, 1998). The following steps were performed in the analysis;

1. Total vertical stresses (σ_{v0}) were estimated for each depth by using equation 5.1,

$$\sigma_{v0} = \rho \times \mathrm{g} \times \mathrm{H} \quad \textbf{(5.1)}$$

where,

ρ: density,

g: acceleration due to gravity and

H: depth.

2. The stress reduction factor (r_d) was obtained for each depth using Figure 5.3,

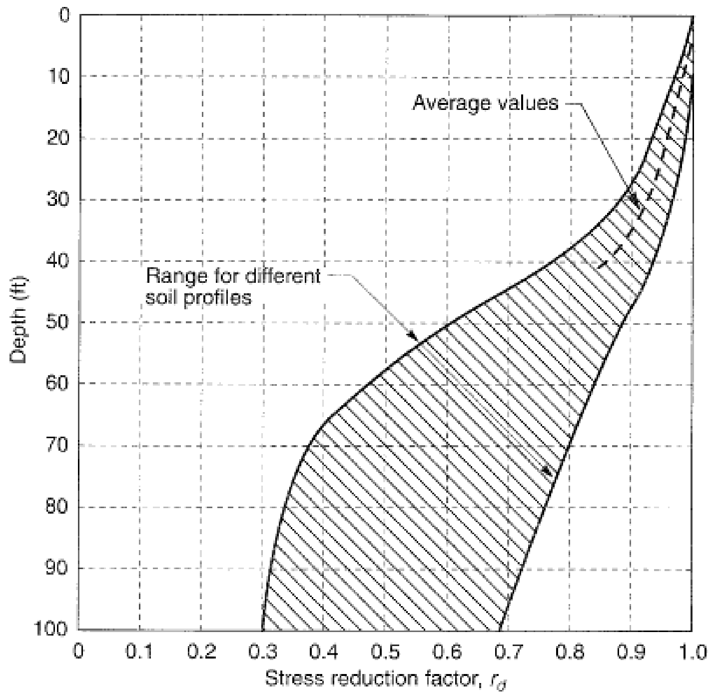

Figure 5.3 : Reduction factor to estimate the variation of cyclic shear stress with depth below level or gently sloping ground surfaces (Seed and Idriss, 1971).

3. The uniform cyclic shear stress amplitude (τ_{cyc}) was estimated by equation 5.2,

$$\tau_{cyc} = 0,65 \frac{a_{\max}}{g} \sigma_v r_d \quad \textbf{(5.2)}$$

where, $a_{\max}$ is peak ground surface acceleration, g is acceleration due to gravity, σ_v is total vertical stress and r_d is stress reduction factor.

4. CSR_L for the given earthquake that is the cyclic stress ratio that causes liquefaction can be determined by first reading cyclic stress ratio (CSR) for M=7,5 from Figure 5.4 and then multiplying by the magnitude scaling factor "$CSR_M/CSR_{M=7,5}$" by using equation 5.3 for M=7,6 (Idriss, 1999).

$$\text{MSF}=6{,}9\exp\left(\frac{-M}{4}\right)-0{,}058 \qquad \textbf{(5.3)}$$

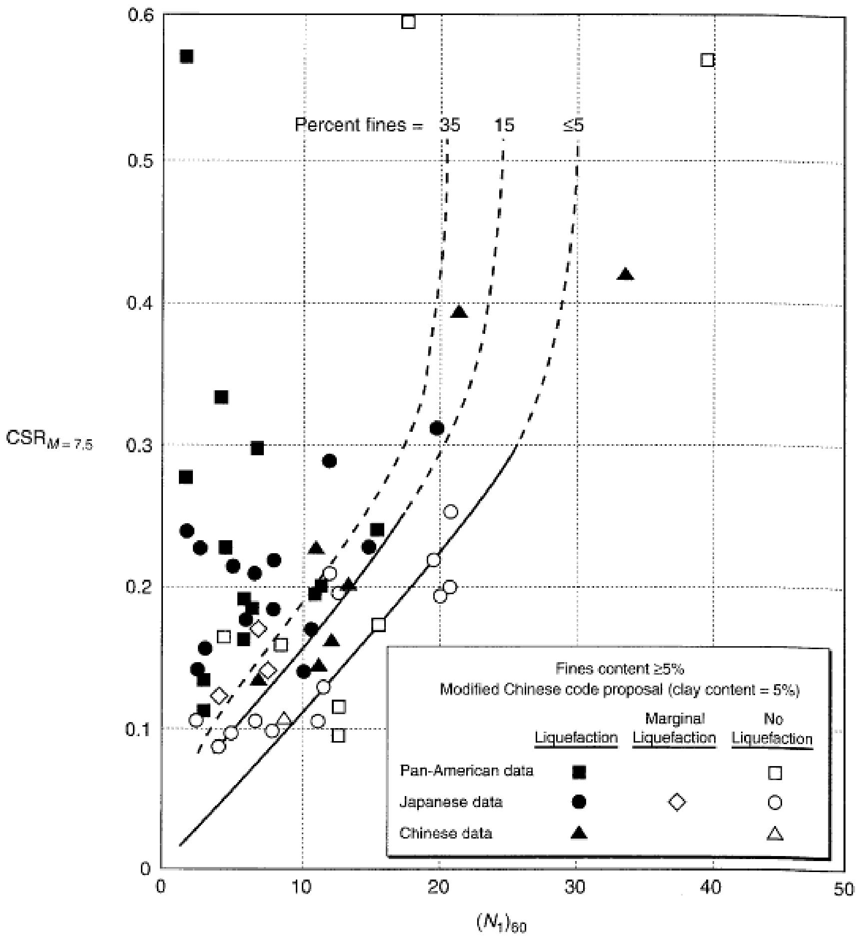

Figure 5.4 : Relationship between cyclic stress ratios and $(N_1)_{60}$ values for silty sands in M=7,5 (Kramer, 1996).

5. The cyclic stress required to initiate liquefaction (τ_{cycL}) was estimated by equation 5.4,

$$\tau_{cycL}=\text{CSR}_L\sigma_{V0}^{'} \qquad \textbf{(5.4)}$$

6. The factor of safety against liquefaction (FS_L) was estimated by equation 5.5 for each sand layer (where liquefaction occurs $FS_L \leq 1$),

$$\text{FS}_L=\frac{\tau_{cycL}}{\tau_{cyc}} \qquad \textbf{(5.5)}$$

Table 5.2 : Liquefaction analysis results through simplified procedure.

D (m)	σ_{v0}	r_d	τ_{cyc}	$(N_1)_{60}$	CSR_L	σ'_{V0}	τ_{cycL}	FS_L
1,2	22,10	0,994	2,57	17,30	NA	22,10	NA	NA
2,2	42,60	0,989	4,93	7,90	0,08	35,68	3,01	0,61
3,2	64,00	0,982	7,35	5,10	0,05	47,25	2,57	0,35
4,2	85,30	0,976	9,74	4,60	0,05	58,83	2,91	0,30
5,2	106,70	0,968	12,08	7,00	0,07	70,41	5,26	0,44
6,2	128,10	0,960	14,39	11,70	0,13	81,98	10,34	0,72
7,2	149,50	0,951	16,63	14,60	0,16	93,56	14,61	0,88
8,2	170,90	0,940	18,80	13,70	0,15	105,13	15,40	0,82
9,2	192,30	0,926	20,83	15,20	0,16	116,71	18,91	0,91
10,2	213,80	0,910	22,76	9,30	0,10	128,29	12,69	0,56
11,2	235,10	0,886	24,37	22,80	0,24	139,86	33,92	1,39
12,2	256,50	0,864	25,93	12,40	0,13	151,44	19,98	0,77
13,2	277,90	0,835	27,15	10,10	0,11	163,01	17,55	0,65
14,2	299,30	0,813	28,47	9,80	0,10	174,59	18,29	0,64
15,2	320,70	0,767	28,78	20,70	0,22	186,16	41,17	1,43
16,2	342,10	0,739	29,58	22,50	0,24	197,74	46,99	1,59
17,2	363,50	0,704	29,94	4,10	0,04	209,32	9,14	0,31
18,2	384,80	0,671	30,21	4,70	0,05	220,89	11,14	0,37
19,2	406,20	0,642	30,51	3,10	0,03	232,47	7,67	0,25
20,2	427,70	0,625	31,28	28,50	0,34	244,04	82,85	2,65

The results of the liquefaction analysis using Simplified Procedure by Seed and Idriss (1971) are shown in Table 5.2. The liquefaction analysis results imply that the sand site is vulnerable to liquefaction even under very low peak ground acceleration (0,18g) and needs mitigation. In the next sections, when IPS mitigation technique is applied in the site, firstly, excess pore pressure ratios to be generated when degree of saturation is lowered down to S=80% will be estimated through all depths and secondly the degree of partial saturation to be induced in each depth for a limiting design level of r_u =0.5 will be determined. For the predictions, both ANN and mathematical models will be used and the results will be compared.

5.3 Estimation of r_u for a Constant Degree of Saturation

In order to show the use of ANN model in practice and for its comparison with the mathematical prediction model, excess pore water pressure ratios in all the liquefiable sand layers of the site given above were estimated for a degree of saturation being equal to 80%. Excess pore water pressures induced in all layers of the sand site were estimated using RuPSS empirical model. The steps of the RuPSS were reported in section 2.5 and also can be referred to Eseller-Bayat (2009):

$$1)\ r_{u\max} = f_1(S, D_r, \gamma)$$

$$2)\ \frac{r_u}{r_{u\max}} = f_2\left(\frac{N_\gamma}{N_{\max}}\right)$$

$$3)\ r_u = f_1 \times f_2$$

A function for N_γ which is the number of equivalent strain cycles for an earthquake with magnitude (M) was developed by Eseller-Bayat (2009). The function f_2 was developed based on the shape of the rate of excess pore water pressure generations during the experimental tests. r_{umax} and N_{max} were predicted in all layers using the ANN models introduced in Chapter 4 and also using the mathematical model developed by Eseller-Bayat (2009). Then, r_u was estimated using the 3 steps of RuPSS. The estimations of r_u using proposed ANNs model and the mathematical model (Eseller-Bayat, 2009) were compared.

5.3.1 Prediction of r_{umax}

As stated in Chapter 2, r_{umax} depends only on S, D_r and γ. Maximum excess pore water pressure ratio (r_{umax}) needs to be predicted when partial saturation is induced in the site for S=80%. Relative density D_r at each layer can be estimated using the SPT resistances by equation 5.6.

$$D_r=15\ (N_1)_{60}^{1/2} \text{ (Boulanger, 2004)} \qquad \textbf{(5.6)}$$

1-D ground motion analysis was performed using Edushake (EduPro Civil System, 1998) to get maximum shear strains (γ_{max}) developed at each layer. Edushake (EduPro Civil System, 1998), assures ground response analysis at any layer of soil by using parameters such as; shear wave velocities (V_s), unit weights (γ) which are obtained from laboratory tests and acceleration time history records of earthquakes. In this program, the shear stress-strain curves of the damping ratio's theoretical models, according to the results of laboratory experiments, are used for sand (Seed and Idriss, 1970), clay (Seed and Sun, 1989) and rock. As considering the SPT resistances $(N_1)_{60}$ are available for each depth, soil profile was generated as 20 layers. At each layer, shear wave velocity (V_s), unit weight (γ), modulus and damping curve were defined. Depending on the fact that V_s and N_m are related, V_s was calculated by equation 5.7.

$$V_s = 80{,}6 \ N_m^{0{,}331} \text{ (Imai, 1977)} \tag{5.7}$$

The estimated D_r and V_s values for each depth are tabulated in Table 5.3.

Table 5.3 : Estimated D_r and V_s with SPT resistances for each layer.

Depth(m)	D_r	V_s (m/s)	Depth(m) Cont'd	D_r Cont'd	V_s (m/s) Cont'd
1,2	0,62	153,5	11,2	0,72	227,5
2,2	0,42	127,5	12,2	0,53	188,4
3,2	0,34	115,9	13,2	0,48	178,3
4,2	0,32	115,9	14,2	0,47	178,3
5,2	0,40	137,3	15,2	0,68	230,8
6,2	0,51	166,8	16,2	0,71	239,9
7,2	0,57	183,5	17,2	0,30	137,3
8,2	0,56	183,5	18,2	0,33	145,8
9,2	0,58	193,1	19,2	0,26	127,5
10,2	0,46	166,8	20,2	0,80	268,7

Unit weights were assigned as 21,4 kN/m^3 for saturated, 18,4 kN/m^3 for dry sand layer. Seed & Idriss average curve was selected for Modulus and Damping curve as depicted in Figure 5.5 and 5.6, respectively.

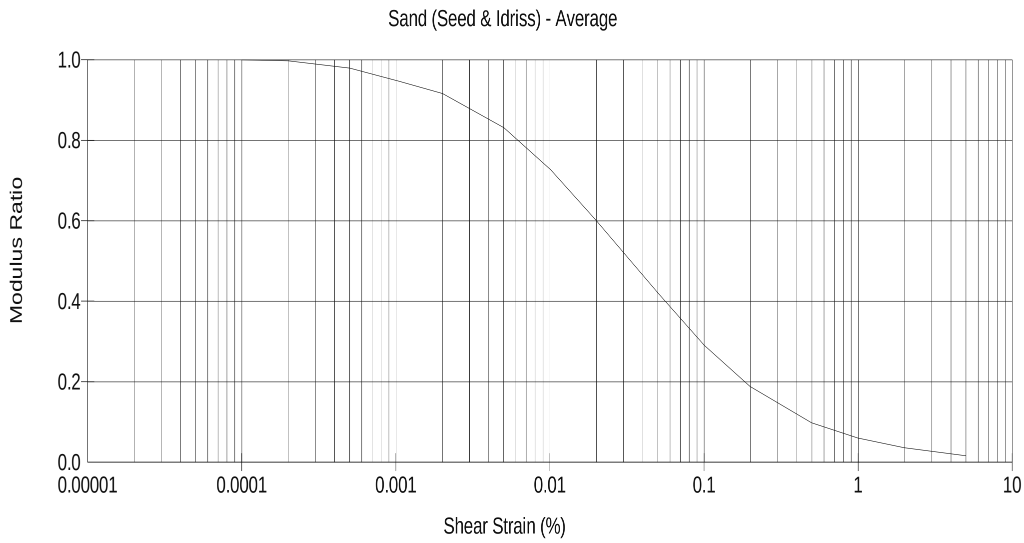

Figure 5.5 : Modulus ratio vs. shear strain graph in Edushake.

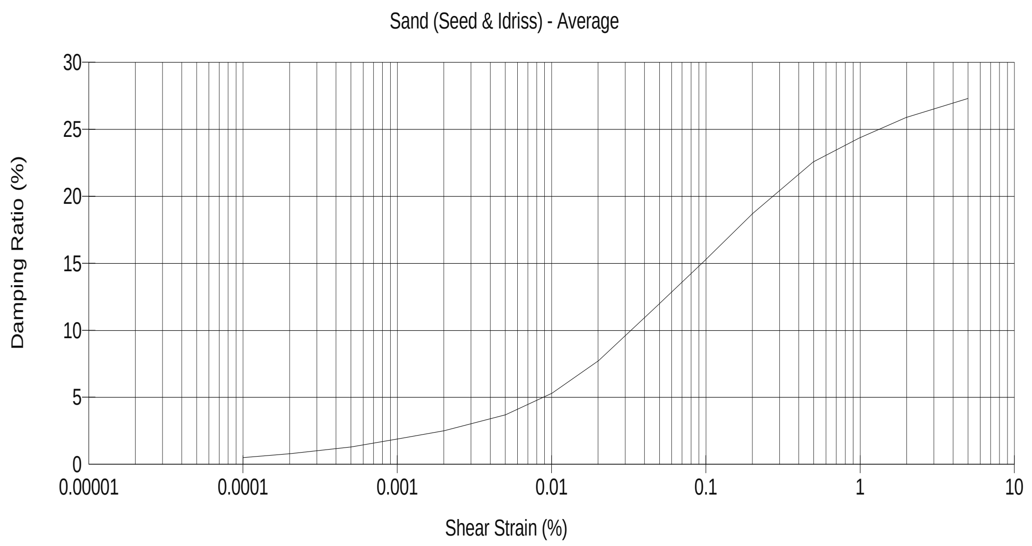

Figure 5.6 : Damping ratio vs. shear strain graph in Edushake.

After assigning all values that were needed, Taft earthquake (M=7,6), was generated in the soil profile to obtain maximum shear strains at each layer. In Figure 5.7, acceleration time history of Taft earthquake (M=7,6) rock motion is displayed.

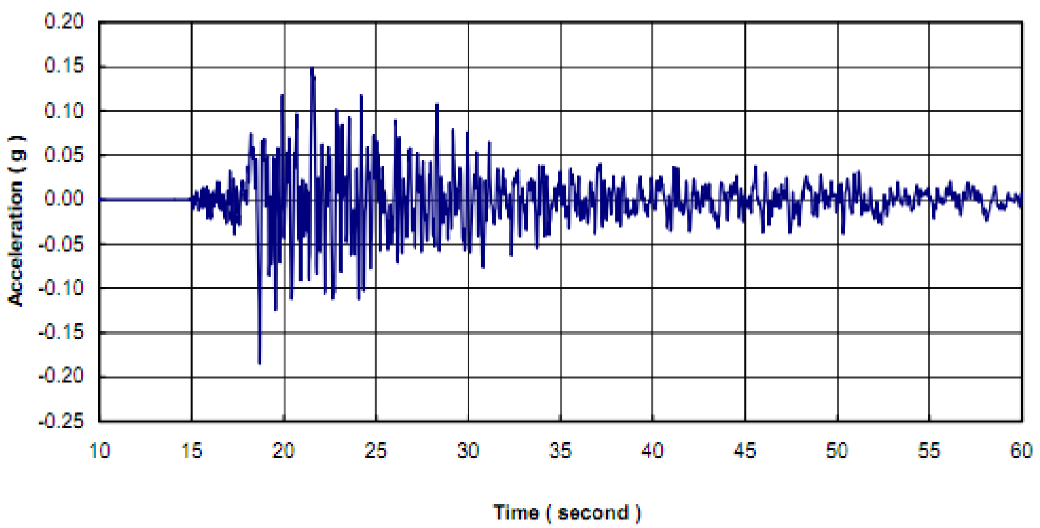

Figure 5.7 : Acceleration time history of Taft earthquake rock motion.

Next step was to get cyclic shear strains which were going to be used in the ANN and mathematical model for estimation of maximum excess pore water pressure ratio (r_{umax}). Figure 5.8 presents the time history of shear strain which was generated in the most critical layer (layer 18). Maximum shear strain was observed as 1,3%.

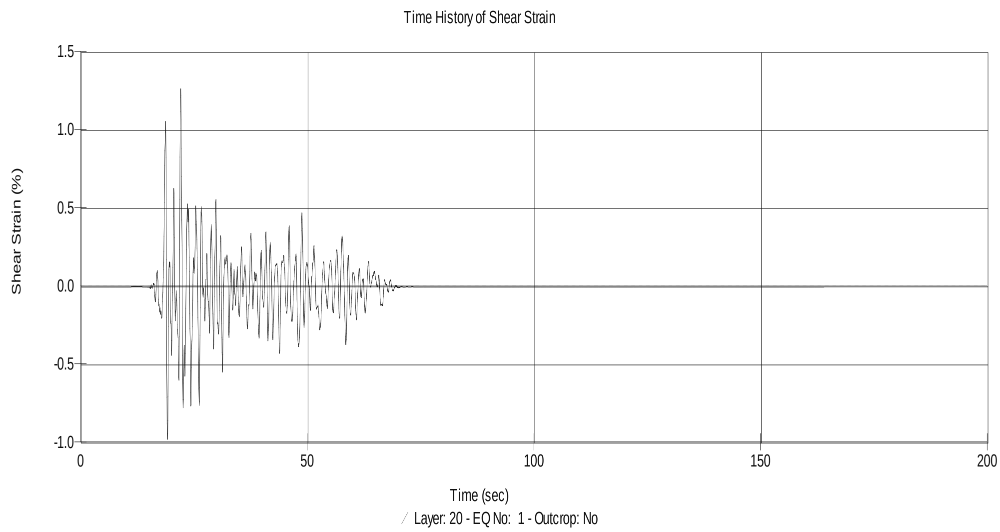

Figure 5.8 : Time history of shear strain in layer 18 in Edushake.

Cyclic shear strains (γ) were estimated by using equations 5.8 and 5.9 and tabulated in Table 5.4 for each depth with γ_{max} which were obtained from Edushake (EduPro Civil System, 1998).

$$\gamma = \gamma_{max} \times R \tag{5.8}$$

$$R = \frac{M-1}{10} \tag{5.9}$$

where, γ is cyclic shear strain, γ_{max} is maximum shear strain, R is the strain ratio and M is earthquake magnitude.

Table 5.4 : γ_{max} obtained from Edushake and estimated γ at each layer.

Depth (m)	γ_{max} (%)	γ(%)	Depth (m) Cont'd	γ_{max} (%) Cont'd	γ (%) Cont'd
1,2	0,016	0,011	11,2	0,086	0,086
2,2	0,042	0,028	12,2	0,13	0,092
3,2	0,08	0,053	13,2	0,14	0,034
4,2	0,069	0,046	14,2	0,051	0,032
5,2	0,047	0,031	15,2	0,048	0,403
6,2	0,044	0,029	16,2	0,61	0,317
7,2	0,052	0,034	17,2	0,48	0,858
8,2	0,053	0,035	18,2	1,3	0,024
9,2	0,12	0,079	19,2	0,037	0,0004
10,2	0,04	0,026	20,2	0,0006	0,086

All the S, D_r and γ values were entered in the ANN prediction model and r_{umax} was predicted at each sand layer. Table 5.5 shows predicted r_{umax} values for each layer by using ANN model.

Table 5.5 : Predicted r_{umax} with ANN model.

Depth (m)	S	D_r	γ (%)	r_{umax}
1,2	0,8	0,62	0,011	NL*
2,2	0,8	0,42	0,028	0,518
3,2	0,8	0,34	0,053	0,664
4,2	0,8	0,32	0,046	0,663
5,2	0,8	0,4	0,031	0,555
6,2	0,8	0,51	0,029	0,396
7,2	0,8	0,57	0,034	0,316
8,2	0,8	0,56	0,035	0,345
9,2	0,8	0,58	0,079	0,376
10,2	0,8	0,46	0,026	0,469
11,2	0,8	0,72	0,057	NL*
12,2	0,8	0,53	0,086	0,483
13,2	0,8	0,48	0,092	0,577
14,2	0,8	0,47	0,034	0,469
15,2	0,8	0,68	0,032	NL*
16,2	0,8	0,71	0,403	NL*
17,2	0,8	0,3	0,317	0,936
18,2	0,8	0,33	0,858	0,912
19,2	0,8	0,26	0,024	0,656
20,2	0,8	0,8	0,0004	NL*

*No liquefaction

Maximum excess pore water pressure ratios were also estimated using the mathematical model by Eseller-Bayat (2009) and the results are tabulated in Table 5.6.

The results from ANN and mathematical model are compared in Figure 5.9. The r_{umax} predictions by two models for S=80% are very close to each other.

The results also imply that when degree of saturation is only reduced by 20%, maximum excess pore water pressure ratios (r_{umax}) generated in the sand layer regardless of the earthquake motion can be still as high as 0,936. In the following section, excess pore water pressure ratios (r_u) will be estimated under the earthquake motion given.

Table 5.6 : Predicted r_{umax} with mathematical model.

Depth (m)	S	D_r	γ (%)	f	F_D	F_γ	r_{umax}
1,2	0,8	0,62	0,011	0,88	0,36	0,70	NL*
2,2	0,8	0,42	0,028	0,88	0,69	0,83	0,500
3,2	0,8	0,34	0,053	0,88	0,82	0,91	0,656
4,2	0,8	0,32	0,046	0,88	0,84	0,89	0,662
5,2	0,8	0,40	0,031	0,88	0,73	0,84	0,538
6,2	0,8	0,51	0,029	0,88	0,54	0,83	0,396
7,2	0,8	0,57	0,034	0,88	0,44	0,86	0,333
8,2	0,8	0,56	0,035	0,88	0,47	0,86	0,356
9,2	0,8	0,58	0,079	0,88	0,42	0,97	0,361
10,2	0,8	0,46	0,026	0,88	0,63	0,82	0,455
11,2	0,8	0,72	0,057	0,88	0,208	0,92	NL*
12,2	0,8	0,53	0,086	0,88	0,52	0,98	0,444
13,2	0,8	0,48	0,092	0,88	0,60	0,99	0,521
14,2	0,8	0,47	0,034	0,88	0,61	0,85	0,458
15,2	0,8	0,68	0,032	0,88	0,26	0,85	NL*
16,2	0,8	0,71	0,403	0,88	0,22	1,19	NL*
17,2	0,8	0,30	0,317	0,88	0,87	1,15	0,880
18,2	0,8	0,33	0,858	0,88	0,84	1,29	0,948
19,2	0,8	0,26	0,024	0,88	0,93	0,81	0,660
20,2	0,8	0,8	0,0004	0,88	0,07	0,26	NL*

*No liquefaction

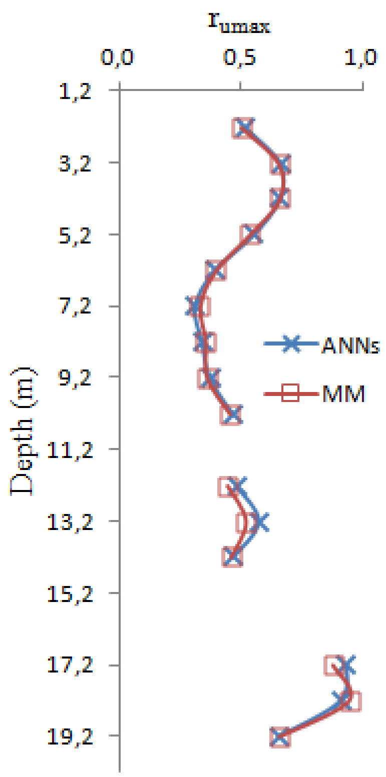

Figure 5.9: Comparison of ANN model with mathematical model for S=80% for r_{umax}.

5.3.2 Estimation of reduction in r_{umax} : r_u/r_{umax}

As stated before, excess pore water pressures generated in partially saturated sands could be much lower than r_{umax} depending on the earthquake record and magnitude. Based on the f_2 function in step 2 of RuPSS model r_u/r_{umax} rate can be calculated at each layer for earthquake magnitude M. The f_2 function developed with N_γ and N_{max} parameters' relation by Eseller-Bayat (2009). N_γ was defined as equivalent number of uniform cyclic shear strains corresponding to an earthquake magnitude M and by using equation 5.10 which was developed by Eseller-Bayat (2009), it was calculated for M=7,6 Taft earthquake. Estimated N_γ was used for both ANN and mathematical models in a way of determination f_2 function. Since N_γ was estimated, Neuroshell 2 was used for N_{max} predictions for ANN model. However N_{max} estimations were done for σ_v'=2,5 kPa, N_{max} results were normalized to N_L: N_{max}/N_L at each depth and actual N_{max} was estimated with different effective stresses by equation 5.11. For mathematical model equation 5.12 was used to predict the number of cycles required to reach maximum excess pore water pressure ratio (N_{max}).

$$N_\gamma = 0,0065 \times e^{\left[\left(\frac{10}{M-1}\right)^{1,8+0,72M}\right]} \qquad \textbf{(5.10)}$$

$$N_{\max,\sigma_v'} = \left[\left(\frac{N_{\max}}{N_L}\right)_{ANN} \right] \left(5.33 \times e^{-2011\gamma} \left(\frac{1}{kPa}\right) \right) \times \sigma_v' \qquad \textbf{(5.11)}$$

$$N_{\max} = 107 \times e^{-(3r_{u\max} + 2011\gamma)} \left(\frac{1}{kPa}\right) \times \sigma_v' \qquad \textbf{(5.12)}$$

In order to eventuate the f_2 function, equation 5.13 was used concerning the condition for $N_\gamma/N_{max} \leq 1$ and equation 5.14 was used for $N_\gamma/N_{max} > 1$.

$$\frac{r_u}{r_{u\max}} = f_2\left(\frac{N_\gamma}{N_{\max}}\right) = \left(\frac{\sin\left[\left(\frac{N_\gamma}{N_{\max}} - 0.5\right) \times \pi \right] + 1}{2} \right)^{0.54} \qquad \textbf{(5.13)}$$

$$\frac{r_u}{r_{u\max}} = 1 \qquad \textbf{(5.14)}$$

The estimation of reduction in r_{umax}: r_u/r_{umax} results were tabulated in Table 5.7 for ANN model, in Table 5.8 for mathematical model.

Table 5.7 : r_u/r_{umax} at each layer with ANN model.

Depth (m)	M	N_γ	γ (%)	S	r_{umax}	N_{max} σ_v'=2,5 kPa	N_L σ_v'=2,5 kPa	N_{max}/N_L	N_L	σ_v	N_{max}	N_γ/N_{max}	$f(N_\gamma/N_{max})=r_u/r_{umax}$
1,2	7,6	12,8	0,011	0,8	NL*	NL*	NL*	NL*	NL*	NL*	NL*	NL*	NL*
2,2	7,6	12,8	0,028	0,8	0,518	15,4	2,6	5,9	108,9	35,7	646,7	0,020	0,024
3,2	7,6	12,8	0,053	0,8	0,664	6,7	2,6	2,6	87,1	47,3	224,1	0,057	0,074
4,2	7,6	12,8	0,046	0,8	0,663	7,2	2,6	2,8	125,5	58,8	349,1	0,037	0,046
5,2	7,6	12,8	0,031	0,8	0,555	10,1	2,6	3,9	201,1	70,4	783,9	0,016	0,019
6,2	7,6	12,8	0,029	0,8	0,396	20,4	2,7	7,7	243,7	82,0	1869,3	0,007	0,008
7,2	7,6	12,8	0,034	0,8	0,316	24,7	3,8	6,5	250,1	93,6	1626,3	0,008	0,009
8,2	7,6	12,8	0,035	0,8	0,345	22,6	3,3	7,0	277,3	105,1	1927,4	0,007	0,008
9,2	7,6	12,8	0,079	0,8	0,376	27,3	4,1	6,7	126,5	116,7	844,2	0,015	0,018
10,2	7,6	12,8	0,026	0,8	0,469	19,4	2,6	7,5	402,1	128,3	2998,5	0,004	0,005
11,2	7,6	12,8	0,057	0,8	NL*	NL*	NL*	NL*	NL*	NL*	NL*	NL*	NL*
12,2	7,6	12,8	0,086	0,8	0,483	20,7	2,7	7,6	143,8	151,4	1085,4	0,012	0,014
13,2	7,6	12,8	0,092	0,8	0,577	19,0	2,6	7,3	135,5	163,0	989,6	0,013	0,015
14,2	7,6	12,8	0,034	0,8	0,469	19,7	2,6	7,6	472,9	174,6	3571,8	0,004	0,004
15,2	7,6	12,8	0,032	0,8	NL*	NL*	NL*	NL*	NL*	NL*	NL*	NL*	NL*
16,2	7,6	12,8	0,403	0,8	NL*	NL*	NL*	NL*	NL*	NL*	NL*	NL*	NL*
17,2	7,6	12,8	0,317	0,8	0,936	5,7	2,6	2,2	1,9	209,3	4,2	3,077	1
18,2	7,6	12,8	0,858	0,8	0,912	5,2	2,6	2,0	0,001	220,9	0,001	170750,118	1
19,2	7,6	12,8	0,024	0,8	0,656	11,0	2,6	4,2	758,3	232,5	3156,2	0,004	0,005
20,2	7,6	12,8	0,0004	0,8	NL*	NL*	NL*	NL*	NL*	NL*	NL*	NL*	NL*

Table 5.8 : r_u/r_{umax} at each layer with mathematical model.

Depth (m)	S	D_r	γ (%)	f	F_D	F_γ	r_{umax}	σ_v	N_{max}	N_γ	N_γ/N_{max}	$f(N_\gamma/N_{max})=r_u/r_{umax}$
1,2	0,8	0,62	0,011	0,88	0,36	0,70	NL*	NL*	NL*	NL*	NL*	NL*
2,2	0,8	0,42	0,028	0,88	0,69	0,83	0,500	35,7	487,9	12,8	0,026	0,032
3,2	0,8	0,34	0,053	0,88	0,82	0,91	0,656	47,3	244,1	12,8	0,052	0,068
4,2	0,8	0,32	0,046	0,88	0,84	0,89	0,662	58,8	345,4	12,8	0,037	0,047
5,2	0,8	0,40	0,031	0,88	0,73	0,84	0,538	70,4	803,4	12,8	0,016	0,019
6,2	0,8	0,51	0,029	0,88	0,54	0,83	0,396	82,0	1491,3	12,8	0,009	0,010
7,2	0,8	0,57	0,034	0,88	0,44	0,86	0,333	93,6	1848,2	12,8	0,007	0,008
8,2	0,8	0,56	0,035	0,88	0,47	0,86	0,356	105,1	1912,4	12,8	0,007	0,008
9,2	0,8	0,58	0,079	0,88	0,42	0,97	0,361	116,7	861,0	12,8	0,015	0,018
10,2	0,8	0,46	0,026	0,88	0,63	0,82	0,455	128,3	2063,5	12,8	0,006	0,007
11,2	0,8	0,72	0,057	0,88	0,21	0,92	NL*	NL*	NL*	NL*	NL *	NL*
12,2	0,8	0,53	0,086	0,88	0,52	0,98	0,444	151,4	761,9	12,8	0,017	0,020
13,2	0,8	0,48	0,092	0,88	0,60	0,99	0,521	163,0	560,7	12,8	0,022	0,028
14,2	0,8	0,47	0,034	0,88	0,61	0,85	0,458	174,6	2401,9	12,8	0,005	0,006
15,2	0,8	0,68	0,032	0,88	0,26	0,85	NL*	NL*	NL*	NL*	NL*	NL*
16,2	0,8	0,71	0,403	0,88	0,22	1,19	NL*	NL*	NL*	NL*	NL*	NL*
17,2	0,8	0,30	0,317	0,88	0,87	1,15	0,880	209,3	3,133106	12,8	4,08	1
18,2	0,8	0,33	0,858	0,88	0,84	1,29	0,948	220,9	4,41E-05	12,8	290035,6	1
19,2	0,8	0,26	0,024	0,88	0,93	0,81	0,660	232,5	2104,7	12,8	0,006	0,007
20,2	0,8	0,80	0,0004	0,88	0,07	0,26	NL*	NL*	NL*	NL*	NL*	NL*

*No liquefaction

5.3.3 Estimation of r_u

First 2 steps of the 3 steps RuPSS model were implemented. Maximum excess pore water pressure ratio (r_{umax}) was obtained for each layer with f_1 function in section 5.2.1 for both ANN and mathematical models as first step of RuPSS model. As a second step of RuPSS model, reduction of r_{umax} based on the f_2 function was estimated at each layer. The generation of r_u by multiplying f_1 and f_2 functions, is the last step in RuPSS model, $r_u = f_1 \times f_2$.

Table 5.9 tabulates r_u results, estimated for both mathematical and ANN models at each layer with constant degree of saturation (S=80%) with earthquake magnitude M.

Table 5.9 : r_u generated at each layer predicted by both mathematical and ANN models.

	Mathematical Model		ANN model	
Depth (m)	$f(N_\gamma/N_{max})=r_u/r_{umax}$	r_u	$f(N_\gamma/N_{max})=r_u/r_{umax}$	r_u
1,2	NL*	NL*	NL*	NL*
2,2	0,032	0,016	0,024	0,012
3,2	0,068	0,044	0,074	0,049
4,2	0,047	0,031	0,046	0,031
5,2	0,019	0,010	0,019	0,011
6,2	0,010	0,004	0,008	0,003
7,2	0,008	0,003	0,009	0,003
8,2	0,008	0,003	0,008	0,003
9,2	0,018	0,006	0,018	0,007
10,2	0,007	0,003	0,005	0,002
11,2	NL*	NL*	NL*	NL*
12,2	0,020	0,009	0,014	0,007
13,2	0,028	0,014	0,015	0,009
14,2	0,006	0,003	0,004	0,002
15,2	NL*	NL*	NL*	NL*
16,2	NL*	NL*	NL*	NL*
17,2	1	0,880	1	0,936
18,2	1	0,948	1	0,912
19,2	0,007	0,005	0,005	0,003
20,2	NL*	NL*	NL*	NL*

*No liquefaction

Figure 5.10 displays the comparison of r_u for both ANN and mathematical models with S=80% and indicates that at most of the layers ANN and mathematical models have similar r_u results. Even soil was affected by strong ground motion response, at most layers r_u values were predicted less than 0,1 by reducing the degree of saturation only 20%. However, r_u had critical values, where 80% degree of saturation was induced with large shear strains (γ>0,3%).

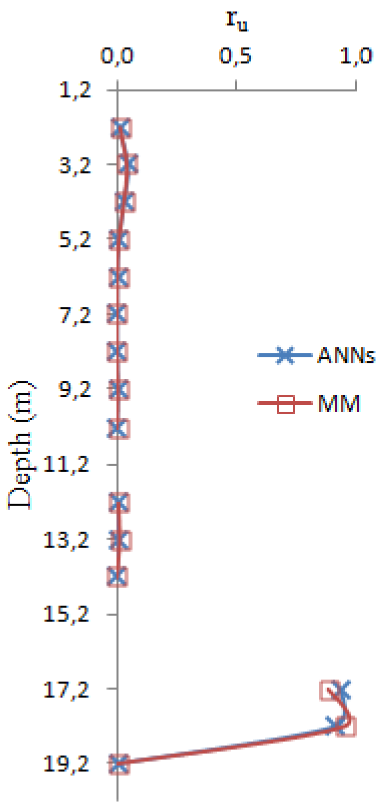

Figure 5.10 : Comparison of ANN model with mathematical model for S=80% for r_u.

5.4 Estimation of Required Partial Saturation for a design r_u

In this section, the degree of partial saturation to be induced in the given liquefiable site was estimated for a limiting design value of r_u, for the implementation of IPS in practice.

Although training the ANNs model with constant r_u was not possible, iteration of S was chosen to predict r_{umax}. Acknowledge the relation between r_u and r_{umax} is related to the relation between N_γ and N_{max} as seen from equation 5.16, r_{umax} and N_{max} was determined to make predictions by using best ANNs model and mathematical model with different degree of saturation (S), relative density (D_r) and γ values from Table 5.6.

$$\frac{r_u}{r_{u\max}} = f\left(\frac{N_\gamma}{N_{\max}}\right)\text{(Eseller-Bayat, 2009)} \tag{5.16}$$

5.4.1 Prediction of r_u

Besides using constant degree of saturation, mentioned steps of RuPSS model above applied on the way of predicting r_{umax}, estimating of reduction in r_{umax} and estimating of r_u. S=80%, S=70%, S=60% and S=50% were used to train ANN model with relative densities and cyclic shear strains from Table 5.6. Also same degree of saturations, relative densities and cyclic shear strains were used for estimations with mathematical model. Figure 5.11 and Figure 5.12 depicts, with different degree of saturations, S=80%, S=70%, S=60% and S=50%, comparison of ANN and mathematical models while estimating maximum excess pore water pressure ratio (r_{umax}), respectively.

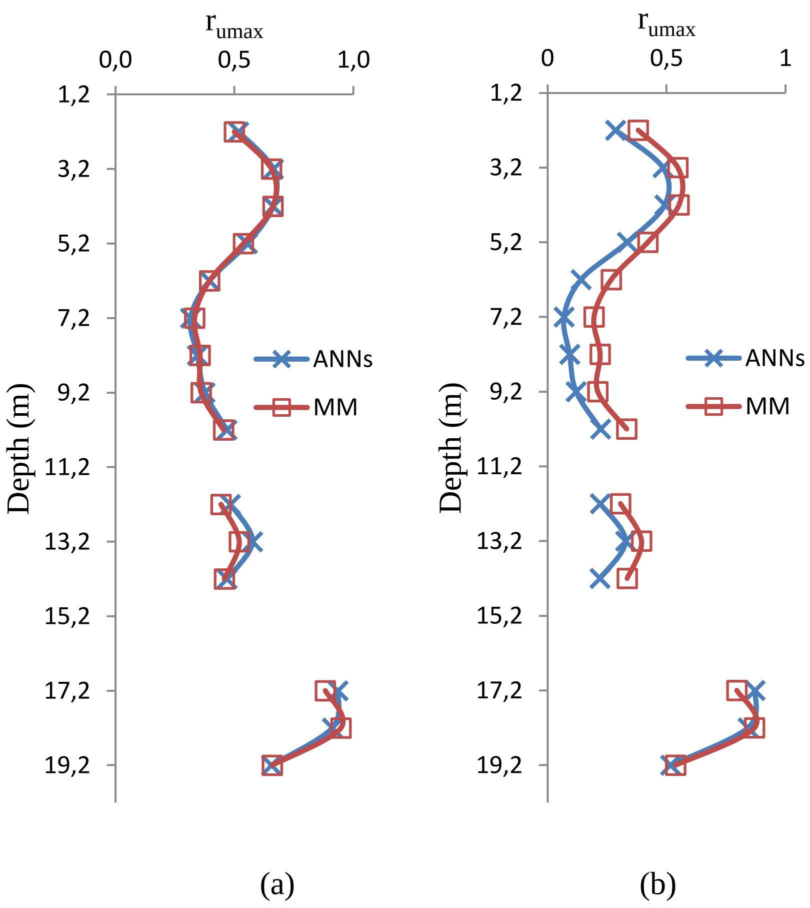

Figure 5.11 : Comparison of ANN model with mathematical model for r_{umax} for S=80% (a) and S=70% (b).

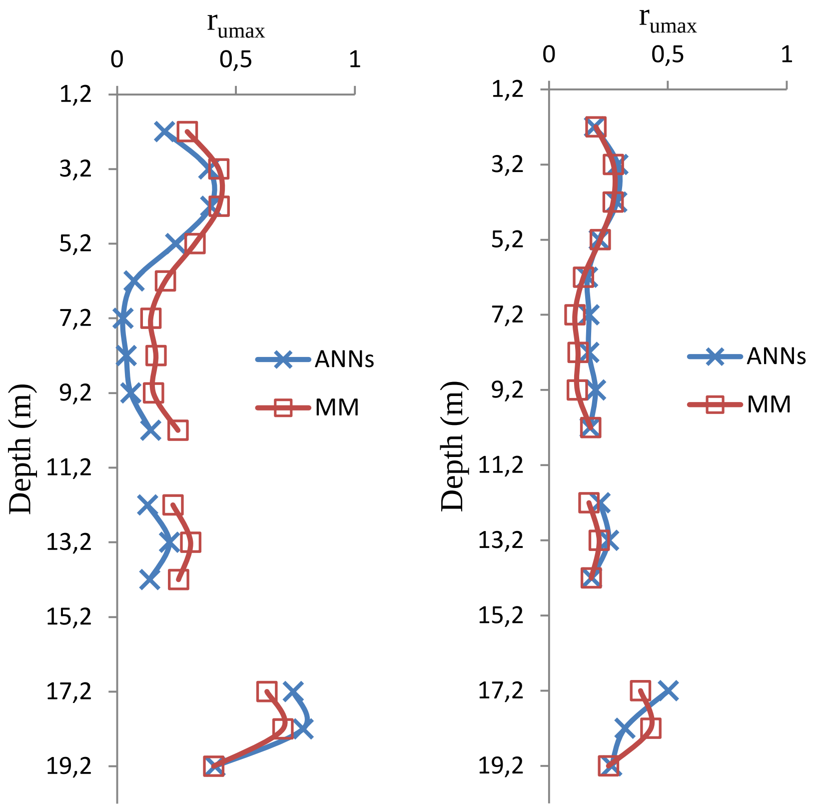

(a) (b)

Figure 5.12 : Comparison of ANN model with mathematical model for r_{umax} for S=60% (a) and S=50% (b).

Since established in Figure 5.10, Figure 5.11 and Figure 5.12, ANN and mathematical models give similar results. After obtaining r_{umax}, considering the steps of RuPSS model, equation 5.16 for reducing r_{umax} was used to estimate limiting design value for r_u. Comparison of both ANN and mathematical models for excess pore water pressure (r_u) with S=80%, S=70%, S=60% and S=50% are shown in Figure 5.13a, Figure 5.13b, Figure 5.14a and Figure 5.14b, respectively.

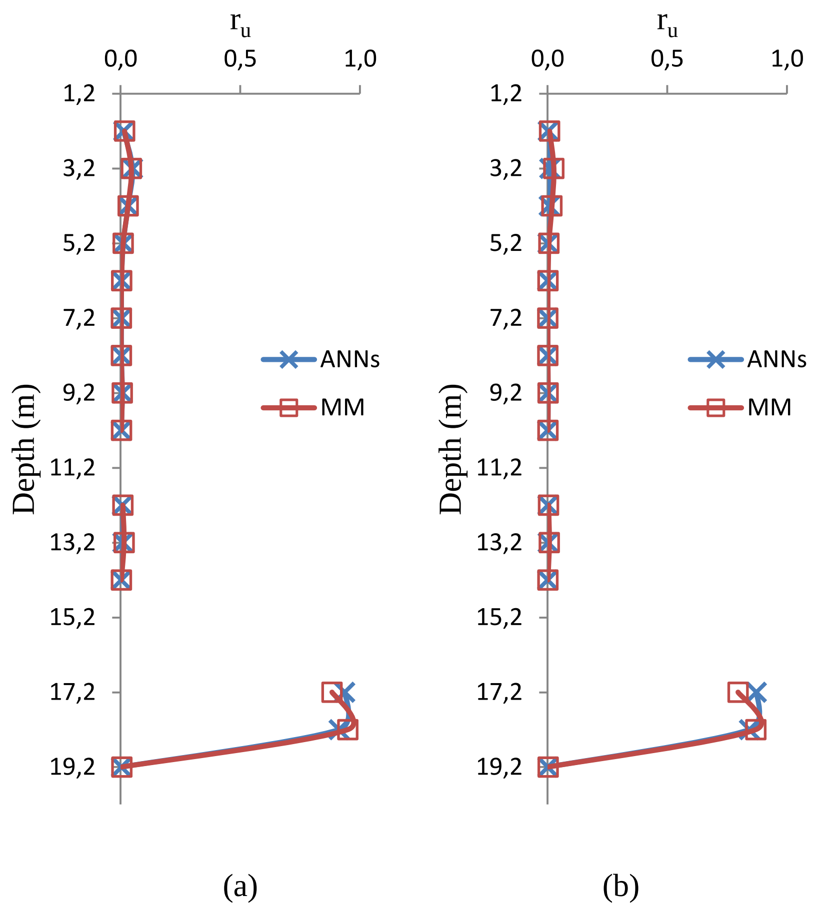

Figure 5.13 : Comparison of ANN model with mathematical model for r_u for S=80% (a) and S=70% (b).

By inducing 80% degree of saturation, at most layers r_u was obtained less than 0,1 values. Correspondingly, 80% partial saturation would be enough to gain reasonable results. If desired, higher degree of partial saturation can be applied but in order to provide uniform distribution in soil, and ensure to be on safe side, inducing 80% partial saturation is suggested. Presence of weak sand layer which is close to rock layer, led to obtain large shear strains in Edushake (EduPro Civil System, 1998). For these shear strains to reduce r_u below 0,5, it is suggested to induce 50% partial saturation.

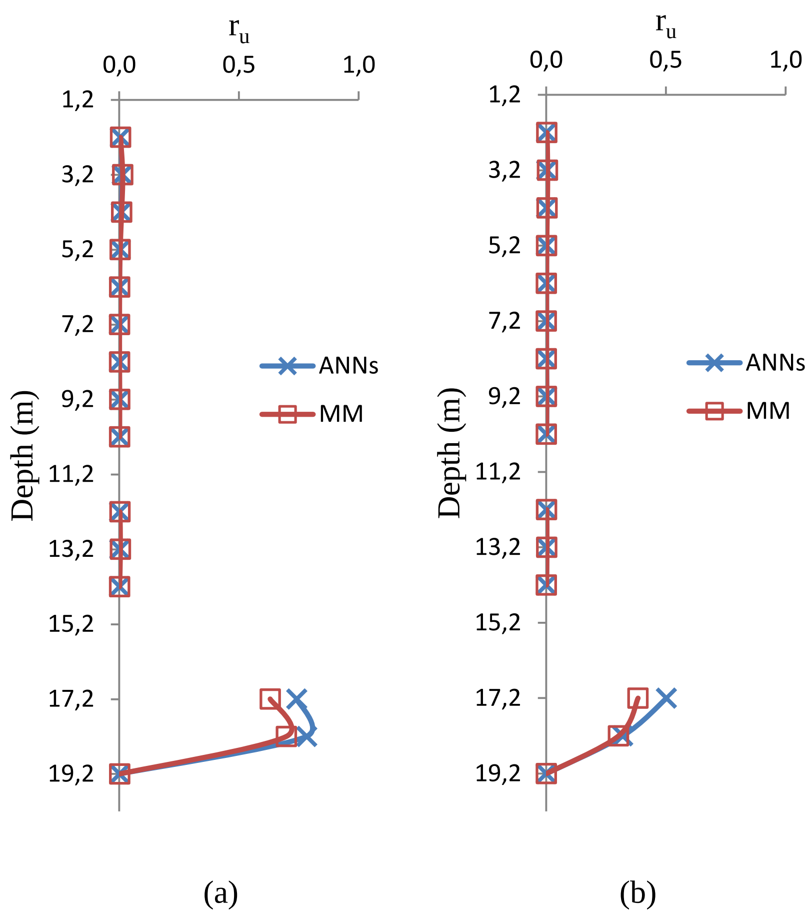

Figure 5.14 : Comparison of ANN model with mathematical model for r_u for S=60% (a) and S=50% (b).

6. SUMMARY AND CONCLUSIONS

This thesis presents the estimation of excess pore water pressure ratio (r_u) in partially saturated sands during earthquakes by using Artificial Neural Networks approach and its comparison with the mathematical model developed by Eseller-Bayat (2009). Using both models partial saturation to be induced in a liquefiable sand site was estimated. To achieve these research goals, the following steps were completed.

1. An ANN model first was developed to predict maximum excess pore water pressure ratio r_{umax} (ultimate value reached under cyclic loading) in partially saturated sands. Different ANN models were explored to train with parameters S, D_r and γ and the best model which eliminates over learning and gives the highest statistical indicator (coefficient of determination, R^2) was obtained. Also, the effect of each parameter on r_{umax} was determined using the relative contributions obtained by ANN.
2. Another ANN model was developed to predict the number of cycles (N_{max}) required to reach maximum excess pore water pressure ratio, also depending on parameters S, D_r and γ for a specific effective stress. Also, a sensitivity analysis was performed to determine the contribution of each parameter on N_{max}.
3. The ANN models for predicting r_{umax} and N_{max} were used to predict excess pore water pressure ratio (r_u) in partially saturated sands during an earthquake.
4. Both ANN and mathematical models were used to estimate the degree of partial saturation to be induced in liquefiable sands by demonstrating in a case example. Edushake (EduPro Civil System, 1998) software program was used to estimate shear strains induced in sand layers for Taft earthquake (M=7,6).

The completed steps were led to following conclusions;

1. The best ANN model to predict r_{umax} was determined as Back Propagation Neural Networks with R^2=96,2% which is a better prediction when compared with mathematical model R^2=92%. Also, the BPNN model can predict r_{umax} with an error range of ±0,1 whereas the mathematical model can predict with an error range of ±0,13 with 90% confidence interval.
2. The best ANN model to predict N_{max} was determined as General Regression Neural Networks with R^2=91,5%. The correlation between N_{max} and S, D_r and γ was very complicated to formulate with a mathematical model. GRNN that was developed was able to correlate the relation between N_{max} and these parameters.
3. According to the sensitivity results from ANN, degree of saturation was determined to be the most dominant parameter on the response of r_{umax} and N_{max}. The second most dominant parameter is shear strain for r_{umax} and relative density for N_{max}.
4. Based on ANN models, prediction plots for r_{umax} and N_{max} were developed for loose and medium dense sands for use in practice.
5. For the given case study site which is susceptible to liquefaction, partial saturation of 80% was suggested to be induced for a design r_u value of 0,5 in the majority of the sand layers which are subjected to Taft earthquake (M=7,6). For only a weak sand layer above the outcrop, 50% partial saturation was suggested to be induced due to high shear strains (γ>0,3%) generated in Edushake (EduPro Civil System, 1998).

The predictions of r_u by ANN and mathematical models were close to each other, confirming the functionality of ANN models. ANN model was found to be more advantageous over the mathematical model since it can predict r_u with higher accuracy and also it can be improved with more field data in the future. Also, ANN was capable to resolve the complexity of the effect of each parameter on r_u. However, since boundary conditions cannot be introduced in an ANN model, mathematical model predicts r_u better in S values close to the boundaries (0-40%, 80-100%). To conclude, through this study ANN models were developed for prediction of r_u in partially saturated sands during earthquakes as an alternative model to mathematical model. The ANN models developed in this thesis will shed light to future studies in investigating the behavior of partially saturated sands during earthquakes. Since these studies have been recently started, there are limited research data. Therefore ANN models presented in this thesis can be improved with more lab and field data in the future to predict r_u's more accurately. Also, the field application of IPS mitigation technique is being studied and ANN models will provide valuable information during developing the field implementation techniques of IPS.

Finally, the study presented in this thesis demonstrates the significant resistance of partially saturated sands to liquefaction and will contribute to the further investigations in Geotechnical and Earthquake Engineering disciplines in understanding the behavior of partially saturated sands to liquefaction during earthquakes.

REFERENCES

Bayrak, B., (2002). Liquefaction Potential: A neural network approach. *Senior Thesis*, I.T.U. Civil Engineering Faculty, Istanbul.

Bayrak, B., (2004). Strong Ground Motion Attenuation Relationship Model by Using Neural Network Methodology, *M.S.c Thesis*, I.T.U. Institute of Science and Technology, Istanbul

Castillo E., (2006). A Very Fast Learning Method for Neural Networks Based on Sensitivity Analysis, Journal of Machine Learning Research 7, 1159–1182

Chang, W.J., Rathje, E.M., Stokoe II, K.H. and Hazirbaba, K., (2007). "In Situ Pore Pressure Generation Behavior of Liquefiable Sand", *Journal of Geotechnical and Geoenvironmental Engineering*, Vol.133, No. 8, pp.921-931.

Cheung V. and Cannons K., (2002). "An Introduction to Neural Networks", Signal and Data Compression Laboratory Group Meeting, University of Manitoba.

Dan Hammerstrom D. (1993). "Working with Neural Networks", IEEE Spectrum, pp. 46-53

Das, B. M., (1993). "Principles of Soil Dynamics", Thomson Learning Academic Resource Center. ISBN 0-534-93129-4

Day, R. W., (2002). "Geotechnical earthquake engineering handbook", McGraw-Hill Handbooks

Dobry, R., Ladd, R.S., Yokel, F.Y. Chung, R.M. and Powell, D., (1982). "Prediction of Pore Water Pressure Buildup and Liquefaction of Sands During Earthquakes By The Cyclic Strain Method", U.S. Dept. of Commerce, Washington, DC, NBS Building Science Series, Vol.138, pp.152.

Edushake, (1998). User's Manual, EduPro Civil Systems. Inc. Redmond, Wash.

Efe, Ö. and Kaynak O., (2000). "Yapay Sinir Ağları ve Uygulamaları", Boğaziçi Üniversitesi, İstanbul, Türkiye

Eseller-Bayat, E.,E. (2009). "Seismic Response and Liquefaction Prevention of Sands Partially Saturated through Introduction of Gas Bubbles", *Ph.D. Thesis*, Northeastern University, Boston, MA.

Fausett L. V., (1993). "Fundamentals of Neural Networks: Architecture, Algorithms and Applications", Prentice Hall, Chapter 1-7, page 1-449

Flood, I. and Kartam, N., (1994). Neural Networks in Civil Engineering I: Principles and Understanding, ASCE, vol.8, pp. 131-148

Flood, I. and Kartam, N., (1994). Neural Networks in Civil Engineering II: Systems and Applications, *Journal of Computing in Civil Engineering,* ASCE, vol.8, iss. 2

Frederick, M.D., (1996). Neuroshell 2 user's manual version 4.2. Ward Systems Group

Ganatra A., Kosta Y P, Panchal G. and Gajjar C. (2011). Initial Classification Through Back Propagation In a Neural Network Following Optimization Through GA to Evaluate the Fitness of an Algorithm, 3(1), 98 – 116

Goh, A.T.C., (1994). "Empirical Design in Geotechnics Using Neural Networks." *Geotechnique*, 45(4), 709-714

Hagan, M.T., H.B. Demuth and M.H. Beale, (1996). Neural Network Design. 1st Edn., PWS Publishing Co., Boston, MA, USA., ISBN: 0-53494332-2.

Hazirbaba, K., (2005). "Pore Pressure Generation Characteristics of Sands and Silty Sands a Strain Approach.", *Ph.D. dissertation,* Univ. of Texas at Austin, Texas.

Ishihara, K., (1985). "Stability of natural deposits during earthquakes", Proceedings, 11th International Conference on Soil Mechanics and Foundation Engineering, San Francisco , Vol. 1, pp.

Juang, C. H., Yuan, H., Lee, D. H. and Lin, P. S. (2003). "Simplified Cone Penetration Test-based Method for Evaluating Liquefaction Resistance of Soils." *Journal of Geotechnical and Geoenvironmental Engineering*, 129(1), 66-80

Kartam, N., **Flood, I. and Garrett, J. H.,** (1997) Artificial Neural Networks for Civil Engineers: Fundamentals and Applications, Publ. ASCE, USA

Kramer, S. L., (1996). Geotechnical Earthquake Engineering, Publ. Prentice Hall, New Jersey, USA

Kulasingam, R., (2008). Liquefaction Potential Analysis, Onondaga Lake ILWD Stability.

Livingstone, D. J., (2009). Artificial Neural Networks, Method sand Applications Series: Methods in Molecular Biology, Vol. 458

Mogami, T. and Kubo K., (1953). The behavior of soil during vibration, Proc. 3rd Inter. Conf. on Soil Mech. And Found. Engi., Vol 1, 152-155

National Research Council, (1985). "Liquefaction of Soils During Earthquakes", National Academy Press, Washington, D.C.

Rauch, A. F., (1997). ''EPOLLS: an empirical method for predicting surface displacements due to liquefaction – induced lateral spreading in earthquakes,'' *PhD dissertation*, Virginia Polytechnic Institute and State University, Blacksburg, Va.

Saygılı, G., (2005). Liquefaction Potential Assessment in Soil Deposits Using Artificial Neural Networks, *M.S.c Thesis*, Concordia University, Montreal, Quebec, Canada

Seed, H. B., (1968). "Land slides caused by soil liquefaction", Eng. vol. P. 73 ff. Reprinted from Journal of Soil Mechanic sand Foundations Division.

Seed, H. B., Arango, I. and Chan, C.K., (1975). Evaluation of Soil Liquefaction Potential During Earthquakes. Report No. EERC 75-28, Earthquake Engineering Research Center, College of Engineering, University of California, Berkeley

Seed, H. B., Idriss, I. M. and Arango, I., (1983). Evaluation of Liquefaction Potential Using Field Performance Data, *Journal of Geotechnical Engineering*, Vol. 109, No. 3, pp. 458-482

Seed, H. B. and Idriss I. M., (1971). Simplified Procedure For Evaluating Soil Liquefaction Potential, *Journal of the Soil Mechanics and Division*, ASCE 97(SM9), 1249-1273.

Seed, H. B., Lee, K. L., Idriss, I. M. and Makdisi, F. I., (1975). "The Slides in the San Fernando Dams During the Earthquake of February 9, 1971," *Journal of Geotechnical Engineering Division*, ASCE, Vol 101,No. GT7, pp 651-688

Shahin, M. A., Maier H. R. and Jaksa M. B., (2000). Predicting the Settlement of Shallow Foundations on Cohesionless Soils Using Back-Propagation Neural Networks, Research Report No. R 167, Department of Civil&Environmental Engineering University of Adelaide.

Shahin, M. A., Jaksa, M. B., and Maier, H. R., (2001). "Artificial neural network applications in geotechnical engineering." Australian Geomechanics, 36(1), 49-62.

Shahin, M. A., Jaksa, M. B., and Maier, H. R., (2005). "Investigation into the Robustness of Artificial Neural Networks for a Case Study in Civil Engineering." Proceedings of the International Congress on Modeling and Simulation, MODSIM 2005, Melbourne (Australia), 79-83.

Shahin, M. A., Jaksa, M. B., and Maier, H. R., (2008). "State of the Art of Artificial Neural Networks in Geotechnical Engineering." *Electronic Journal of Geotechnical Engineering*, Vol. 8, pp. 1–26.

Smith K. A. and Gupta J. N. D., (1997). Neural networks in business: techniques and applications, Idea Group Inc (IGI).

Specht, D. F., (1991). A General Regression Neural Network. IEEE Transactions on Neural Networks, 2 (6), 568-576.

Specht, D. F., (1996). Fuzzy Logic and Neural Network Handbook, Mc Graw-Hill Companies, Inc.

Tao C.W., Nguyen H.T., Yao J.T. and Kreinovich V., (2003). "Sensitivity Analysis of Neural Control", Proceedings of the International Conference on Information Technology InTech'03. Page(s) 478-482

Therón, R. and Paz, J.F.D., (2006). Visual Sensitivity Analysis for Artificial Neural Networks. In Proceedings of IDEAL., 191-198.

Tolon, M., (2007). Artificial Neural Network Approaches for Slope Stability, *M.S.c Thesis*, I.T.U. Institute of Science and Technology, Istanbul

Ural, D. and Saka, H., (1998). “Liquefaction Prediction by Neural Networks”, *Journal of Geotechnical Engineering*, ISSN 1089-3032, Vol. 3, pp.1-4.

Url-1 <*http://geomaps.wr.usgs.gov/sfgeo/liquefaction*>, date retrieved 23.08.2011

Vaid, Y.P. and Chern, J.C., (1983). "Effect of static shear on resistance of liquefaction", Soils and Foundations, Vol. 23, No. 1, pp. 47-60

Yegian, M. K., Eseller-Bayat, E., Alshawabkeh, A., and Ali, S., (2007). "Induced Partial Saturation (IPS) for Liquefaction Mitigation: Experimental Investigation.", *Journal of Geotechnical and Geoenvironmental Engineering*, 133(4), 372-380.

Yeung D. S., Cloete I., Shi D. and Ng W. W.Y. (2010). Sensitivity Analysis for Neural Networks, Springer Heidelberg Dordrecht London New York

APPENDICES

APPENDIX A.1 : Network design in Neuroshell 2.

APPENDIX A.2 : r_{umax} data used in Neuroshell 2.

APPENDIX A.3 : N_{max} data used in Neuroshell 2.

APPENDIX A.1

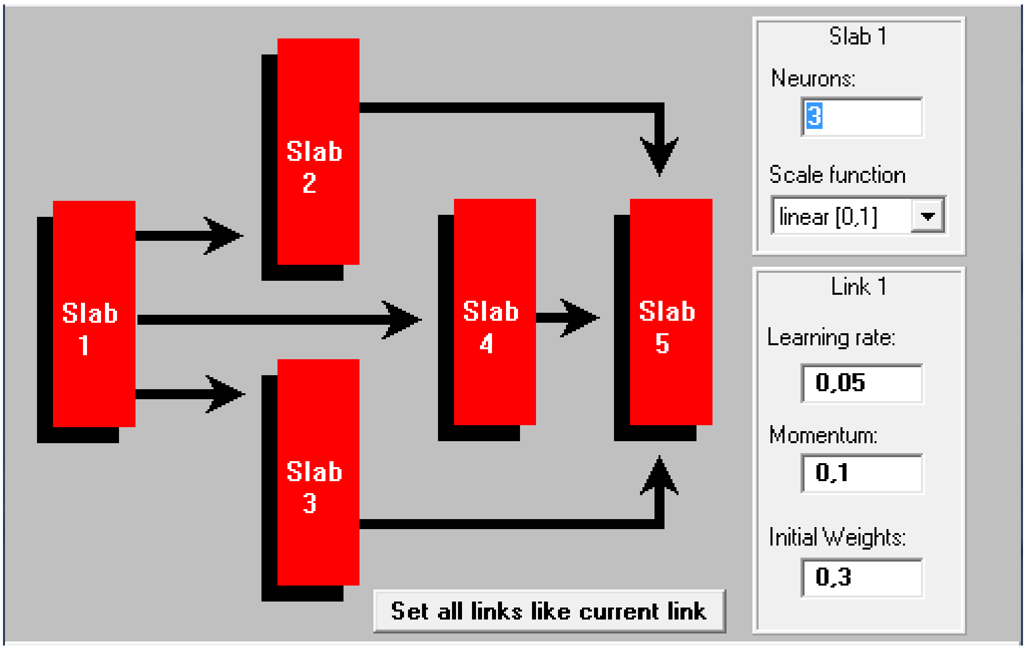

Figure A.1 : Slabs and links for r_{umax} for BPNN in Neuroshell 2.

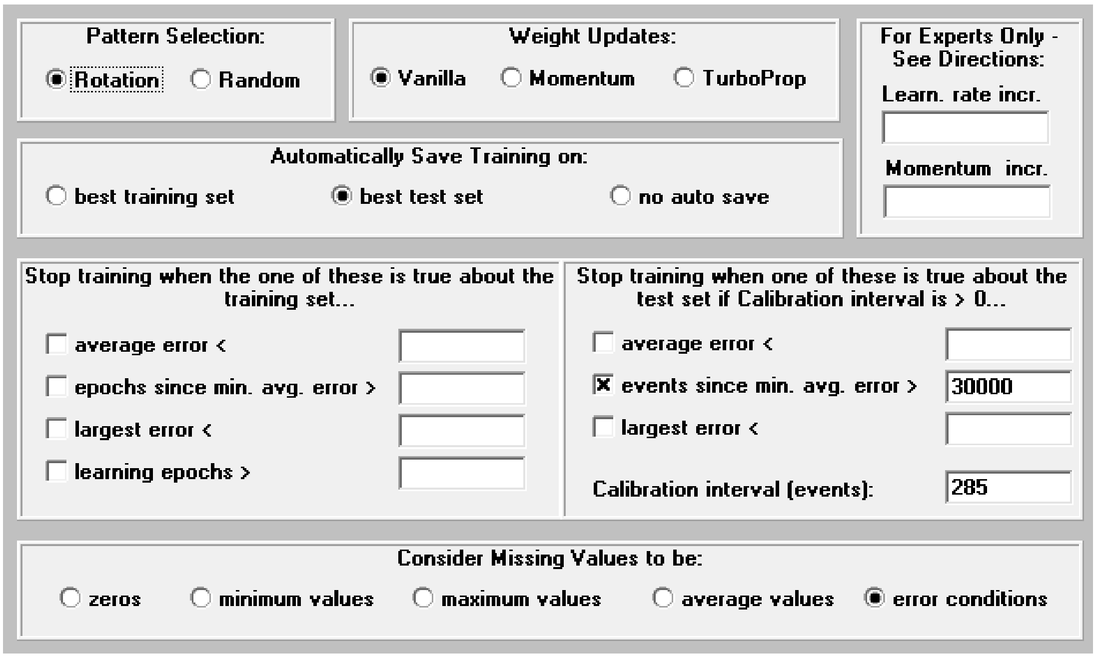

Figure A.2 : Training and stop training criteria for r_{umax} for BPNN in Neuroshell 2.

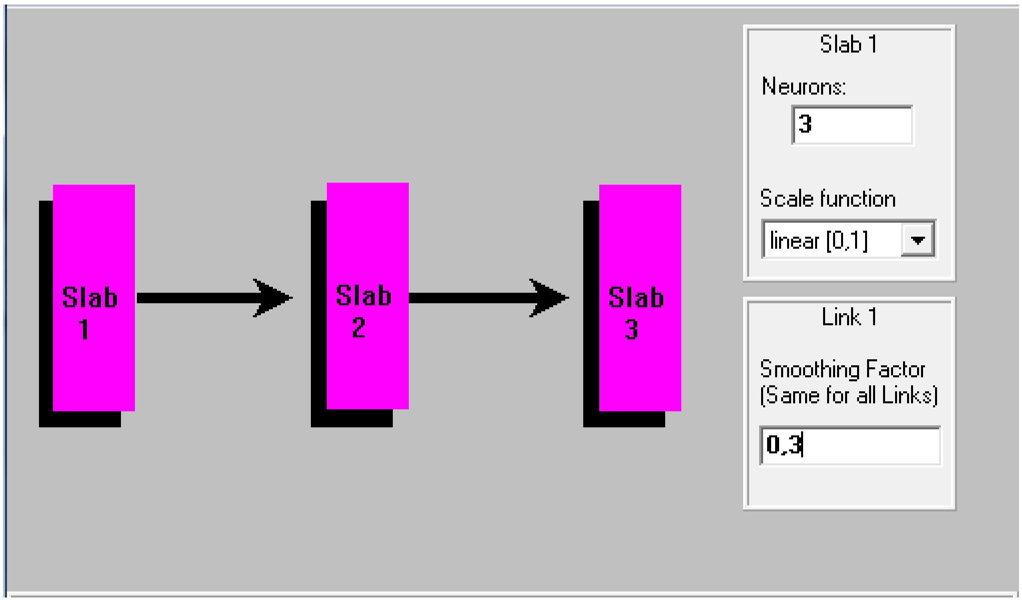

Figure A.3 : Slabs and links for N_{max} for GRNN in Neuroshell 2.

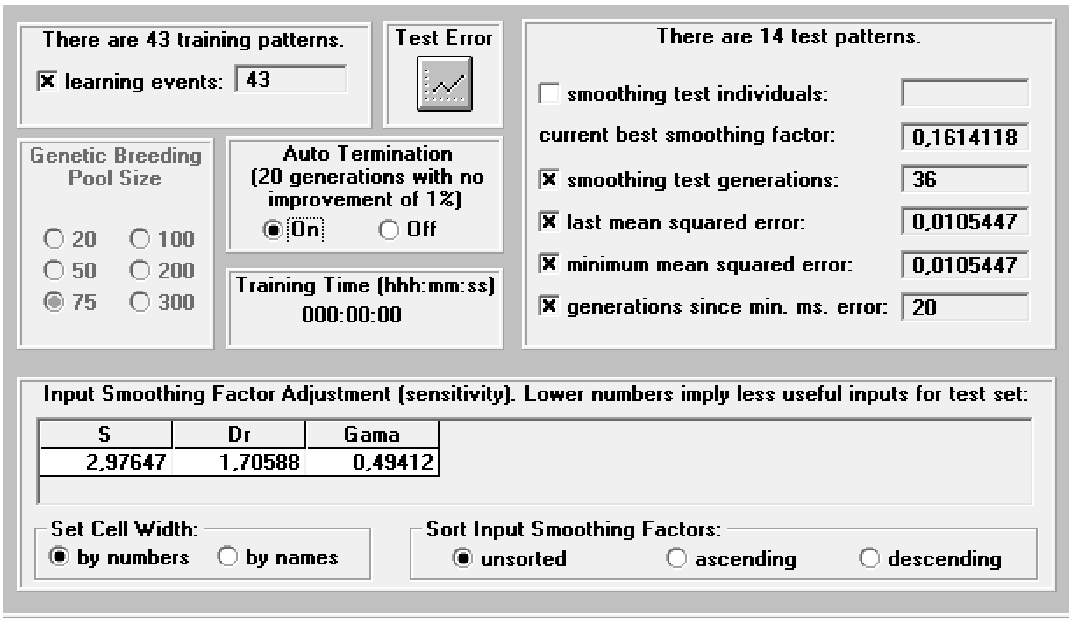

Figure A.4 : Training and stop training criteria for N_{max} for GRNN in Neuroshell 2.

APPENDIX A.2

Table A.1: r_{umax} data (Eseller-Bayat, 2009).

S	D_r	γ %	r_{umax}
0,4763	0,2	0,0225	0,16
0,84	0,2	0,1	0,89
0,63	0,21	0,022	0,47
0,62	0,21	0,057	0,64
0,4646	0,24	0,21	0,44
0,745	0,24	0,055	0,76
0,62	0,25	0,2	0,75
0,4608	0,26	0,31	0,42
0,7	0,27	0,1	0,71
0,741	0,28	0,016	0,37
0,453	0,29	0,015	0,13
0,453	0,29	0,0475	0,16
0,5	0,29	0,1	0,32
0,62	0,29	0,018	0,32
0,58	0,29	0,1	0,46
0,61	0,31	0,053	0,44
0,7317	0,31	0,2	0,78
0,84	0,31	0,06	0,85
0,85	0,32	0,1	0,94
0,78	0,33	0,1	0,74
0,71	0,33	0,1	0,76
0,9	0,33	0,11	0,94
0,74	0,34	0,05	0,62
0,83	0,34	0,1	0,7
0,7262	0,35	0,011	0,3
0,6	0,35	0,1	0,49
0,84	0,35	0,095	0,84
0,44	0,36	0,012	0,06
0,44	0,36	0,1	0,17
0,62	0,36	0,1	0,41
0,74	0,36	0,2	0,78
0,7245	0,37	0,0516	0,41
0,6	0,37	0,2	0,61
0,83	0,38	0,2	0,89
0,43	0,39	0,2	0,22
0,7186	0,39	0,105	0,51
0,57	0,4	0,016	0,12
0,7174	0,4	0,205	0,64

Table A.1 (continued): r_{umax} data (Eseller-Bayat, 2009).

S	D_r	γ %	r_{umax}
0,85	0,4	0,1	0,68
0,56	0,42	0,049	0,21
0,7096	0,44	0,011	0,07
0,56	0,44	0,1	0,31
0,42	0,45	0,013	0,02
0,42	0,45	0,09	0,09
0,7085	0,45	0,052	0,24
0,7029	0,46	0,108	0,31
0,55	0,47	0,013	0,09
0,41	0,47	0,2	0,14
0,55	0,47	0,049	0,14
0,81	0,47	0,052	0,68
0,84	0,47	0,1	0,78
0,53	0,48	0,1	0,32
0,6971	0,48	0,206	0,45
0,6875	0,5	0,0106	0,1
0,84	0,5	0,1	0,69
0,686	0,51	0,107	0,17
0,54	0,51	0,2	0,28
0,81	0,52	0,2	0,69
0,63	0,53	0,1	0,32
0,6816	0,54	0,205	0,26
0,8	0,55	0,011	0,3
0,53	0,56	0,012	0,08
0,53	0,56	0,2	0,15
0,8	0,57	0,051	0,39
0,8	0,59	0,1	0,39
0,6464	0,64	0,011	0,01
0,6464	0,64	0,052	0,03
0,6464	0,64	0,2	0,08
0,8	0,64	0,01	0,14
0,79	0,66	0,1	0,2
0,79	0,67	0,2	0,28
0,4763	0,2	0,05	0,25
0,4734	0,2	0,1	0,36
0,86	0,21	0,02	0,8
0,86	0,21	0,1	0,92
0,63	0,22	0,1	0,74
0,72	0,26	0,1	0,78
0,7343	0,28	0,1	0,77
0,453	0,29	0,1	0,22

Table A.1 (continued): r_{umax} data (Eseller-Bayat, 2009).

S	D_r	γ %	r_{umax}
0,88	0,32	0,1	0,78
0,453	0,33	0,2	0,28
0,81	0,35	0,1	0,81
0,44	0,36	0,048	0,09
0,74	0,36	0,1	0,79
0,8	0,44	0,1	0,59
0,42	0,45	0,046	0,06
0,55	0,46	0,2	0,4
0,71	0,46	0,1	0,45
0,55	0,49	0,1	0,24
0,6875	0,5	0,0516	0,14
0,81	0,51	0,1	0,63
0,53	0,56	0,1	0,11
0,53	0,56	0,012	0,03
0,8	0,61	0,2	0,44
0,6464	0,64	0,108	0,05
0,8	0,64	0,05	0,2

APPENDIX A.3

Table A.2: N_{max} data (Eseller-Bayat, 2009).

S	D_r	γ %	N_{max}
0,453	0,29	0,015	60
0,4608	0,26	0,31	40
0,4734	0,2	0,1	60
0,4763	0,2	0,0225	80
0,62	0,21	0,057	25
0,62	0,25	0,2	15
0,63	0,21	0,022	31
0,63	0,22	0,1	25
0,7343	0,28	0,1	19,6
0,741	0,28	0,016	29,4
0,86	0,21	0,1	2,7
0,86	0,21	0,1	2,5
0,86	0,21	0,02	18
0,64	0,31	0,053	14,2
0,7186	0,39	0,105	23
0,7245	0,37	0,0516	25
0,7317	0,31	0,2	8,6
0,81	0,35	0,1	4,7
0,83	0,38	0,2	4,5
0,84	0,31	0,06	12
0,84	0,35	0,095	7
0,85	0,32	0,1	2,7
0,85	0,32	0,1	2,5
0,9	0,33	0,11	2,6
0,42	0,45	0,013	55
0,6875	0,5	0,0106	35
0,6971	0,48	0,206	38
0,7029	0,46	0,108	40
0,7085	0,45	0,052	40
0,7096	0,44	0,011	45,4
0,7174	0,4	0,205	22
0,81	0,47	0,052	24
0,84	0,47	0,1	4,4
0,6464	0,64	0,011	45
0,6464	0,64	0,108	90

Table A.2 (continued): N_{max} data (Eseller-Bayat, 2009).

S	D_r	γ %	N_{max}
0,6816	0,54	0,205	45
0,686	0,51	0,107	45
0,79	0,66	0,1	50
0,79	0,67	0,2	45
0,8	0,57	0,051	21
0,8	0,61	0,2	29
0,8	0,64	0,05	30
0,81	0,51	0,1	20
0,453	0,29	0,0475	70
0,4763	0,2	0,05	80
0,62	0,29	0,018	24
0,745	0,24	0,055	8,7
0,86	0,21	0,1	2,7
0,7262	0,35	0,011	23,6
0,81	0,35	0,1	5,5
0,85	0,32	0,1	2,5
0,55	0,47	0,013	40
0,6875	0,5	0,0516	46
0,84	0,5	0,1	5,4
0,6464	0,64	0,052	90
0,8	0,59	0,1	30
0,81	0,52	0,2	15

CIRRICULUM VITAE

Name Surname:	Çağdaş ÇAYAKAN
Place and Date of Birth:	London, 06.12.1986
Address:	Balçova / İzmir
E-Mail:	cagdascayakan@hotmail.com
B.Sc.:	Civil Engineering